

**TOWARDS A HIGH-QUALITY INTERANNUAL TO MILLENNIAL ICE-CORE
BASED TEMPERATURE RECONSTRUCTION FOR EAST-ANTARCTICA:**

- Developments for characterizing the spatial and temporal variability of the isotopic composition in low accumulation areas

- Assessment of regional non-climatic isotopic variations induced by topography

Dissertation

for the award of the degree

"Doctor rerum naturalium" (Dr.rer.nat.)

of the Georg-August-Universität Göttingen

within the doctoral program Geosciences of the Georg-August University School of Science

(GAUSS)

submitted by

Rémi Dallmayr

from Geneva, Switzerland

Göttingen, 2021

Thesis Committee

- Prof. Dr. Frank Wilhelms, Department of Crystallography, Geoscience Centre of the University of Göttingen
- Prof. Dr. Andreas Pack, Department of Isotope Geology, Geoscience Centre of the University of Göttingen
- Prof. Dr. Thomas Laepple, Alfred-Wegener-Institut Helmholtz Centre for Polar and Marine Research, Professor at MARUM, department of Geoscience (University of Bremen)
- Dr. Maria Hörhold, Alfred-Wegener-Institut Helmholtz-Zentrum für Polar- und Meeresforschung

Members of the Examination Board

- Reviewer: Prof. Dr. Frank Wilhelms, Department of Crystallography, Geoscience Centre of the University of Göttingen
- Second Reviewer: Prof. Dr. Andreas Pack, Department of Isotope Geology, Geoscience Centre of the University of Göttingen

Further members of the Examination Board:

- Prof. Dr. Julia Kowalski, Computational Geoscience, Geoscience Centre of the University of Göttingen
- Dr. Johannes Freitag, Alfred-Wegener-Institut Helmholtz-Zentrum für Polar- und Meeresforschung

Date of the oral examination: December 10th, 2021

ABSTRACT

Instrumental observations of climate cover only the past ~200 years. Our knowledge about historical natural climate variability beyond this time is exclusively based on climate proxies, stored within natural archives. The polar ice sheets of Greenland and Antarctica have formed by continuous accumulation of snow over > hundred-thousand of years, recording local climate conditions such as the air temperature by means of the isotopic composition of the water molecules composing the snow and ice. However, in regions with very little snow accumulation, multiple processes hamper the interpretation of isotopic data in terms of climate variations and temperature reconstructions from ice-cores from the East Antarctic Plateau are still highly uncertain on decadal to millennial timescales. One approach to overcome the local spatial noise in isotope records was to stack several independent vertical profiles of a specific site. In order to extend this approach into space and time, innovative developments are required to enable (1) the extensive spatial sampling of the snowpack in the field, (2) the temporal analysis providing high-quality isotope records of an increasing amount of profiles from Antarctic snow- and ice-cores.

As a part of the AWI Strategyfund project COMB-i, this dissertation addresses the technical development of tools to meet both requirements and to be applicable to the East Antarctic snowpack and ice column:

- 1) Spatially, I developed a novel sampling technique for a fast and precise sampling of the snow, allowing to investigate the spatial variability of the isotopic composition of the snowpack. We applied this new tool in a study to regionally investigate the relationship between local topography, accumulation rate and isotopic composition. We identify a new mechanism leading to a non-climatic variability in isotopic records retrieved from ice cores, which may impact a large area of the East Antarctic Plateau. Such a finding will improve the interpretation of existing ice-core records, affect the choice of future ice-core drilling site, and contribute to develop statistical models for non-climatic variations of water isotope record.
- 2) Temporally, I enabled the analysis of isotopic composition with high-precision of snowpack profiles using the Continuous Flow Analysis (CFA) technique. This will allow high-pace

measurement of snow-cores, and hence increase statistics of temporal analyzes in order to ultimately strengthen the understanding of the isotopic signal formation. The CFA setup was further applied to generate high-quality paired records of stable water isotopes and chemical impurities along the top 70-meters of an ice-core from East Antarctica. The data produced will foster the newly developed method within the COMB-i project to utilize impurity records to improve the temperature reconstruction from East Antarctic ice-cores.

Overall, through technical innovations and their application, this thesis contributes to push further the limit towards high-quality temperature records on the interannual to millennial time scales in East Antarctica.

PUBLICATIONS AND AUTHOR CONTRIBUTIONS

This thesis is comprised of three publications addressing the characterization of the spatial and temporal variability of the isotopic composition in near-surface snow in low accumulation rate area of East-Antarctica. Studies are introduced in the Results sections 6.1, 6.2.1, and 6.3.1, respectively.

Publication-I: A DUAL-TUBE SAMPLING TECHNIQUE FOR SNOWPACK STUDIES

Dallmayr R., Freitag J., Hörhold M., Laepple T., Lemburg J., Della-Lunga D., Wilhelms F.

Status: The manuscript was published in the peer-reviewed “Journal of Glaciology” 67(261), 84–90. <https://doi.org/10.1017/jog.2020.85>

Authors Contribution: JF actively contributed to this work by participating in the design of the technique, the fieldwork, regularly discussed preliminary results and provided guidance to the first author. In addition to motivating and enabling the device development, TL suggested relevant insights, comments and statistical calculus for this manuscript. Via AWI’s technical services, JL contributed to the device realization and provided the technical illustrations for the manuscript. MH participated during different stages of the study (philosophy, fieldwork, paper preparation). DDL helped with sampling the presented datasets. FW contributed to the results and discussion sections and edited the language of the paper. RD designed and coordinated the realization of the sampling device, led its use in the field, analyzed the results and prepared this manuscript.

Publication-II: TOPOGRAPHIC EFFECT CREATES NON-CLIMATIC VARIATIONS IN ICE-CORE BASED TEMPERATURE RECORDS OF THE LAST MILLENNIUM

Dallmayr, R., Freitag, J., Laepple, T., Wilhelms, F., Jansen, D., Behrens, M. and Hörhold, M.

Status: The manuscript was submitted to the peer-reviewed journal “Geophysical Research Letters” in September 2021.

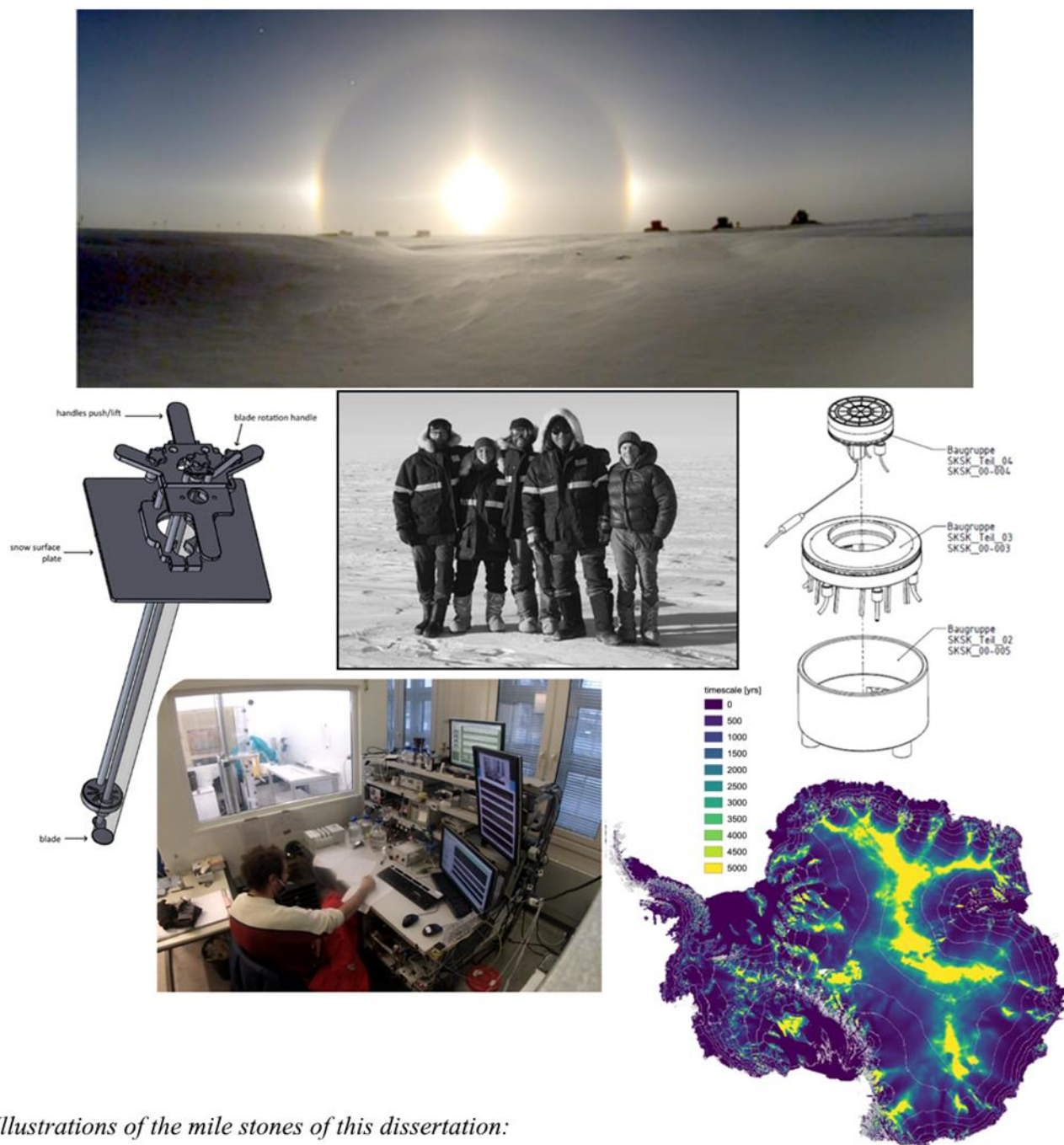
Authors Contribution: T.L. and M.H. enabled the project. T.L. M.H. and J.F. designed the traverse, performed the field-work, and provided support and guidance to the first author for the preparation of the manuscript. M.H. supervised this part of the PhD project. F.W. contributed to the discussion sections and edited the language of the paper. D.J. provided the Figure 4 using the geographic information system Q-GIS, and MB conducted all isotopic measurements at AWI-Bremerhaven. R.D. performed the field-work, analyzed the data and prepared this manuscript, reviewed by all co-authors.

Publication-III: HIGH-PRECISION PROFILES OF WATER ISOTOPES IN SNOW-CORES MEASURED BY CFA; ASSESSMENT OF LIMITATIONS AND TECHNICAL IMPROVEMENT

Dallmayr, R., Meyer, H., Lemburg, J., Gkinis, V., Laepple, T., Behrens, M., Wilhelms, F., and Hörhold, M.

Status: The manuscript is a draft, with a submission planned to the peer-reviewed journal “Environmental Science and Technology”.

Authors Contribution: Through her master-thesis HM participated to the experiments, developed all the algorithms to characterize the isotopic diffusion using the R-software, and participated actively to the preparation of this manuscript with the main author. In addition to the original algorithms, VG provided his expertise on CFA and characterization of isotopic diffusion, and provided insights of the storage-effect based on firn-diffusion. Through initiating the COMB-i project, MH and TL motivated the use of CFA with snow-cores, and provided guidance to the main author. JL designed the new Melt-Head with the main author, manufactured it at the AWI-workshop and provided technical illustrations for the manuscript. MB conducted all discrete isotopic measurements at AWI-Bremerhaven. FW. RD developed the CFA-system, designed and proceeded to the tests and experiments, co-supervised the diffusion characterization Master-thesis, designed the new Melt-Head, analyzed all data and prepared this manuscript.



Illustrations of the mile stones of this dissertation:

At start the magic dance between the surface snow and the wind under a Halo after a storm, redistributing the fresh snow along the local topography; The Kohnen-QK traverse crew: Johannes Freitag, Maria Hörhold, Rémi Dallmayr, Klaus Trimborn and Thomas Laepple); Technical designs of the dual-tubes tool, and of the improved Melt-Head for snow-cores; The Continuous Flow Analysis system of the Alfred-Wegener Institut analyzing the core B56; Time scales of the topographic effect across the Antarctic continent.

Acknowledgments

My first thoughts are to my Referent Prof. Dr. Frank Wilhelms for his trust and supportive attitude all along this thesis and earlier, actually since my first visit to the AWI back in September 2016. Despite your highly busy schedules, you were always here for me when advices and/or reassurance were needed, always with your full-support and without putting pressure. *Merci!*

Thank you so much Dr. Maria Hörhold and Dr. Johannes Freitag for your nearly every day support with constant enthusiasm, for regularly meeting, repeating, again and again, for putting me back on track, for pushing me with care when needed, for proofreading, again and again... for basically guiding me towards changing my way of thinking from a Research-Engineer to a Scientist. *Merci!*

Without the COMB-i project this thesis would not exist, so a big thanks to its original initiator, Prof. Dr. Thomas Laepple. For enhancing the project and for all your relevant ideas and valuable comments leading to these publications. Your way of thinking is as impressive as it is inspiring, I feel lucky having you in my committee thesis. *Merci!*

Thank you, Prof. Dr. Andreas Pack, for your time and for your advises during the committee meetings! *Merci!*

I want to thanks Dr. Johannes Lemburg for our successful collaborations! *Merci Lemmi!*

Merci Prof. Dr. Julia Kowalski for accepting being a member of my examination board.

Without great facilities and good data generated, outstanding science cannot be done. So merci to all technical members of the AWI-Glaciology group and the whole AWI-technical support.

Without great coffee and a good atmosphere, outstanding science cannot be done. So big merci to all the colleagues for the stimulating, enriching, or just relaxing times in the Dome D, up on the AWI-terrasse, or during lunch times. From glaciology or from other sections, building-D or elsewhere, the list of names is long as AWI has this interdisciplinary-family spirit like nowhere else. (Alex, Andreas, Cesar, Damiano, Diana & Topher, Ilka & Christian, Jan, Jean-Louis, Mariano & Miri, petit-frère Nico, Olaf, Sophie, Steven, Tetsuro, Tobi, for just few names...).

The last but far away from the least, I have deep thoughts for Dr. Kipfstuhl, a.k.a. Sepp! Your level of experience and your vision of Science are priceless, and besides lots of fruitful lessons, nice philosophical and personal talks, everything I experienced in the last ~ 5 years is connected to this one-day you visited my previous ice-core lab in Tokyo. *Merci Sepp!*

Looking further back, since my graduation in 2004 several mile stones made my professional path up to this new step. Patrick, Sonia, Amaëlle & Valérie in Paris; Dominique, Jérôme, & Joël in Grenoble; Kumiko & Kenji in Tokyo; the colleagues from Bern, Copenhagen, in the USA. Thank you all for your trust through all the opportunities you gave me.

Living abroad is as challenging as it is enriching, and we need even more the support of our roots, our family. I do feel blessed with mines:

Papa & Maman, vous m'avez offert une vie tellement privilégiée, j'espère qu'aujourd'hui je vous rend un petit peu de tout ce que vous avez fait pour moi. Même si ils paraissaient dénués de sens à vos yeux, vous avez toujours accepté mes choix et m'avez toujours soutenu. Encore merci pour votre présence, votre écoute, votre patience, votre réconfort et votre aide dans les moments difficiles traversés pendant toutes ces années, et spécialement ces >10 derniers mois...!! Lionel & Sonia, sans vous je ne serai certainement pas arrivé jusqu'ici non-plus, merci pour vos réajustements permanents. Mathias, Emie, une petite pensée pour vous; j'espère qu'un jour vous lirez cet ouvrage sans vous endormir, et comprendrez qu'avec travail et persévérance on peut réaliser tous nos rêves! Michèle, j'espère que tu es satisfaite de ton filleul qui a décidé de suivre tes traces. Merci pour tes conseils, pro & perso.

Une belle pensée et merci à ma belle Mariane qui n'a jamais abandonné, malgré tous ces mois de constante préoccupation et ces phases de stress intense.

Et enfin, à tous mes amis et collègues du 74, du 64, de Paris, de Grenoble et de toute la France, et à toutes celles et ceux rencontrés le long de ces 15 années de vie-yage aux extrêmes-Nord, -Est et -Ouest pour atteindre l'extrême-Sud.

Je sais c'est cliché, mais vous avez quelque-part tous contribué à ces travaux...

Je ne crois pas qu'il y ait de bonne ou de mauvaise situation. Moi, si je devais résumer ma vie aujourd'hui avec vous, je dirais que c'est d'abord des rencontres. Des gens qui m'ont tendu la main, peut-être à un moment où je ne pouvais pas, où j'étais seul chez moi. Et c'est assez curieux de se dire que les hasards, les rencontres forgent une destinée... Parce que quand on a le goût de la chose, quand on a le goût de la chose bien faite, le beau geste, parfois on ne trouve pas l'interlocuteur en face je dirais, le miroir qui vous aide à avancer. Alors ça n'est pas mon cas, comme je disais là, puisque moi au contraire, j'ai pu : et je dis merci à la vie, je lui dis merci, je chante la vie, je danse la vie

Otis, créateur de sans-efforceur

TABLE OF CONTENTS

| | |
|---|-----------|
| 0/ GENERAL INTRODUCTION | 1 |
| 1/ ICE CORE, A UNIQUE CLIMATE ARCHIVE | 2 |
| 1.1. Accumulation rate and variability across Antarctica | 5 |
| 1.2. Firn densification and Δ age..... | 6 |
| 2. TEMPERATURE RECONSTRUCTION BASED ON ICE-CORE RECORDS | 7 |
| 2.1. Fractionation of stable water isotopes and global hydrological cycle | 7 |
| 2.2. Measuring the stable water isotopes | 8 |
| 2.3. Stable water isotopes as paleothermometer | 9 |
| 3/ CHALLENGES OF ISOTOPE-BASED TEMPERATURE RECONSTRUCTION | 11 |
| 3.1. Pre-depositional processes | 11 |
| 3.2. Surface (post-)depositional processes | 12 |
| 3.3. Buried firn diffusion process..... | 12 |
| 3.4. Progress and remaining challenges | 13 |
| 4/ THE COMB-I PROJECT (COMB-ING IMPURITY RECORDS WITH WATER ISOTOPES)..... | 14 |
| 4.1. Outlines and deliverables | 14 |
| 4.2. Work-plan for the COMB-i project..... | 15 |
| 4.3. Contribution of this PhD-thesis..... | 16 |
| 5/ METHODS | 16 |
| 5.1. Development of the snow-sampling technique | 16 |
| 5.2. Continuous Flow Analysis system for firn- and ice-cores | 17 |
| 5.2.1. Experimental setup | 17 |
| 5.2.2. System and data-processing software | 19 |
| 5.2.3. Quality assessment of water isotopes analyzes and correction | 20 |
| 6/ RESULTS | 21 |
| 6.1. The dual-tubes snow-sampling technique | 21 |
| 6.2. Regional-scale variability of water isotopes and impurities | 21 |

| | |
|--|-----------|
| 6.2.1 Water-isotopes composition related to accumulation, topography | 21 |
| 6.2.2 Impurity concentrations related to accumulation, water-isotopes | 22 |
| 6.3. Continuous Flow Analysis system | 23 |
| 6.3.1. Adaptation of the system to snow-cores | 23 |
| 6.3.2. ExNGTB27/28 firn core analysis: characterization of diffusion and correction | 24 |
| 6.3.3. The B56 firn core analysis | 26 |
| 6.3.3.1. Reconstructed depth-scale and uncertainties | 26 |
| 6.3.3.2. Datasets synchronization and uncertainties | 27 |
| 6.3.3.3 Water-isotopes measurement and uncertainties | 28 |
| 6.3.3.4. Impurities measurement and uncertainties | 29 |
| 6.3.3.5. Dataset cleaning | 29 |
| 6.3.4. Preliminary results | 30 |
| 7/ SUMMARY AND CONCLUSIONS | 32 |
| 8/ OUTLOOK | 33 |
| 9/ DATA GENERATED WITHIN THE PHD-THESIS | 35 |
| 9.1. Datasets | 35 |
| 9.2. Technical drawings | 36 |
| 9.3. Software, code, user manual | 36 |
| 10/ References..... | 36 |
| 11/ Appendices..... | 47 |
| PUBLICATION-I: A DUAL-TUBE SAMPLING TECHNIQUE FOR SNOWPACK STUDIES | |
| PUBLICATION-II: TOPOGRAPHIC EFFECT CREATES NON-CLIMATIC VARIATIONS IN ICE-CORE BASED TEMPERATURE RECORDS OF THE LAST MILLENNIUM | |
| PUBLICATION-III: HIGH-PRECISION PROFILES OF WATER ISOTOPES IN SNOW-CORES MEASURED BY CFA; ASSESSMENT OF LIMITATIONS AND TECHNICAL IMPROVEMENTS..... | |
| PORT-FOLIO/ ANT LAND-18..... | |

LIST OF FIGURES

| | |
|---|----|
| Figure 1. Drilling sites in Antarctica and Greenland | 3 |
| Figure 2. Schematic of the archival process of the polar-ice | 4 |
| Figure 3. Modelled Surface Mass Balance | 5 |
| Figure 4. Principle of a CRDS device..... | 9 |
| Figure 5. $\delta^{18}\text{O}$ -temperature slopes found in literature | 10 |
| Figure 6. Correlation between ice cores and observations | 11 |
| Figure 7. Melting Unit of the CFA-system for firn/ice cores | 19 |
| Figure 8. Example of CFA, discrete, and deconvolved-CFA signals..... | 26 |
| Figure 9. Top 70-meters B56 depth scale | 27 |
| Figure 10. Delays of detection unit for the B56 analysis..... | 28 |
| Figure 11. Preliminary results of the B56-core..... | 30 |

LIST OF TABLES

| | |
|---|----|
| Table 1. Relative abundances of stable water isotopes..... | 7 |
| Table 2. Analytical measurements of the CFA-system for firn/ice cores..... | 18 |
| Table 3. Diffusion lengths of the CFA-system | 24 |
| Table 4. Diffusion lengths of the CFA-analysis | 25 |
| Table 5. Statistics of the B56 depth scale construction | 27 |
| Table 6. Precision, accuracy, and drift of the water isotopes measurement | 29 |

LIST OF APPENDICES

| | |
|--|----|
| APPENDIX-A: SETUP OF THE CFA-SYSTEM FOR FIRN AND ICE CORES AT THE AWI..... | 47 |
| APPENDIX-B: CUTTING PLAN OF A FIRN/ICE CORE..... | 48 |
| APPENDIX-C: MELT-HEAD FOR FIRN AND ICE CORE..... | 49 |
| APPENDIX-D1: AWI-CFA-PROCESSING/DEPTH ASSIGNMENT | 50 |
| APPENDIX-D2: AWI-CFA-PROCESSING/DATASETS DELAYS | 51 |
| APPENDIX-D3: AWI-CFA-PROCESSING /WATER-ISOTOPES CALIBRATION | 52 |
| APPENDIX-D4: AWI-CFA-PROCESSING /DATASET CLEANING..... | 53 |
| APPENDIX-E: IMPURITIES RECORDS ALONG THE B56 FIRN CORE..... | 55 |
| APPENDIX-F1: SPATIAL VARIABILITY OF IMPURITIES WITH RESPECT TO THE LOCAL ACCUMULATION RATE ALONG THE KOHNEN-QK TRAVERSE | 56 |
| APPENDIX-F2: SPATIAL VARIABILITY OF IMPURITIES THROUGH SITES-GROUP ALONG THE KOHNEN-QK TRAVERSE..... | 57 |
| APPENDIX-F3: IMPURITIES AGAINST $\delta^{18}\text{O}_{\text{anomalies}}$ ALONG THE KOHNEN-QK TRAVERSE | 58 |
| APPENDIX-G: TOP-20M PROFILES OF δD FOR FIRN CORES B56, B53, B54, AND TOP-4M LINER T15-X | 59 |
| APPENDIX-H: EGU21/PRESENTATION OF THE DUAL-TUBE SAMPLING TECHNIQUE..... | 60 |

ABBREVIATION

AWI: Alfred-Wegener-Institut Helmholtz-Zentrum für Polar-und Meeresforschung

DML: Dronning Maud Land

EDC: Epica Dome Charlie Deep Ice Drilling

EDML: Epica Dronning Maud Land Deep Ice Drilling

EPICA: European Project for Ice Coring in Antarctica

NEEM: North Greenland Eemian Ice Drilling

KOHNEN-QK: Quantitative reconstruction of millennial climate variability around Kohnen

0/ GENERAL INTRODUCTION

"Whilst rapid attribution studies have shown the clear link between human-induced climate change for the unprecedented heatwave episodes recorded in the Western United States and Canada, weather patterns over the whole northern Hemisphere have shown an unusual planetary wavy patterns in this summer. This has brought unprecedented heat, droughts, cold and wet conditions in various places." (Baddour, World Meteorological Organization, 2021). The increase in intensity and frequency of extreme meteorological events suggested in 1990 by the 1st report of experts composing the Intergovernmental Panel on Climate Change (IPCC) became such a reality that questioning the climate change induced by human-kind is no longer discussed. And about thirty years later, the very recent 6th assessment IPCC-report was qualified as *"a code red for humanity"* by the UN Secretary-General (Guterres, 2021).

However, implying a not-changing climate refers only to the considered window of time as the climate system on Earth varies periodically, naturally. This variability is due to (1) external forcing, i.e. solar cycle and orbital factors (eccentricity, obliquity, precession; the Milankovitch cycles), and (2) internal interactions between atmosphere, hydrosphere, cryosphere, lithosphere, and biosphere, from which the anthroposphere should now be distinguished. As driven by the modern human society, the latter can evaluate, predict, and modulate its impact in consequence. But this requires at first a profound knowledge of all the contemporary mechanisms involved in the global system, as well as their variability over the past. Paleo-studies are then necessary via a variety of climate archives recording parameters directly or indirectly related to the climate at different time-scales. Such archives are provided by Nature, within the oceans (e.g. marine sediment and coral) and the continents (e.g. lake sediment, speleothem, tree-ring and mountain or polar glacier) (Evans et al., 2013). Amongst them, the polar-ice is of particular interest.

1/ ICE-CORES, A UNIQUE CLIMATE ARCHIVE

Ice-cores provide a unique contribution to our view of past climates as they represent the only natural archive preserving (past)samples of the atmosphere contained within the trapped bubbles. Measuring the composition of the gas offers information about past atmospheric condition on similar timescale than multiple parameters contained within the ice (EPICA community members, 2004). These parameters are called climate proxies as they indirectly give climate information. Amongst others are the stable isotopologues of the water molecule (i.e. the ice matrix itself), as they allow for inferring past temperature changes (section 2 and further). For instance, the Vostok ice-core showed for the first time that the atmospheric concentrations of greenhouse gases CO₂ and CH₄ oscillated in close harmony with global temperature changes through several past glacial-interglacial cycles (Lorius et al., 1985; Barnola et al., 1987; Petit et al., 1999).

A glacier is composed from layers of snow formed during colder winters and warmer summers, accumulated on top of each other with a distinct seasonal distribution of stable water isotope, but also of compounds such as chemical impurities (Figure 2). These soluble ions are present in the buried ice, and provide information about the composition of the atmosphere and its natural variability (Legrand and Mayewski, 1997). They are additionally typically used to identify past volcanic events (Traufetter et al., 2004). As a result, dating each depth of an ice-core is commonly based on counting distinct seasonal layers combined to known volcanic age (Legrand and Mayewski, 1997).

Since the first successful deep ice-core drilling in Greenland (Camp Century, 1966), and in West Antarctica (Byrd station, 1968), numerous deep ice-core studies started in several places on the both ice sheets. The Figure 1 shows the locations of retrieved deep ice-cores which were dated back to the last glacial period or earlier, covering our current interglacial period, the Holocene.

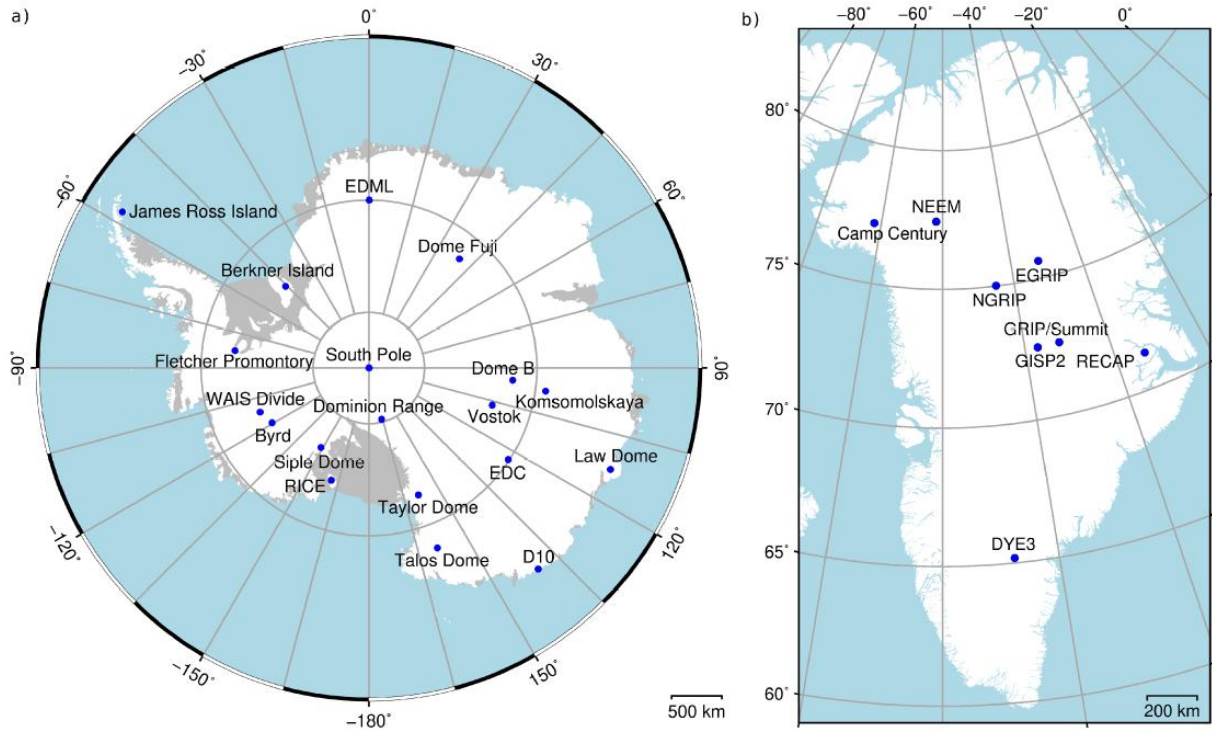


Figure 1. Overview of a) Antarctic and b) Greenlandic ice cores spanning at least 14'000 years, i.e. extending to the last glacial. For Antarctica, ice sheets (white) and ice shelves (gray) are distinguished. The EDML deep core drilling site refers to Kohnen station, Dronning Maud Land (DML).

While ice cores from the East Antarctic plateau can cover a time scale up to ~800'000 years before present including eight glacial-interglacial cycles (EDC ice-core, 3190m depth, EPICA community members, 2004), the oldest climatic record retrieved on the Greenlandic plateau spans ~130'000 years (NEEM ice-core, 2540m depth, NEEM community members, 2013), and reaches the previous interglacial period called Eemian. Intuitively, one may guess that the length of the extracted core is the main reason of such different time-scales spanned. This is partly true, but the

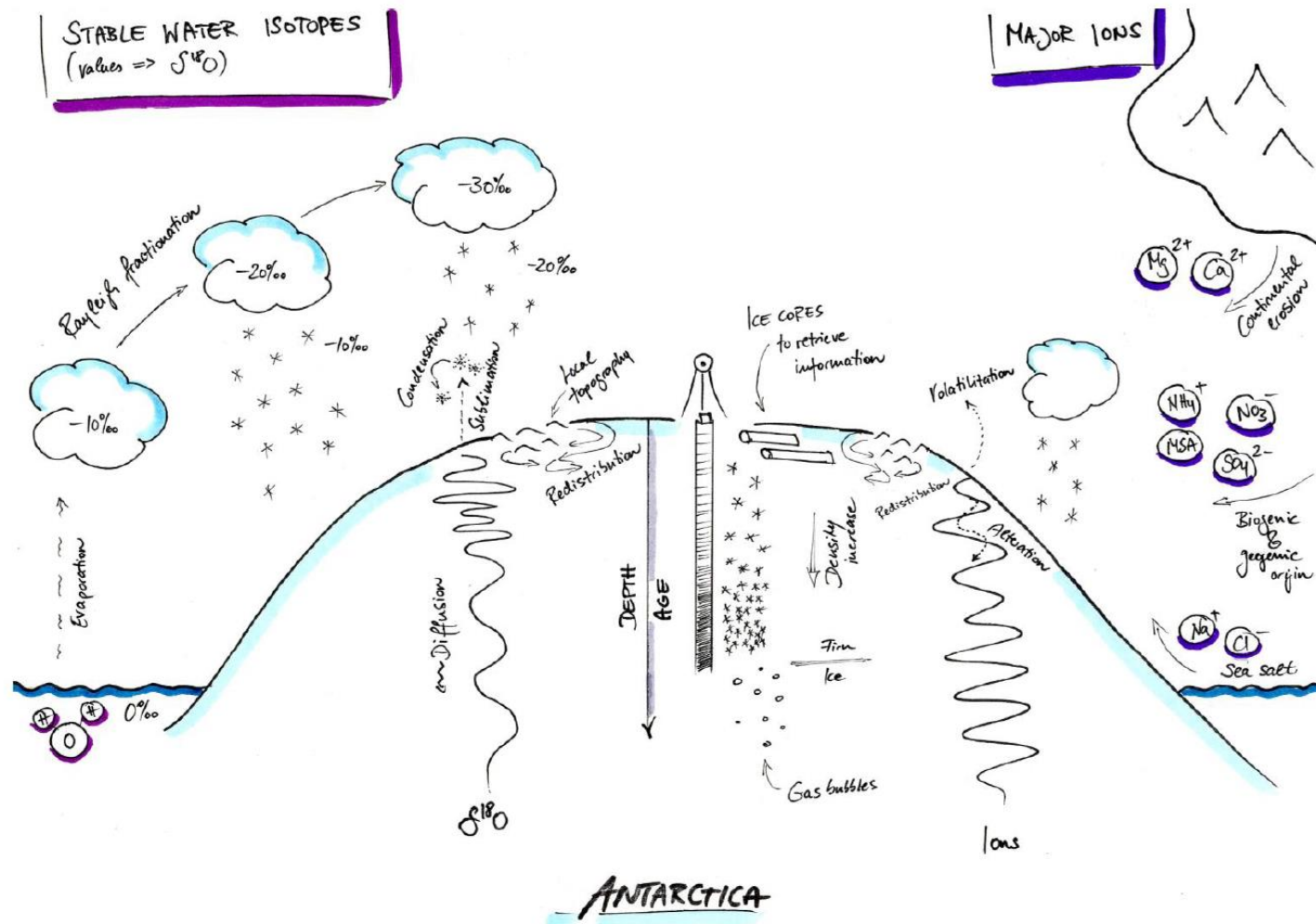


Figure 2. Schematic of the archival process of the polar-ice: stable water isotopes (left); densification (middle); and chemical impurities (right). The figure shows the seasonal variabilities of both climate proxies, as well as different processes that hamper their interpretation on short time scales in low accumulation areas.

Courtesy of Alexander Weinhart (modified).

the main driver is the yearly amount of snow added at the surface of the ice sheet, also called accumulation rate. On the desertic East Antarctic plateau, the accumulation rate is at least 10 times less than on the central plateau of Greenland (Landais et al., 2017).

1.1. Accumulation rate and variability across Antarctica

Accumulation rate is expressed in $\text{kg m}^2 \text{yr}^{-1}$, or more commonly in annual millimeter water equivalent (mm w.e. a^{-1}), the latter considering the density of the snow. From the very low 27 mm w.e. a^{-1} at Dome C (Casado et al., 2016) to 74 mm w.e. a^{-1} at Kohnen station (Steinhage et al., 2013) and South Pole (Winski et al., 2019), further up to the 220 mm w.e. a^{-1} of central West Antarctic Ice Sheet at WAIS-Divide (Buizert et al., 2015) up to

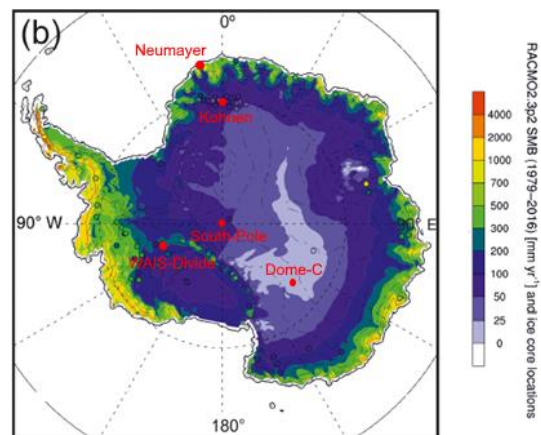


Figure 3. Modelled Surface Mass Balance (RACMO2.3p2) - accumulation rates (1976-2016) (from Thomas et al., 2017, modified)

the coastal 340 mm w.e. a^{-1} at Neumayer station, the Antarctic continent features a wide spatial variability of accumulation rates as indicated in Figure 3. On average, the dry Antarctic plateau is characterized by an accumulation rate below 80 mm w.e. a^{-1} (Casado et al., 2016), with a high regional variability (Fujita et al., 2011).

Such little annual gain is synonym of long exposure times of the surface snow to an atmosphere with a quasi-constant wind, and to intense solar radiations. The cumulative recording of climate in these areas is significantly challenged, and consequently the very low accumulation rate is assumed to be a major source of uncertainty at the different stages of the paleoclimatic use of ice-

core records, from the temperature reconstruction (section 2 and further) to its synchronization with the air samples.

1.2. Firn densification and Δ age

The samples of the past atmosphere are contained within the enclosed bubbles which are not encountered before reaching a certain depth, corresponding to a density of 830 kg.m^{-3} (Schwander and Stauffer, 1984). Starting with a surface snow density $>300 \text{ kg.m}^{-3}$ (Weinhart et al., 2020), the densification process slowly compacts snow to ice, via the state of firn (Figure 2). Depending on local conditions such as the accumulation rate and the temperature, 50 to 120 meters depth (Talalay, 2016) are typically required for the full densification (i.e. a few hundred to a few thousand years, Schwander et al., 1997). In the upper-part of the firn-column, strong ventilation mixes rapidly the surrounding atmosphere and the large open pores (the convective zone, Schwander et al., 1993), while deeper down air transport is dominated by diffusion (the diffusive zone, Sowers et al., 1992).

The air trapped is thus always younger than the surrounding ice, resulting in a Δ age (i.e. mean difference $\text{age}_{\text{ice}} - \text{age}_{\text{gas}}$ along the column), a parameter of first order importance for a correct interpretation of both the information archived in the air (e.g. greenhouse gases, Nakazawa et al., 1993) and ice (e.g. thermometry, Jouzel et al., 1997, section 2 and further). A reliable estimation of the Δ age and the remaining mismatches (especially on the Low-accumulation-rate East Antarctic plateau with up to 2000 years difference, Bender et al., 2006; Parrenin et al., 2012) depends on the constantly improved understanding of the densification process. As an example, the recent identification of the impurities-effect along the process (Hörhold et al., 2012) enabled improvements of firn densification models (Freitag et al., 2013a; Breant et al., 2017).

2. TEMPERATURE RECONSTRUCTION BASED ON ICE-CORE RECORDS

2.1. Fractionation of stable water isotopes and global hydrological cycle

Table 1. Relative abundances of the four major stable water isotopologues (Nassar et al., 2007).

| Isotope | Abundance (%) |
|--------------------------------|---------------|
| H ₂ ¹⁶ O | 99.731700 |
| H ₂ ¹⁸ O | 0.199983 |
| H ₂ ¹⁷ O | 0.037200 |
| HD ¹⁶ O | 0.031069 |

Isotopes are atoms whose atomic nuclei have the same number of protons but a different number of neutrons. Dependent on their inner energy equilibrium, isotopes can either be stable or radioactive; the latter decay with a characteristic half-life time for each radioactive element. Water naturally occurs in several different stable isotopologues (Table1). During phase changes, enrichment or depletion of one isotope specie relative to another occurs. Such change is called fractionation of the isotopic composition, and can originate both from equilibrium or kinetic effect. The equilibrium fractionation refers to slow-enough processes leading to a constant equilibrium between both phases with a fractionation factor related to temperature (Majoube, 1971a,b), while kinetic effects lead to additional fractionation during rapid phase changes (Jouzel and Merlivat, 1984).

The isotopic composition of a water sample is usually expressed as mixing ratio by delta values

$$\delta = \left(\frac{R_{sample}}{R_{VSMOW}} - 1 \right) * 10^3, \text{ and is measured in per mil (‰).}$$

With R_{sample} the abundance ratio of the rare to the common (H₂¹⁶O) isotope in the sample, and R_{VSMOW} correspond to the ratio of the standard reference water. Delta (δ) values are thus reported to the isotopic composition of the Vienna Standard Mean Ocean Water scale (hereafter VSMOW scale, Gonfiantini, 1978) which represents the average isotopic composition of the global ocean.

Based on the Rayleigh model assuming isotopic equilibrium with the additional kinetic effects (Jouzel and Merlivat, 1984), the Rayleigh fractionation describes a process where the condensate is immediately removed from the vapor, depending on temperature (Dansgaard, 1964). This process is of major interest because it occurs in the global hydrological cycle. Initial ocean water (δ -value of 0 ‰) evaporates, with the resulting vapor and the subsequent clouds depleted in heavy isotopes - enriched in lighter ones. During the transport to higher latitudes, further phase change and fractionation take part and the resulting snow falling inland of high latitudes is strongly depleted in the both heavy isotopes $\delta^{18}\text{O}$ and δD (Figure 2).

2.2. Measuring the stable water isotopes

High-precision analysis of stable water isotope are traditionally performed by isotope ratio mass spectrometry (hereafter IRMS). The method is based on the difference of the isotopes mass-to-charge ratio, and while high -precision and -accuracy can be achieved by IRMS systems, water isotope analysis is here a highly demanding process. In common IRMS techniques, water molecules are not measured as such but are converted into a different gas before measurement; for $\delta^{18}\text{O}$ analysis, the CO_2 equilibration method (Epstein and Mayeda, 1953); for δD analysis, reduction of water to hydrogen gas over hot uranium (Vaughn et al., 1998). Thus, measuring simultaneously both isotopes requires the combination of methods.

The laser absorption spectroscopy (LAS) at the near and mid-infrared regions has been demonstrated as an alternative for water isotope analysis to measure simultaneously both isotopic ratios of oxygen and hydrogen with high-quality by injecting directly the sampled water vapor into the optical cavity of the spectrometer (Kerstel et al., 1999).

Laser Absorption Spectrometry by Cavity Ring-Down Spectroscopy

The Cavity Ring-Down Spectroscopy (hereafter CRDS) technique was established as a state-of-the-art technique for stable water isotope analysis (Gupta et al., 2009; Maselli et al., 2013). Such analyzer consists of a tunable infrared diode, a cavity functioning at a low 40 Torr pressure, and a detector unit. The cavity contains three mirrors and receives the laser beam. Once the laser intensity reaches a threshold, the diode is turned off and the light in the cavity circulates within the cavity as reflected by the mirrors, with exponential intensity

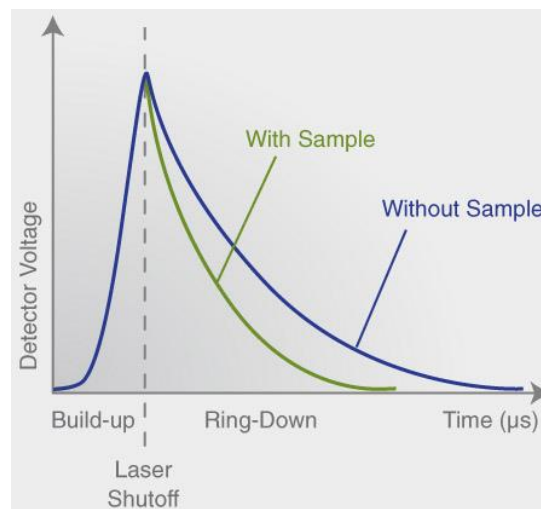


Figure 4. Principle of a CRDS device, with light intensity as a function of time with (green line) and without (blue line) sample absorption.

decay along a pathway increased to ~20 km length. This decay (“ring-down”) time changes once a vaporized sample is passed into the cavity due to additional absorption of light by molecules (Figure 4). Each gas-phase molecule having a unique absorption spectrum, the ring-down at specific wavelength quantifies the absorption of the molecule (i.e. isotopic composition).

2.3. Stable water isotopes as paleothermometer

Since the first stable water isotopes measurements by IRMS, empirical relationships between water isotopic composition of precipitation and air temperature in the mid- and high- latitudes were observed (Epstein and Mayeda, 1953). Traverses to inland stations in Antarctica and Greenland started to sample surface snow along and early studies determined the spatial relationship between

isotopic composition of snow precipitation and local temperature (Dansgaard, 1964; Lorius et al., 1969). Assuming that this relationship remains valid over time, the spatial slope is used as a surrogate for temporal slope changes from past to present. This assumption is however largely discussed and debated (Landais et al., 2017), as it has been shown that the relationship between

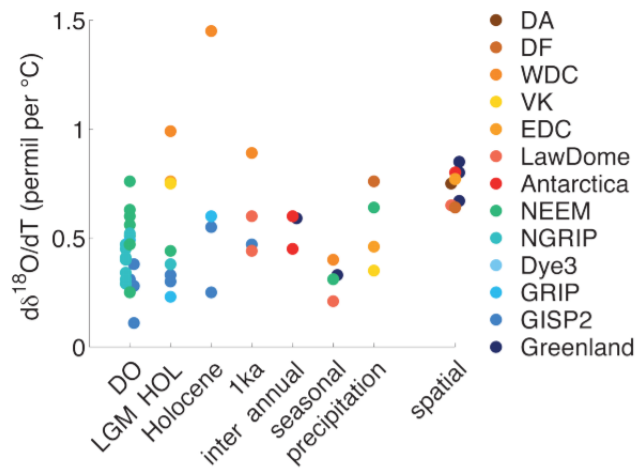


Figure 5. $\delta^{18}\text{O}$ -temperature slopes found in literature.

(from Casado et al., 2017)

isotopes and temperature present a high range of variability in time and space (Figure 5). An adapted calibration of the isotopic paleothermometer to the investigated time scales should be applied, based on weather station data for seasonal and interannual scale, or borehole temperature for longer time scales (e.g. glacial-interglacial millennial transition, Dahl-Jensen et al., 1998).

3/ CHALLENGES OF ISOTOPE-BASED TEMPERATURE RECONSTRUCTION

Recent studies show that the water isotopic composition in shallow snow-pits in Antarctica does not follow the recent temporal evolution of temperature, especially in the regions of low accumulation on the East Antarctic plateau (Masson-Delmotte et al., 2008; Touzeau et al., 2016). The temperature reconstructions based on firn cores records from such areas (1) shows a significantly low correlation with observations of the past 50 years (Klein et al., 2019; Figure 6), and (2) are inconsistent with observations and climate model simulations

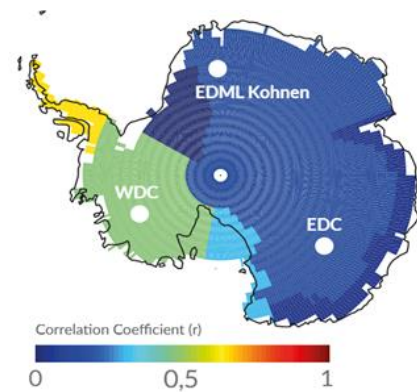


Figure 6. Correlation between ice cores and observations over the period 1958-2005 (Klein et al., 2019, modified).

including anthropogenic forcing for the past 200 years (Jones et al., 2016), and (3) fail to provide a reliable temperature history for the last 2000 years (Stenni et al., 2017; Klein et al., 2019). Indeed, from the atmosphere to the buried firn, multiple processes affect the archiving of the isotopic records at different scales, each adding uncertainties and challenges to the reliability of the thermometry relationship.

3.1. Pre-depositional processes

In addition to precipitation, “diamond dust” deposition represents up to 65% of the annual accumulation rate at Dome C (Stenni et al., 2016), and 40% at Dome Fuji (Fujita and Abe, 2006). Both types of deposition differing in their relationships with temperature, the isotopic temperature should refer to precipitation-weighted temperature (Fujita and Abe, 2006). On the interior plateau of DML, only several precipitation events per year are responsible for a large part (>50%) of the annual precipitation (Fujita et al., 2011; Van den Broeke, 2003). Such inhomogeneous distribution

of events (i.e. precipitation intermittency) on a seasonal and interannual scale strongly influences the accumulation conditions spatially and temporally, and by extension the annual cycle of the isotopic record. As a result, an initial bias on the mean isotopic composition of the surface snow is introduced (Laepplé et al., 2011).

3.2. Surface (post-)depositional processes

Due to the sparse and irregular distribution of precipitation, the snow stays at the surface for a large amount of time. Meanwhile, mechanical interaction with wind erodes the top snow layer and deposits the snow in a new location (Figure 2; Birnbaum et al., 2010; Lenaerts et al., 2012). This re-distribution is locally routed by the topography (Wilhans, 1975) and enables a vertical mixing of both drifted snow and snowfall, leading to a significant depositional noise in the isotopic record (Münch et al., 2016), commonly called stratigraphic noise (Fisher et al., 1985).

Additionally, evidence of water vapor exchanges has been observed on a daily (Steen-Larsen et al., 2011) as well as diurnal basis (Steen-Larsen et al., 2014; Ritter et al., 2016). The isotopic composition of surface snow is modified by physico-chemical interactions with the overlaying atmosphere (Neumann et Waddington, 2004; Town et al., 2008), and within these processes of ventilation the sublimation-condensation is shown to have significant impact on the isotopic composition (Hugues et al., 2021; Ma et al., 2020b).

3.3. Buried firn diffusion process

After burial, the isotopic record is then affected by diffusion through the air channels of the porous firn (Whilans and Grootes, 1985; Johnsen et al., 2000) and results in an attenuation of the

amplitude of the signal (Figure 2) without affecting its absolute composition. The effect of diffusion is negatively related to the depth due to firn densification and the decay of the porosity (section 1.2). However, while the oscillations are not fully erased, this process can be overcome by the use of constantly improved firn-diffusion models (Johnsen et al., 2000; Gkinis et al., 2014; 2021) allowing to back-diffuse the attenuated record and retrieve the original signal.

3.4. Progress and remaining challenges

The magnitude of these (post-)depositional processes being mainly related to the exposure time at the surface, their impact is stronger on the dry Antarctic plateau. For these areas, the isotopic signal is dominated by depositional noise (low Signal-to-Noise ratio, hereafter SNR, Laepple et al., 2016; 2018). But recent trench-studies near Kohnen station (Münch et al., 2016; Laepple et al., 2016) showed that the decorrelation length of vertical profiles of the snowpack was there less than 10 meters, and that stacking an array of independent profiles allows for increasing sufficiently the SNR and overcome the depositional noise. The isotopic signal can be retrieved, its formation and propagation along the upper-firn constrained, enabling thus improved temperature reconstruction on a local-scale (Münch et al., 2017). However, such approach demands a large number of upper-meter profiles analyzed in high resolution, and the low-pace of the liner sampling technique (Schaller et al., 2016) combined to labor-intensive analyzes of discrete samples limit an extensive use of the approach. As a result, extending the stacked-profiles strategy to larger spatial scales remains a logistical challenge and has yet only been applied to small-scale trench studies.

Consequently:

- **On a regional scale, the representative spatial variability of the upper-meter isotopic composition remains an open question.**
- **Interannual to millennial isotope-based temperature reconstruction for East Antarctica cannot be reliably inferred.**

4/ THE COMB-I PROJECT (COMB-ING IMPURITY RECORDS WITH WATER ISOTOPES)

4.1 Outlines and deliverables

The above described challenges call for new statistical and analytical attempts. Within the AWI-internal Strategy fund, new and not-validated approaches can be developed and tested. Within this frame, the COMB-i project was initiated, to explore and push the statistical, analytical, theoretical knowledge and actively tackle the problem of temperature reconstruction in East Antarctica. The major idea behind the COMB-i approach is that, similar to the water isotopes, chemical impurities (e.g. Fluoride, MSA, Chloride, Bromide, Sulfate, Nitrate, Sodium, Ammonium, Potassium, Magnesium, Calcium) records present a seasonal variability (Legrand et Delmas, 1988) and are partly affected by similar (post)depositional processes (e.g. wind-redistribution, Figure 2). Therefore, the project aims to use impurities as a second order parameter to separate the effect of seasonality, noise, and long-term climate variations on the isotope records in order to ultimately propose the first high-quality temperature records from the East Antarctic Plateau on the interannual to millennial time scales.

The deliverables of the project are: (a) a new quantitative temperature reconstruction method based on combining the water isotope signal with impurities, (b) paired high-resolution and dated records of impurity concentrations and water isotopes of firn cores of the East Antarctic Plateau to apply the new reconstruction method, and finally (c) high-resolution temperature reconstruction of East Antarctica for the last millennium.

4.2. Work-plan of the COMB-i project

Along its way to the validation of a new temperature reconstruction method, the project contains the following major mile stones and goals:

0. Theoretical development of the method: Statistical analysis of temperature-isotope, impurities-isotopes, and snow-to-firn relationships (observations from coastal Neumayer station to inland plateau Kohnen station; model simulations, Werner et al., 2011).
1. Field work: the Kohnen-QK traverse is designed to quantify the parameters variability on regional scale (~100 km) around Kohnen station, as related to the varying accumulation conditions. In parallel, excavation of the T4M (Trench 4 meters depth, 50 m length) which offers two-dimensional observations covering the ~20 years period of an automatic weather station.
2. Temporal-tests and tuning of the method through comparison with the T4M combined datasets.
3. Spatial-tests (regional-scale) of the method with the isotope-impurities relationship with respect to the seasonal variability of the accumulation conditions.

- Best combination of impurity species
- Optimal sampling
- Stacking strategy

4. High-resolution paired datasets from firn/core, analyzed by Continuous Flow Analysis.
5. Application of the method and new temperature reconstruction.
6. Validation and extension to East-Antarctica, and further.

4.3 Contribution of the current thesis

As part of the COMB-i project, this thesis aims at addressing the mile stones and goals 1 and 4, with a focus of developing the tools and methods. More specifically, the goals of the thesis are:

- A) The development of a new technique for a clean and fast sampling of upper-meter profiles to overcome the logistical challenge of large-scale representative snowpack content.
- B) Application of A in order to quantify the large-scale spatial variability of parameters and the investigation of the relationships as related to the varying accumulation rate conditions.
- C) The development of a Continuous Flow Analysis (hereafter CFA) system for firn/ice cores providing paired, dated, and high-resolution datasets with high-quality.

5. METHODS

5.1 Development of the snow-sampling technique

With the goal of developing a device offering a fast but precise sampling of the snowpack, we conducted initial tests related to the tubing size, thickness and material type in the Bavarian Alps. Later on, at the Greenlandic camp EGRIP, a first trial based on a piston-effect approach failed in retrieving precise and consistent lengths of snow-cores. Creating an access to the bottom of the

sample tube using a second hole/tube appeared then to be an ideal solution, and the dual-tube technique was born. The original designs of the method were first prepared with the Computer Aided Design software (CAD) Design-Spark Mechanical, while the final designs were implemented/built at the AWI workshop with Solidworks.

5.2 Continuous Flow Analysis system for firn- and ice-cores

5.2.1. Experimental setup

A Continuous Flow Analysis (CFA) system consists of a cold melting unit, and measurement units in an ambient temperature laboratory. In a typical melting unit, a longitudinal subsection of a firn/ice core remains frozen while the end is melted continuously on a chemically inert Melt-Head (MH), adapted to provide two or more streams of water and air bubbles from both inner- and outer-parts of the core. Only the uncontaminated inner-part of the core sample is drained to a degassing unit (Debubbler, DB) before its distribution to analytical devices for online measurements, and/or collection of fractions (Table 2). When the melting unit is not generating melted water, the analytical units are fed with ultrapure water (Millipore Advantage, Milli-Q $\geq 18.2 \text{ M}\Omega\cdot\text{cm}^{-1}$, hereafter MQ). The detailed setup of the CFA-system developed at the AWI used for firn and ice cores is presented in Appendix-A. Following the work of Dallmayr et al. (2016), a high-accuracy laser positioning sensor determines the distance to the top of the melting sample 10 times per seconds with a precision of 0.1 mm in order to derive an accurate melt-speed, and to assign to each data generated the precise corresponding depth.

In order to fulfill the requirements of the COMB-i project, the developed CFA-system generates paired datasets of water isotopes and chemical impurities. The online isotopic measurement

technique applied is described in detail in Publication-III, and in Dallmayr et al. (2016), while for the impurities the system collects cleaned fractions at variable depth-resolution in 20 ml vials (made of polypropylene) under a laminar flow bench. The aliquots are then analyzed offline by the established Ion Chromatography (IC) method (Fischer et al., 2007; Wolff et al., 2006). The results shown for the B56-core (section 6.3.3) were realized with a system Dionex ICS-5000. Ionic species are separated by using columns CG12A-5 μ m, CS12A-5 μ m for cations, and AG18- 4 μ m, AS18-4 μ m for anions.

The system performs additionally the continuous counting and sizing of micro-particles (detection of shadowing and scattering of the transmitted light, Ruth et al., 2002) as well as the online detection of Ca²⁺ by fluorimetry. Finally, continuous measurement of electrical conductivity (Breton et al., 2012) is realized and duplicated along the system for the synchronization of the different datasets (Dallmayr et al., 2016, section 6.3.3.2).

Table 2. Analytical measurements of the CFA-system for firn/ice cores.

| Measurement | Electrical conductivity | Stable water isotopes | Micro- particles | Calcium (Ca ²⁺) | Fraction Collectors |
|-----------------|----------------------------|--------------------------|---------------------|--------------------------------|--|
| Analytical unit | Model 3082 | L2140-i | Abakus | Fluorimetry | SC-4DX |
| (Manufacturer) | (Amber Sciences Inc.) | (Picarro Inc.) | (Klotz GmbH) | (Dr Göbbel GmbH) | (Elemental Service Instruments - ESI) |

The CFA-system for firn/ice cores features a Melt-Head with a square shape of outer-channel of typically 35x35 mm matching the dimension of a typical firn/ice CFA-stick (Appendix-B), and an inner-channel of 31x31mm. The device used at the AWI was developed and manufactured at the

Physics of Ice, Climate and Earth (PICE), Niels Bohr Institute, University of Copenhagen (Figure 7-right, technical drawing in Appendix-C).

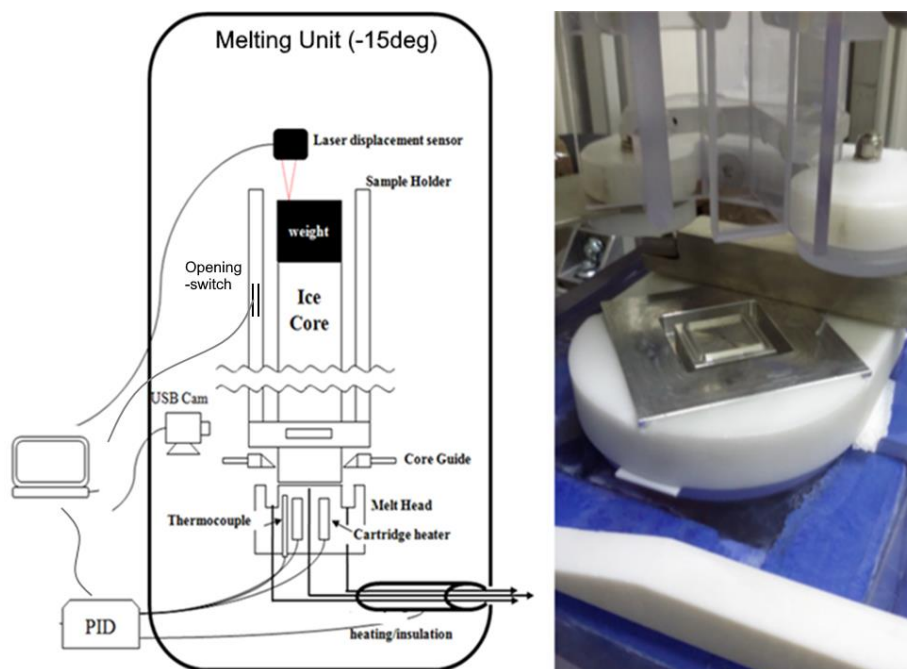


Figure 7. Melting Unit of the CFA-system for firn/ice cores. (left) schematic of the structure and heating setup, (right) photograph of the Danish-design firn/ice Melt-Head.

The core holding structure is adapted to the dimensions of the sample-core and offers an opening mechanism that allows for stacking-up CFA-sticks and performing the continuous analysis of several meters at once. This mechanism is connected to the main software for an efficient depth assignment during the processing (section 6.3.3.1).

5.2.2. System and data processing software

All devices are connected to the controlling computer, using a software developed with LabView 2012. Drivers are either provided by manufacturers (pumps, flowmeters), or developed to suit the purpose (Laser positioning, actuated valves, core holder opener, all analytical units...). All the

technical signals are monitored at $\geq 4\text{Hz}$ and averaged to fit with the 1Hz recording rate of the analytical measurements. Afterwards, the generated datasets are processed using a complementary software also developed with LabView 2012, which realizes (1) a high-precision depth-assignment, (2) a straightforward and efficient synchronization of all datasets, (3) the calibration of the water isotopes to the VSMOW-scale, and (4) a multi-option cleaning procedure of the datasets. The Appendix-D shows the corresponding procedures as applied to the firn core B56 analysis.

5.2.3. Quality assessment of water isotope analyzes and correction

The major disadvantage of the CFA technique consists of its attenuation of the original isotopic signal (smoothing). The performances of a system are thus commonly characterized by its diffusion length (Gkinis et al., 2011; Jones et al., 2017, Publication-III). With the aim to develop procedures and algorithms at the AWI in order to quantify and correct for the diffusion on a routine base, I co-supervised the Master thesis of Hannah Meyer with Dr. Maria Hörhold (collaboration with Vasielios Gkinis, Niels Bohr Institute, Copenhagen). Using the software R, the Master student developed algorithms assessing the isotopic diffusion length of the CFA-system by (1) means of isotopic abrupt changes at relevant points of the system, and by (2) investigating continuous records with respect to discrete records. Based on the results, a mathematical technique was developed to address a correction of the isotopic dataset.

6/ RESULTS

6.1 The dual-tubes snow-sampling technique

Here we address the challenge of extending the stacked-profiles strategy to larger scales. By using a mechanical approach, the developed tool avoids the use of electricity and potential issues in such extreme and isolated conditions. Two juxtaposed tubes are pushed down into the snowpack, one containing the sample core while the second is used to create an access to the bottom of the former. Once the second tube is emptied, a designed structure is inserted to cut the snow and cover below the sample tube. The manuscript describes the successful technique and additionally addresses the 5 km variability of the upper-meter isotopic composition with respect to the accumulation rate in the vicinity of Kohnen station on the plateau of DML. An illustration of the sampling is further shown in Appendix-G, as presented at the European Geosciences Union (EGU) in May 2021.

Publication I: A dual-tube sampling technique for snowpack studies

6.2 Regional-scale variability of water isotopes and impurities

6.2.1 Water-isotopes composition related to accumulation, topography

Using the presented tool in Publication-I, we address here the 100 km regional-scale spatial variability of the upper-meter isotopic composition and its non-climatic variability with respect to the accumulation rate driven by the local topography. The isotopic composition of the surface is widely inhomogeneous, and we observe its anti-correlation to the deposition of snow which is strongly influenced by changes in the surface slope as small as $<0.1^\circ$. Hence, topographic anomalies induce indirectly surface snow isotopic anomalies, that will get buried through time,

and slowly migrate due to ice flow. This dynamic enables a spatial-to-temporal transfer, and generates in our study case ~1000 years non-climatic variability on a magnitude comparable to the climatic variations over the last millennium. Ice flow and topographic features being omnipresent across the East-Antarctic plateau, we estimated similar non-climatic variabilities at specific time scales in order to assist the interpretation of existing cores as well as to optimize future coring activities.

Publication II: Topographic effect creates non-climatic variations in ice-core based temperature records of the last millennium

6.2.2 Impurity concentrations related to accumulation, water-isotopes

We further investigate the regional variability of impurities with respect to the variations of local accumulation rate (accumulation rate anomalies, Publication-II). Regression analyses are presented in Appendix-F1. MSA and Nitrate show a positive correlation with local deposition (R^2 0.3 and 0.44, p-values 0.004 and 0.0003, respectively). For other species, no significant linear relations are observed. In Appendix-F2, we discriminate sites with low/high accumulation rate (i.e. negative/positive accumulation rate anomalies, respectively) and average the impurities concentrations for each group. While the local isotopic composition detrended from elevation ($\delta^{18}\text{O}_{\text{anomalies}}$, Publication-II) shows a clear pattern, the distribution of impurities is sparse, with globally higher concentrations at the depositional sites. Finally, Appendix-F3 shows the regression analyses of impurities against $\delta^{18}\text{O}_{\text{anomalies}}$. Only the Nitrate compound gives a significant anti-correlation (R^2 0.34, p-value 0.007). But the Nitrate cycle is only weakly defined with a tendency

toward higher summer concentration (Fischer et al., 1998) and processes involved in its deposition are indeed shown to be temperature- and/or accumulation rate-dependent (Röthlisberger et al., 2002).

6.3 Continuous Flow Analysis system

6.3.1. Adaptation of the system to snow-cores

For temporal tests of the COMB-i method, large number of paired isotopes-impurities of upper-meters profiles are needed. Therefore, in addition to the CFA-system required to provide high-resolution paired datasets along a firm core, we address an adaptation of the technique to analyze isotopic profiles of snow-cores. Here, we (1) assess the limitations due to the instrumental setup and the high-smoothing induced by the low density of the snow samples, and (2) propose technical improvements to overcome the analytical challenge. We also observe a significant attenuation of the isotopic signal between datasets separated by 4 years, which indicates additional diffusion during the storage in cold facilities.

Publication III: High-precision profiles of water isotopes in snow-cores measured by CFA; assessment of limitations and technical improvements.

6.3.2. ExNGTB27/28 firn core analysis: characterization of diffusion and correction

We conducted a 32.15 upper-meters firn analysis using the core ExNGT-B27/28 (North Greenland Traverse, Weissbach et al., 2016). By stacking-up artificial ice-cores of different isotopic composition at the Melt-Head, we estimate the diffusion length of the full experimental setup (σ_{system} , Table 3). The Gaussian Cumulative Distribution Function (CDF) was used, as described in Publication-III. To emphasize the high-quality of the developed experimental setup, the improved system proposed by Jones et al. (2017) exhibits diffusion lengths of 17.4 and 19.1 seconds for $\delta^{18}\text{O}$ and δD , respectively.

| | $\delta^{18}\text{O}$ | δD |
|--------------------------------|-----------------------|------------------|
| σ_{system} (sec) | 12.5 (1.4) | 13.2 (1.4) |
| σ_{system} (mm) | 8.3 (1.7) | 8.8 (1.8) |

Table 3. Mean diffusion lengths and standard-deviation in parenthesis of the full experimental setup for both isotopologues, expressed in second and in mm. Conversion from second to mm is based on the considered melt-speed. 20 isotopic steps realized by stacking-up cores are considered.

We further estimate the real diffusion of the continuous analysis with respect to a discrete record. Gkinis et al. (2011) proposed an assessment of diffusion length in the frequency-domain by contrasting the power spectral densities (PSD) of the continuous and discrete datasets. In our upper-firn study, this approach appeared neither being efficient nor precise, and an alternative PSD approach was developed (Meyer, 2020, not published). We used an assessment approach in the depth-domain (described in Publication-III) to estimate the variability of diffusion induced by our continuous analysis (σ_{CFA}) along the upper > 30 meters of firn. As the meter-to-meter results along the core show a high variability (which can be explained by several severe depth-mismatches between datasets), we applied the approach over 4-meter sections (Table 4).

The high diffusion for the top 5-meters underlines the message of Publication-III and the use of a specific and improved experimental setup for such core samples. However, further down the diffusion is surprisingly relatively constant while the depth (density) keeps increasing. Higher density implying more liquid stream generated, this observation is partially explained by the voluntary progressive decrease of the melt-speed to maintain stability in the liquid flow in order to optimize the resolution of the analysis.

| Depth (meters) | $\sigma_{\text{CFA}} - \delta\text{D}$ (mm) | $\sigma_{\text{CFA}} - \delta^{18}\text{O}$ (mm) |
|-------------------|--|---|
| 1-5 | 42 | 39 |
| 5-9 | 17 | 14.9 |
| 9-14 | 18.9 | 18.7 |
| 14-18.01 | 17.5 | 17.2 |
| 18-21.6 | 19.9 | 19.1 |
| 29-32.17 | 18.8 | 13.9 |

Table 4. Diffusion lengths (mm) for δD and $\delta^{18}\text{O}$, as retrieved from the depth-domain approach using a Gaussian CDF over ~4m sections.

Correction of the CFA-induced diffusion

As the CFA-system acts as a smoothing filter convolving the original record of the core, a reciprocal deconvolution can be applied once the diffusion length factor was estimated. To avoid amplifying the frequencies corresponding to the noise induced by the system, we used a Wiener filter (Wiener, 1949). Here, the signal part is assumed to be an exponential multiplied by a constant, and the noise part to be red (or white) noise. Based on the power spectral density of the CFA dataset, a cut-off frequency is manually chosen to separate and amplify the low signal frequencies while smoothing out the high noise frequencies (Meyer, 2020, not published).

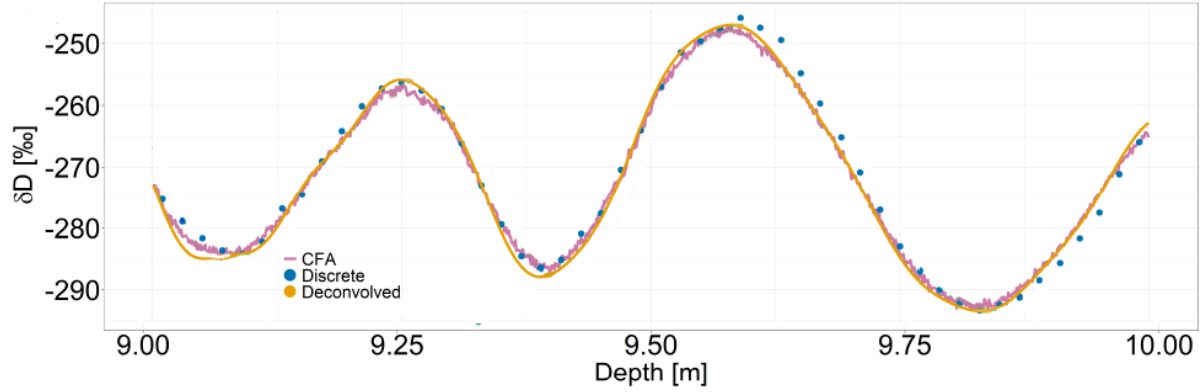
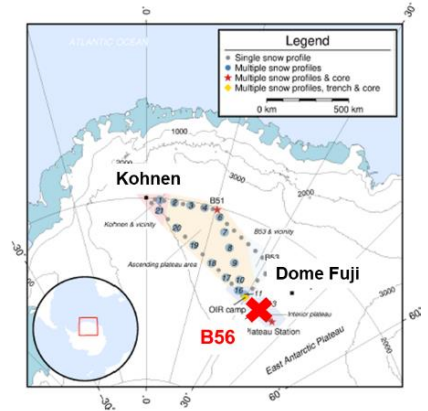


Figure 8. Example of CFA, discrete, and deconvolved-CFA signals, [9:10] meters depth. We see the amplification of low frequencies while high frequencies are smoothed out. Additionally, the depth mismatches between datasets is shown (e.g. depths ~9.6m to 10m).

6.3.3. The B56 firn core analysis

We delivered paired measurements of stable water isotopes and chemical impurities of the top 70-meters of the firn core B56 (34. 97°E, 79.33°S, 3544 m.a.s.l.) to apply the COMB-i method. The core B56 was drilled during the “COFI” traverse (2016/17) in the high interior plateau of DML, in the vicinity of the Dome Fuji station.



(from Weihart et al. 2020, modified)

6.3.3.1. Reconstructed depth-scale and uncertainties

The firn/ice core setup allowing to stack-up cores, runs of 4 cores (4-meter runs) were realized during the CFA-campaign. During a run, melting-events (e.g. start/end of run, new core starting, break in a core) are recorded by the user, while the status of the core-holder (opened when adding

a new core) is continuously recorded. Using such information together with the positioning laser data, the processing software can reconstruct the length and positions along each core automatically and straightforwardly. Positions identified as outliers are replaced by interpolated positions by the software. The user can tune for the optimal reconstruction of the run by using the statistics of each core (e.g. difference experiment-theory, resolution, proportion of interpolated points) and obtain a high-quality depth-assignment for each core and each run. The result of the full depth-scale for the B56 analysis is shown in Figure 9, with the associated statistics in Table 5. An example of the “depth-assignment” procedure is given in Appendix-D1.



Figure 9. Depth-scale of top 70-meters B56 analysis.

| | |
|-----------------------------------|------|
| Mean theory-experiment error (mm) | 4.58 |
| Mean resolution (mm) | 0.71 |
| Mean standard-deviation (mm) | 0.13 |
| Interpolated points (%) | 17.9 |

Table 5. Statistics of the B56 depth-scale construction.
70 cores are considered.

6.3.3.2. Datasets synchronization and uncertainties

The analytical units being located at specific distances in the laboratory with sub sample streams arriving at specific flow rates, each dataset presents a specific delay. Duplicated measurements of electrical conductivity allow for a straightforward approach to identify each delay and synchronize all datasets (Dallmayr et al., 2016). While online measurements present variations allowing to identify the start and end of sample, such approach is essential for the collected-vials and the resulting dataset of chemical impurities. The result of delays obtained of each detection unit and their stability along the 17 runs of the B56 campaign is shown in Figure 10. The strong outlier (water isotopes, run 6) was related to the 10 μm frits-filter (Appendix 1 of Publication-III) getting

blocked, and changed after the run. An example of the “Get-delays” procedure is given in Appendix-D2.

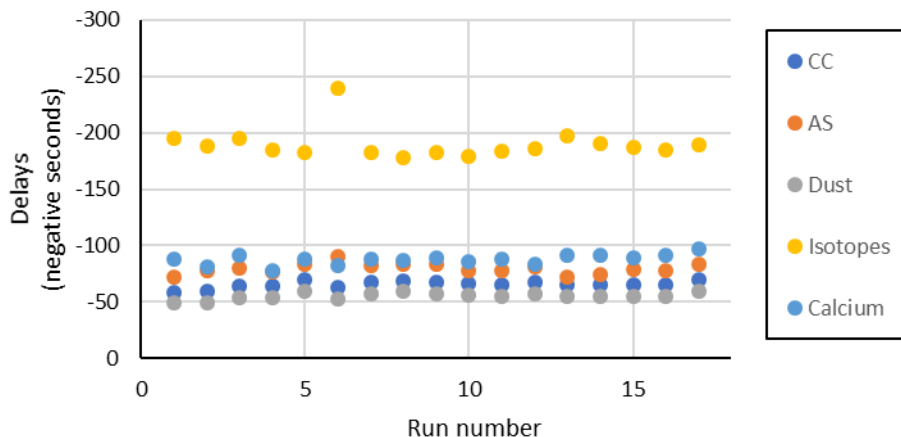


Figure 10. Delays of each detection unit along the 17 runs of the B56 analysis. CC stands for electrical conductivity, AS for the vials collected, Dust for the micro-particles, Isotopes for the stable waster isotopes, and Calcium for the online measurement of Ca^{2+} .

6.3.3.3 Water-isotopes measurement and uncertainties

In contrast to the three-points linear regression used with snow-cores (Publication-III), we updated the calibration procedure for firn-ice core campaigns to a two-point linear regression, the third standard injected acting as a quality-check. Thus, in addition to the precision of the measurement (level of agreement among independent measures) comes the accuracy of the measurement (proximity of measurement to the true value). Furthermore, due to several cores analyzed per run the CRDS instrumental drift must be considered; thus, a first calibration is applied before analyzing the sample and a second after the analysis. The in-between drift of composition is estimated via the quality standard, and a drift-correction of the calibration coefficients is applied. Table 5 shows the isotopic measurement uncertainties of the B56 campaign. An example of the “Water-isotopes calibration” procedure is given in Appendix-D3.

| | Precision | | Accuracy | | Drift | |
|------------------------|-----------------------|------------------|-----------------------|------------------|-----------------------|------------------|
| | $\delta^{18}\text{O}$ | δD | $\delta^{18}\text{O}$ | δD | $\delta^{18}\text{O}$ | δD |
| Mean (‰) | 0.23 | 0.47 | -0.31 | -0.34 | 0.04 | 0.62 |
| Standard-deviation (‰) | 0.01 | 0.03 | 0.08 | 0.60 | 0.14 | 0.85 |

Table 6. Precision, accuracy, and drift of the water isotopes measurement along the 20 calibrations considered during the B56 analysis.

6.3.3.4. Impurities measurement and uncertainties

The chemical impurities of the B56 core were measured with the new system acquired by AWI in 2017. The uncertainty is of about 10% of the value, i.e. a similar precision than the previous system (Göktas et al., 2002). However, the results are now achieved more than twice faster thanks to the rapid separation columns.

6.3.3.5. Dataset cleaning

Additionally, the CFA-system proposes a semi-automated cleaning functionality, which allows for the identification and/or deletion of contaminated/artefact-data from real signal-data. Amongst others, the procedure cleans (1) the contamination due to melting-events such as the “new-core” or the “breaks in core”, (2) the detected presence of air-bubbles downstream of the Debubbler, and (3) the introduction of MQ water in the system, which is a standard procedure in case of melting issues when no sample stream is temporarily generated. An example of the “Cleaning_dataset” procedure is given in Appendix-D4.

6.3.4. Preliminary results

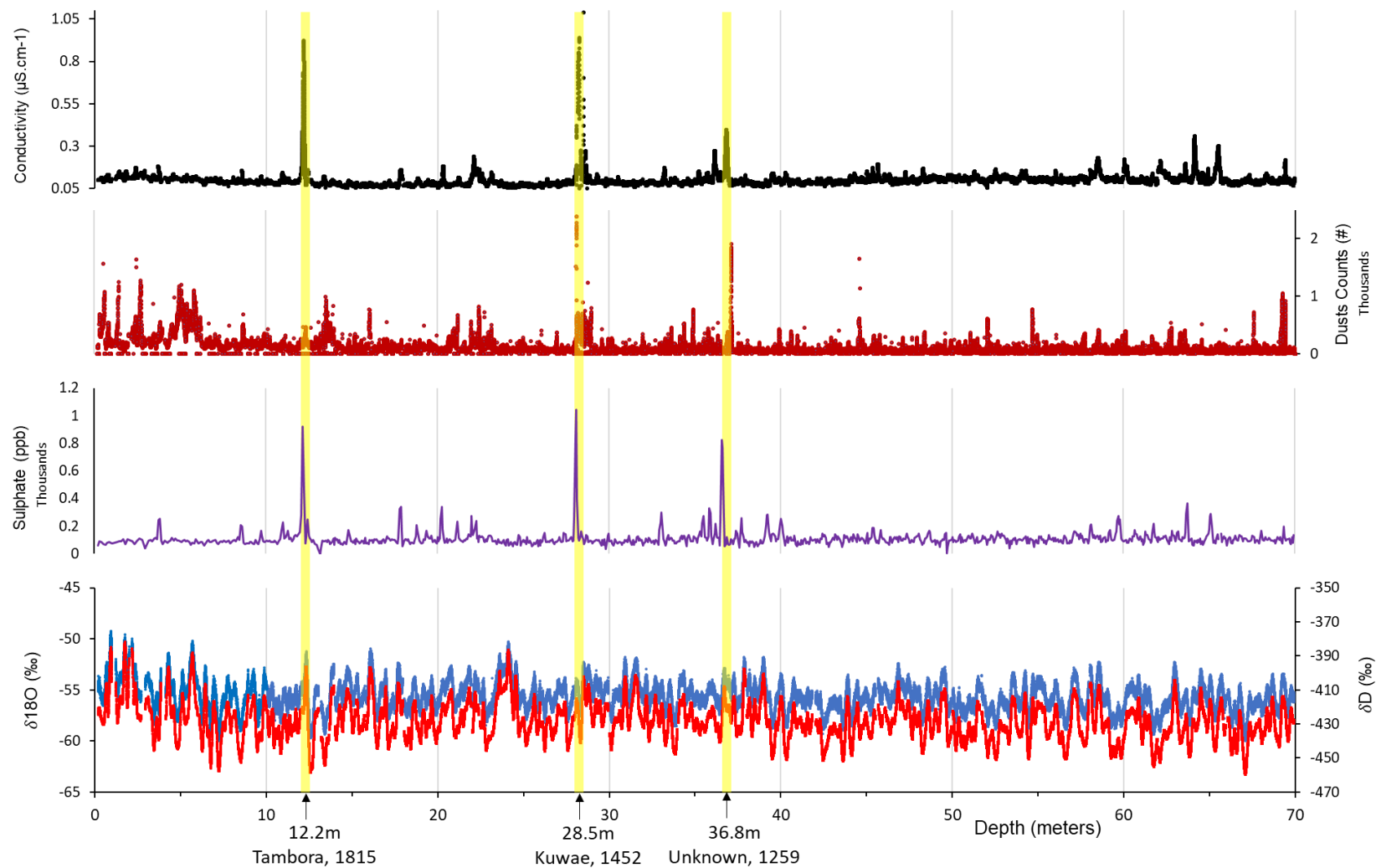


Figure 11. Preliminary results of electrical Conductivity, Micro-particles, Sulphate, and stable water isotopes ($\delta^{18}\text{O}$, δD) along the B56-core.

With the online measurements of electrical conductivity, micro-particles, and Ca^{2+} , we are able to identify promptly three dated volcanic eruptions at depths 12.2 m, 28.5 m, and 36.8 m corresponding to (1) Tambora in 1815, (2) Kuwae in 1452, and (3) Unknown in 1259 (Figure 11; Igarashi et al., 2001; Traufetter et al., 2004; Narcisi et al., 2019). Further volcanic identifications are necessary to correctly date the 70-meters of the core to allow for a first application of the COMB-i method. All impurities (except Fluoride and Bromide) results are shown in Appendix-E.

Based on a preliminary analysis of the processed data, we observe a significant trend towards enrichment of the isotopic composition within the top 10-meters of the core of $>2\text{‰ } \delta^{18}\text{O}$ and $>10\text{‰ } \delta\text{D}$ (Figure 11). Our quality-check data shows a consistent level of reliability for this section compared to the rest of the core. The B56 firn core may thus indicate a trend towards warming over the last <200 years. A 4-meter depth snow profile also taken at the site B56 (Weinhart et al., 2020) agrees with the firn core profile and shows a similar trend (Appendix-G). However, nearby cores (B53 ~ 200 km and B54 ~ 100 km away, both analyzed on the CFA-system of the Desert Research Institute, Reno, USA, Maselli et al., 2013) do not show such tendency (Appendix-G). The comparison also shows that the record of B56 presents colder events than the other cores, like if this site was more sensitive to temperature fluctuations. Further investigation is required, and a parallel look on the past accumulation conditions at site with a detailed topography may be relevant, as a corresponding reduction of snow deposition may indicate a case of non-climatic variations.

7/ SUMMARY AND CONCLUSIONS

As part of the COMB-i project, the presented PhD-thesis actively contributed to improving the millennial-scale temperature reconstruction in East-Antarctica by overcoming challenges of the characterization for both the spatial and the temporal variability of the isotopic composition of the snowpack.

(A) Spatially, we provided an innovative tool easing the sampling of the snowpack (Publication-I). An extensive application of the technique on a 100 km scale in the interior DML permits to investigate the regional variability of the near-surface isotopic composition. By quantifying these variations with respect to the accumulation conditions and the local topography, we inferred the non-climatic isotopic variability (Publication-II). We identified a widely spread within the interior of the continent mechanism that transfers isotopic anomalies at the surface into the firn/ice column. With the map of time scales estimates for this topographic-effect, we open a door to improve the last millennial temperature reconstruction by (1) assisting the interpretation of existing ice-cores, and (2) optimizing the sites for further firn/ice coring. It will additionally contribute to develop statistical models for isotopic non-climatic variations, essential to correct the climate variability estimates from ice-cores.

At this stage, our datasets do not confirm the COMB-i hypothesis that impurities and isotopic variations can be combined to detect and correct for seasonal accumulation effects. We note however the significant relations of Nitrate with accumulation conditions and isotopic composition, but further investigations are needed.

(B) Temporally, we enabled the possibility of high-pace continuous analysis of isotopic composition of the snowpack in low accumulation areas (Publication-III). This work will ease

studies of extended arrays of snow profile, thus increase statistics of temporal analyzes in order to ultimately strengthen the understanding of isotopic signal formation as realized in the Kohnen area (Münch et al., 2017). Following the concept of the COMB-i project, such analysis technique with a great sample throughput allows for isotopic profiles paired with a variety of other proxies at high-resolution. As a result, this development contributes to a better knowledge of the true temporal variability of a multitude of records. We also demonstrated the need of collaboration with manufacturers to push the limits and fit with the constraints of very low accumulation rate sites. In addition, the significant attenuation of the isotopic signal induced by the storage in cold-facilities must be addressed, either via a strategy to preserve the original signal (e.g. cutting discrete samples in the field), or via prompt analysis of the cores by such a development.

(C) Following the deliverables of the COMB-i project, we generated high-resolution paired isotopic and impurities datasets for the first application of the COMB-i method. Cleaned sample fractions are collected and combined to a precise depth-assignment of each vial, efficiently synchronized to the isotopic data. For the latter, beyond an experimental setup optimized to limit the instrumental smoothing (higher performances than the state-of-the-art system at the Institute of Arctic and Alpine Research, Boulder, Colorado, USA; section 6.3.2), we developed procedures to routinely assess and correct for the imprecision of the analyzes in order to provide the highest quality.

8/ OUTLOOK

In addition to the improvements for a precise spatial and temporal characterization of the isotopic content of the snowpack, this work also opens new possibilities for large-scale studies. A modified

sampling device to extract 10 cm diameter sample cores down to several meters used with the CFA-system for snow-cores will popularize the stacked profiles strategy for large-areas. The observed storage effect stressing the need of near-time analyzes, coupling our improved continuous analysis of water isotopes to an on-site system (e.g. Kjaer et al., 2021) will optimize the quality of the record and allow for shipping only frozen fractions for offline measurements. Thinking further, a similar CFA-system also proposing online chemical impurity analysis (Severi et al., 2015) might be implemented in a state-of-the-art mobile-laboratory-container within a traverse train. Then, in addition to an efficient characterization of the complete content of the snowpack at site, such facility may also analyze scrapped surface snow along its way.

I attempted a doctoral summer-school at the University of Svalbard related to the detection and quantification of organo-chemical pollutants in accumulated snow in the Arctic with Professor Roland Kallenborn. Such type of compounds (e.g. polycyclic aromatic hydrocarbon) is directly related to human activities and present a distinct seasonal variability (Kawamura et al., 1994; Jaffrezzo et al., 1994; Masclet et al., 2000). My initial objective was to evaluate technically the potential of using a CFA-system to generate high-resolution profiles of organics from polar ice sheets. The conventional quantification of organics by Gas Chromatography Mass Spectrometry would offer at best ~20 cm depth-resolution via offline analyzes of fractions collected, but coupling recent technologies such as a Proton Transfer Reaction Mass Spectrometry (PTR-MS, Ionicon Inc.) or an Aerosol mass Spectrometer (AMS, Aerodyne Research Inc.) can offer online high-resolution profiles, and further options of potential proxies-combination.

The anti-correlation between isotopic composition and accumulation rate (Publication-II) is of high-interest and further studies are strongly needed. The B31 site represent a perfect location to investigate the prolonged post-depositional alteration of isotopic composition. Assuming a

constant ice flow of 3.5 m yr^{-1} , getting a deeper ice core from B31 covering the last ~14000 years would present full isotopic oscillations due to the cumulated effects of several topographic hollows/bumps up to ~50 km upstream.

Other firm core analyzes are needed by the COMB-i project to obtain a reliable method and to deliver the expected high-quality temperature reconstruction to the community. The AWI CFA-system will naturally respond to this need, but the amount of time for the analyzes of several full firm core may require collaboration with other institution possessing similar CFA-systems of high-quality (e.g. Institute of Arctic and Alpine Research, Boulder, USA; Niels Bohr Institute, Copenhagen, Denmark; Desert Research Institute, Reno, USA; or my previous achievement at the National Institute of Polar Research, Tokyo, Japan,).

9/ DATA GENERATED WITHIN THE PHD-THESIS

9.1/ Datasets

The small 100 m scale and 5 km-transect isotopic datasets (Publication-I) were published at <https://doi.pangaea.de/10.1594/PANGAEA.921928>; <https://doi.pangaea.de/10.1594/PANGAEA.921930>, respectively. For the Kohnen-QK traverse (Publication-II), the isotopic dataset, the surface elevation, the surface elevation of the traverse-00/01, and the GPR profiles of the traverse-00/01 were published at <https://doi.pangaea.de/10.1594/PANGAEA.935029>, <https://doi.pangaea.de/10.1594/PANGAEA.935030>, <https://doi.pangaea.de/10.1594/PANGAEA.935031>, and <https://doi.pangaea.de/10.1594/PANGAEA.935129>, respectively. All discrete and continuous isotopic profiles of the Publication-III, have not yet been published but will be submitted for

publication to PANGAEA. The continuous analysis of the firn cores ExNGTB27/28 and B56 are intended to be added to IceDB data management platform of the Glaciology section at the AWI.

9.2/ Technical drawings

The technical drawings of all the components of the dual-tube sampling device and their assembly are available at the digital library Zenodo, under <https://doi.org/10.5281/zenodo.4001469>.

The technical drawings of all the components of the Melt-Head for snow-cores and their assembly will be published at the digital library Zenodo.

9.3/ Software, code, and user manual

The codes developed for the characterization of isotopic diffusion and correction are available at: https://github.com/Ice-core-Paleo-Proxies/AWI_CFA_Isotope

The CFA-software, the CFA-processing software, and the operating manual are available at: https://github.com/Ice-core-Paleo-Proxies/AWI_CFA_Operation

The report “Continuous Flow Analysis system and organic compounds quantification” written at the Norwegian University of Svalbard was not published.

10/ REFERENCES

Baddour, O. (2021, July). Summer of extremes: floods, heat and fire, <https://public.wmo.int/en/media/news/summer-of-extremes-floods-heat-and-fire>

- Barnola, J., Raynaud, D., Korotkevich, Y. et al. (1987), Vostok ice core provides 160,000-year record of atmospheric CO₂. *Nature* 329, 408–414, doi.org/10.1038/329408a0
- Bender, M. L., G. Floch, J. Chappellaz, M. Suwa, J.-M. Barnola, T. Blunier, G. Dreyfus, J. Jouzel, and F. Parrenin (2006), Gas age-ice age differences and the chronology of the Vostok ice core, 0-100 ka, *J. Geophys. Res.*, 111 (D21115), doi:10.1029/2005JD006488.
- Birnbaum, G., Freitag, J., Brauner, R., König-Langlo, G., Schulz, E., Kipfstuhl, S., Oerter, H., Reijmer, C. H., Schlosser, E., Faria, S. H., Ries, H., Loose, B., Herber, A., Duda, M. G., Powers, J. G., Manning, K. W. and van den Broeke, M. R. (2010), Strong-wind events and their influence on the formation of snow dunes: observations from Kohnen station, Dronning Maud Land, Antarctica, *J. Glaciol.*, 56 (199), 891–902. doi:10.3189/002214310794457272.
- Breant, C., P. Martinerie, A. Orsi, L. Arnaud, and A. Landais (2017), Modelling firn thickness evolution during the last deglaciation: constraints on sensitivity to temperature and impurities, *Clim. Past*, 13 (7), 833–853, doi:10.5194/cp-13-833-2017.
- Breton, D.J., Koffman, B.G., Kurbatov, A.V., Kreutz, K.J. and Hamilton, G.S. (2012): Quantifying Signal Dispersion in a Hybrid Ice Core Melting System. *Environ. Sci. Technol.*, 46(21), 11922–11928, doi:10.1021/es302041k.
- Buizert, C., Cuffey, K. M., Severinghaus, J. P., Baggenstos, D., Fudge, T. J., Steig, E. J., Markle, B. R., Winstrup, M., Rhodes, R. H., Brook, E. J., Sowers, T. A., Clow, G. D., Cheng, H., Edwards, R. L., Sigl, M., McConnell, J. R., and Taylor, K. C. (2015), The WAIS Divide deep ice core WD2014 chronology – Part 1: Methane synchronization (68–31 ka BP) and the gas age–ice age difference, *Clim. Past*, 11, 153–173, doi.org/10.5194/cp-11-153-2015
- Casado, M., Landais, A., Picard, G., Münch, T., Laepple, T., Stenni, B., Dreossi, G., Ekaykin, A., Arnaud, L., Genthon, C., Touzeau, A., Masson-Delmotte, V., and Jouzel, J. (2016), Archival processes of the water stable isotope signal in East Antarctic ice cores. *The Cryosphere*, 12, 1745–1766, doi.org/10.5194/tc-12-1745-2018
- Casado, M., A.J. Orsi, A. Landais (2017), On the limits of climate reconstruction from water stable isotopes in polar ice cores. *Past Global Changes Magazine, Past Global Changes (PAGES) project*, 25 (3), pp.146-147. <10.22498/pages.25.3.146>. <hal-03260040>
- Dahl-Jensen et al. (1998), Past Temperatures Directly from the Greenland Ice Sheet, *Science*, Vol. 282(5387), 268-271, doi: 10.1126/science.282.5387.268

- Dallmayr, R., Goto-Azuma, K., Kjær, H. A., Azuma, N., Takata, M., Schüpbach, S. and Hirabayashi, M. (2016), A High-Resolution Continuous Flow Analysis System for Polar Ice Cores, *Bull. Glaciol. Res.*, 34, 11–20, doi.org/10.5331/bgr.16R03.
- Dansgaard, W. (1964). Stable isotopes in precipitation, *Tellus*, 16:4, 436-468, doi 10.3402/tellusa.v16i4.8993
- EPICA Community Members (2004), Eight glacial cycles from an Antarctic ice core. *Nature* 429(6992), 623–628. doi:10.1038/nature02599
- Epstein, S., Mayeda, T. (1953), Variation of O18 content of waters from natural sources, *Geochimica et Cosmochimica Acta*, 4(5), 213-224, doi.org/10.1016/0016-7037(53)90051-9
- Evans, M.N., Tolwinski-Ward, S.E., Thompson, D.M., Anchukaitis, K.J. Applications of proxy system modeling in high resolution paleoclimatology, *Quaternary Science Reviews*, 2013, 76, 16-28. doi.org/10.1016/j.quascirev.2013.05.024.
- Fischer, H., D. Wagenbach, and J. Kipfstuhl (1998), Sulfate and nitrate firn concentrations on the Greenland ice sheet: 1. Large-scale geographical deposition changes, *J. Geophys. Res.*, 103(D17), 21,927–21,934.
- Fischer, H., Fundel, F., Ruth, U., Twarloh, B., Wegner, A., Udisti, R., Becagli, S., et al. (2007), Reconstruction of millennial changes in dust emission, transport and regional sea ice coverage using the deep EPICA ice cores from the Atlantic and Indian Ocean sector of Antarctica, *Earth and Planetary Science Letters*, 260 (1–2), 340-354, doi.org/10.1016/j.epsl.2007.06.014
- Fisher, D., Reeh, N., and Clausen, H. (1985). Stratigraphic noise in time series derived from ice cores. *Annals of Glaciology*, 7, 76–83. doi:10.3189/S0260305500005942
- Freitag, J., S. Kipfstuhl, T. Laepple, and F. Wilhelms (2013a), Impurity-controlled densification: a new model for stratified polar firn, *J. Glaciol.*, 59 (218), 1163–1169, doi:10.3189/2013JoG13J042.
- Fujita, K. and Abe, O. (2006), Stable isotopes in daily precipitation at Dome Fuji, East Antarctica, *Geophys. Res. Lett.*, 33 (L18503), doi: 10.1029/2006GL026936.
- Fujita, S., Holmlund, P., Andersson, I., Brown, I., Enomoto, H., Fujii, Y., et al. Fujita, K., Fukui, K., Furukawa, T., Hansson, M., Hara, K., Hoshina, Y., Igarashi, M., Iizuka, Y., Imura, S., Ingvander, S., Karlin, T., Motoyama, H., Nakazawa, F., Oerter, H., Sjöberg, L. E., Sugiyama, S., Surdyk, S., Ström, J., Uemura, R., and Wilhelms, F. (2011). Spatial and temporal variability

- of snow accumulation rate on the East Antarctic ice divide between Dome Fuji and EPICA DML. *The Cryosphere*, 5, 1057–1081, doi:10.5194/tc-5-1057-2011
- Gkinis, V., Popp, T.J., Blunier, T., Bigler, M., Schüpbach, S., Kettner, E. and Johnsen, S.J. (2011): Water isotopic ratios from a continuously melted ice core sample. *Atmos. Meas. Tech.*, 4(11), 2531-2542, doi:10.5194/amt-4-2531-2011.
- Gkinis, V., Simonsen, S. B., Buchardt, S. L., White, J. W. C. and Vinther, B. M. (2014), Water isotope diffusion rates from the NorthGRIP ice core for the last 16,000 years – Glaciological and paleoclimatic implications, *Earth Planet. Sci. Lett.*, 405, 132–141, doi:10.1016/j.epsl.2014.08.022,
- Gkinis, V., Holme, C., Kahle, E., Stevens, M., Steig, E., & Vinther, B. (2021), Numerical experiments on firn isotope diffusion with the Community Firn Model. *Journal of Glaciology*, 67(263), 450-472. doi:10.1017/jog.2021.1
- Gonfiantini, R. (1978), Standards for stable isotope measurements in natural compounds, *Nature*, 271 (5645), 534–536, doi: 10.1038/271534a0.
- Gupta, P., D. Noone, J. Galewsky, C. Sweeney, and B.H. Vaughn (2009), Demonstration of High-Precision Continuous Measurements of Water Vapor Isotopologues in Laboratory and Remote Field Deployments Using Wavelength-Scanned Cavity Ring-Down Spectroscopy (WS-CRDS) Technology, *Rapid Commun. Mass Spectrom.* 23, 2534. doi: 10.1002/rcm.4100.
- Guterres, A. (August 9, 2021). IPCC report: ‘Code red’ for human driven global heating, warns UN chief, <https://news.un.org/en/story/2021/08/1097362>
- Hörhold, M.W., Laepple, T., Freitag, J., Bigler, M., Fischer, H., Kipfstuhl, S. (2012), On the impact of impurities on the densification of polar firn, *Earth and Planetary Science Letters*, 325–326, 93-99, doi.org/10.1016/j.epsl.2011.12.022
- Hughes, A. G., Wahl, S., Jones, T. R., Zühr, A., Hörhold, M., White, J. W. C., & Steen-Larsen, H. C. (2021). The role of sublimation as a driver of climate signals in the water isotope content of surface snow: Laboratory and field experimental results. *The Cryosphere Discuss.* doi:10.5194/tc-2021-87.
- Intergovernmental Panel on Climate Change, and J. T. Houghton. 1990. IPCC first assessment report. Geneva: WMO.
- IPCC, 2021: Climate Change 2021: The Physical Science Basis. Contribution of Working Group I to the Sixth Assessment Report of the Intergovernmental Panel on Climate Change by Masson-

- Delmotte, V., P. Zhai, A. Pirani, S. L. Connors, C. Péan, S. Berger, N. Caud, Y. Chen, L. Goldfarb, M. I. Gomis, M. Huang, K. Leitzell, E. Lonnoy, J. B. R. Matthews, T. K. Maycock, T. Waterfield, O. Yelekçi, R. Yu and B. Zhou. Cambridge University Press, 2021.
- Jaffrezo, J.L., Clain, M.P., Masclet, P. (1994), Polycyclic aromatic hydrocarbons in the polar ice of Greenland. Geochemical use of these atmospheric tracers. *Atmospheric Environment*, 28(6), 1139-1145, doi.org/10.1016/1352-2310(94)90291-7
- Jones, J., Gille, S., Goosse, H. et al. (2016), Assessing recent trends in high-latitude Southern Hemisphere surface climate. *Nature Clim Change* 6, 917–926. doi.org/10.1038/nclimate3103
- Jones, T.R.; White, James W C; Steig, Eric J.; Vaughn, Bruce H.; Morris, Valerie; Gkinis, Vasileios; Markle, Bradley R.; Schoenemann, Spruce W. (2017), "Improved methodologies for continuous-flow analysis of stable water isotopes in ice cores", *Atmos. Meas. Tech.*, 10, 617–632, doi.org/10.5194/amt-10-617-2017
- Johnsen, S. J., Clausen, H. B., Cuffey, K. M., Hoffmann, G., Schwander, J. and Creyts, T. (2000), Diffusion of stable isotopes in polar firn and ice: the isotope effect in firn diffusion, *Physics of Ice Core Records*, vol. 159, pp. 121–140, Hokkaido University Press.
- Jouzel, J. and Merlivat, L. (1984), Deuterium and Oxygen 18 in Precipitation: Modeling of the Isotopic Effects During Snow Formation, *J. Geophys. Res.*, 89 (D7), 11749–11757, doi:0.1029/JD089iD07p11749.
- Jouzel J., Alley, R. B., Cuffey, K. M., Dansgaard, W., Grootes, P., Hoffmann, et al. G., Johnsen, S. J., Koster, R. D., Peel, D., Shuman, C. A., Stievenard, M., Stuiver, M., White, J. (1997). Validity of the temperature reconstruction from water isotopes in ice cores. *Journal of Geophysical Research* 102(C12), 471–487 doi: 10.1029/97JC01283.
- Kawamura, K.; Suzuki, I.; Fujii, Y.; Watanabe, O. (1994), Ice Core Record of Polycyclic Aromatic Hydrocarbons over the Past 400 Years. *Naturwissenschaften* 81, 502-505.
- Kerstel, E.R.T., R. Trigt van, N. Dam, J. Reuss, and H.A.J. Meijer (1999), Simultaneous Determination of the $2\text{H}/1\text{H}$, $17\text{O}/16\text{O}$ and $18\text{O}/16\text{O}$ Isotope Abundance Ratios in Water by Means of Laser Spectrometry, *Anal. Chem.* 71, 5297. doi.org/10.1021/ac990621e
- Kjaer et al. (2021), A portable Lightweight In Situ Analysis (LISA) box for ice and snow analysis, *The Cryosphere*, 15, 3719–3730, 2021 doi.org/10.5194/tc-15-3719-2021
- Klein, F., Abram, N. J., Curran, M. A. J., Goosse, H., Goursaud, S., Masson-Delmotte, et al. V., Moy, A., Neukom, R., Orsi, A., Sjolte, J., Steiger, N., Stenni, B., and Werner, M. (2019).

- Assessing the robustness of Antarctic temperature reconstructions over the past 2 millennia using pseudoproxy and data assimilation experiments. *Climate of the Past*, 15, 661–684, doi: 10.5194/cp-15-661-2019.
- König-Langlo, G., King, J. C., & Pettré, P. (1998), Climatology of the three coastal Antarctic stations Dumont d'Urville, Neumayer, and Halley. *Journal of Geophysical Research*, 103, 10,935– 10,946, doi.org/10.1029/97JD00527
- Laepple, T., Werner, M. and Lohmann, G. (2011), Synchronicity of Antarctic temperatures and local solar insolation on orbital timescales, *Nature*, 471 (7336), 91–94, doi: 10.1038/nature09825.
- Laepple, T., Hörhold, M., Münch, T., Freitag, J., Wegner, A. and Kipfstuhl, S. (2016), Layering of surface snow and firn at Kohnen Station, Antarctica: Noise or seasonal signal?, *J. Geophys. Res. Earth Surf.*, 121 (10), 1849–1860, doi: 10.1002/2016JF003919.
- Laepple, T., Münch, T., Casado, M., Hoerhold, M., Landais, A. and Kipfstuhl, S. (2018), On the similarity and apparent cycles of isotopic variations in East Antarctic snow pits, *The Cryosphere*, 12 (1), 169–187, doi: 10.5194/tc-12-169-2018.
- Landais A., Casado, M., Prié, F., Magand O., Arnaud, L., Ekaykin, A., Petit, J.R., Picard, G., Fily, M., Minster, B., Touzeau, A., Goursaud, S., Masson-Delmotte, V., Jouzel, J., Orsi, A. (2017), Surface studies of water isotopes in Antarctica for quantitative interpretation of deep ice core data. *Comptes Rendus Geoscience*, 349(4), 139-150, doi.org/10.1016/j.crte.2017.05.003
- Legrand, M., Delmas, R. (1988). Soluble Impurities in Four Antarctic Ice Cores Over the Last 30 000 Years. *Annals of Glaciology*, 10, 116-120. doi:10.3189/S0260305500004274
- Legrand, M., and P. Mayewski (1997), Glaciochemistry of polar ice cores: A review. *Rev. Geophys.*, 35 (3), 219–243, doi:10.1029/96RG03527.
- Lenaerts, J. T. M. and van den Broeke, M. R. (2012), Modeling drifting snow in Antarctica with a regional climate model: 2. Results, *J. Geophys. Res.*, 117, D05109, doi.org/10.1029/2010JD015419
- Lorius, C., Merlivat, L., and Hagemann, R. (1969), Variation in the Mean Deuterium Content of precipitations in Antarctica. *J. Geophys. Res.*, 74, 7027–7031, doi.org/10.1029/JC074i028p07027
- Lorius, C., Jouzel, J., Ritz, C. et al. (1985), A 150,000-year climatic record from Antarctic ice. *Nature* 316, 591–596, doi.org/10.1038/316591a0

- Ma T., Li L., Shi G., Li Y. (2020). Acquisition of Post-Depositional Effects on Stable Isotopes ($\delta^{18}\text{O}$ and δD) of Snow and Firn at Dome A, East Antarctica. *Water*, 12(6):1707. doi:10.3390/w12061707
- Majoube, M. (1971a), Fractionnement en ^{18}O entre la glace et la vapeur d'eau [Fractionation in ^{18}O between ice and water vapour], *J. Chim. Phys.*, 68, 625–636, doi: 10.1051/jcp/1971680625.
- Majoube, M. (1971b), Fractionnement en oxygène 18 et en deutérium entre l'eau et sa vapeur [Oxygen-18 and deuterium fractionation between water and vapour], *J. Chim. Phys.*, 68, 1423–1436, doi: 10.1051/jcp/1971681423.
- Masclat, P., Hoyau, V., Jaffrezo, J.L., Cachier, H. (2000), Polycyclic aromatic hydrocarbon deposition on the ice sheet of Greenland. Part I: superficial snow, *Atmospheric Environment*, 34(19), 3195-3207, doi.org/10.1016/S1352-2310(99)00196-X
- Maselli, O. J. et al. (2013). “Comparison of water isotope-ratio determinations using two cavity ring-down instruments and classical mass spectrometry in continuous ice-core analysis”. *Isotopes in Environmental and Health Studies* 49.3. pp. 387–398. doi: 10.1080/10256016.2013.781598.
- Masson-Delmotte, V., Hou, S., Ekaykin, A., Jouzel, J., Aristarain, A., Bernardo, R. T., Bromwich, D., Cattani, O., Delmotte, M., Falourd, S., Frezzotti, M., Gallée, H., Genoni, L., Isaksson, E., Landais, A., Helsen, M. M., Hoffmann, G., Lopez, J., Morgan, V., Motoyama, H., Noone, D., Oerter, H., Petit, J. R., Royer, A., Uemura, R., Schmidt, G. A., Schlosser, E., Simões, J. C., Steig, E. J., Stenni, B., Stievenard, M., van den Broeke, M. R., van de Wal, R. S. W., van de Berg, W. J., Vimeux, F. and White, J. W. C. (2008), A Review of Antarctic Surface Snow Isotopic Composition: Observations, Atmospheric Circulation, and Isotopic Modeling, *J. Climate*, 21 (13), 3359–3387, doi: 10.1175/2007JCLI2139.1
- Meyer, H., Lohmann, G., Laepple, T., Hörhold, M., Dallmayr, R. (2020) Characterization of a continuous-flow analysis facility and development of data correction techniques, University of Bremen Institute of Environmental Physics. Not published.
- Münch T, Kipfstuhl S, Freitag J, Meyer H & Laepple T. (2016). Regional climate signal vs. Local noise: a two-dimensional view of water isotopes in Antarctic firn at Kohnen station, Dronning Maud Land. *Climate of the Past*, 12, 1565–1581. doi:10.5194/cp-12-1565-2016

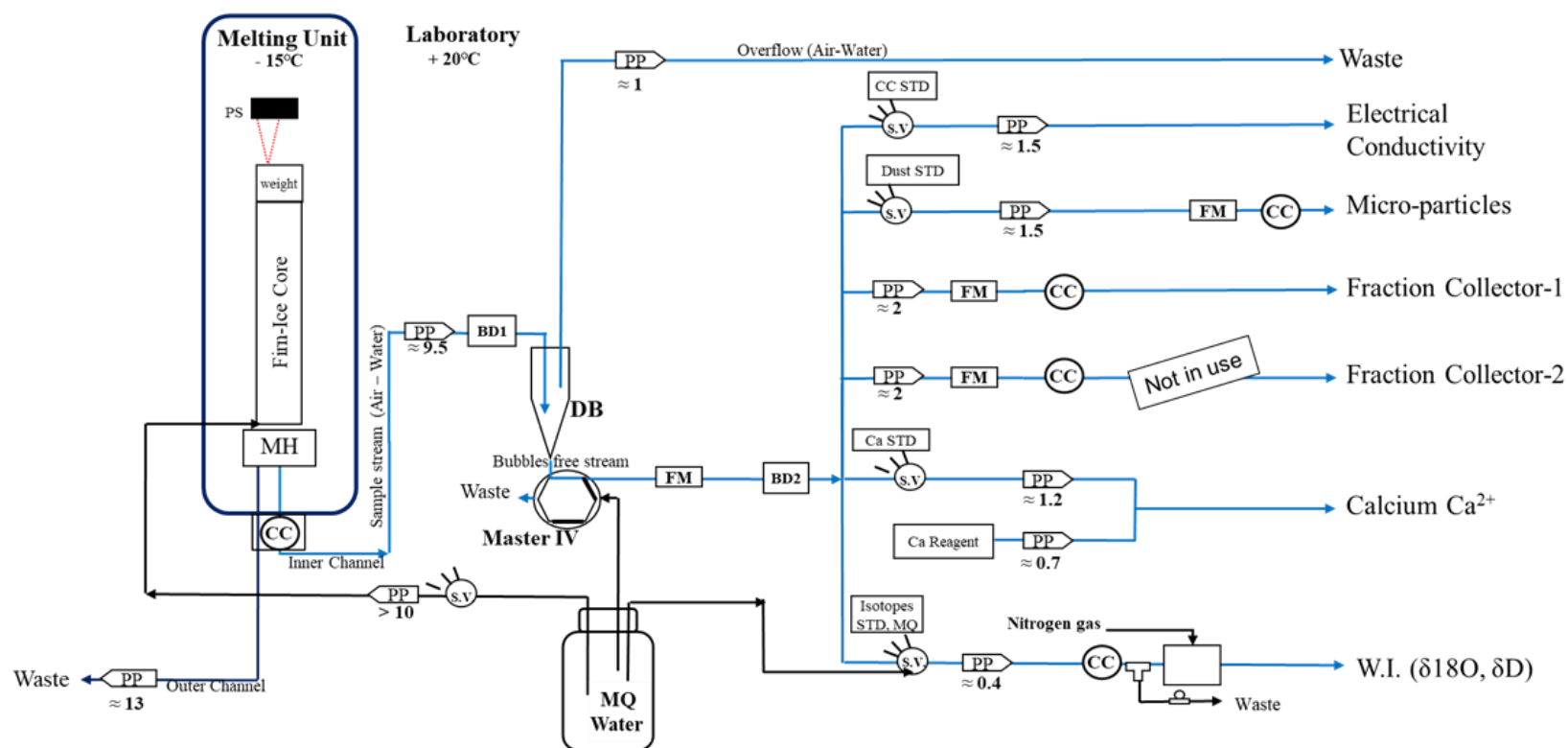
- Münch, T., Kipfstuhl, S., Freitag, J., Meyer, H., and Laepple, T. (2017), Constraints on post-depositional isotope modifications in East Antarctic firn from analysing temporal changes of isotope profiles, *The Cryosphere Discuss.*, 2017, 1–21, doi:10.5194/tc-2017-35.
- Münch, T. and Laepple, T. (2018): What climate signal is contained in decadal- to centennial-scale isotope variations from Antarctic ice cores?, *Clim. Past*, 14, 2053–2070, doi.org/10.5194/cp-14-2053-2018
- Nakazawa, T., Machida, T., Esumi, K., Tanaka, M., Fujii, Y., Aoki, S., & Watanabe, O. (1993). Measurements of CO₂ and CH₄ concentrations in air in a polar ice core. *Journal of Glaciology*, 39(132), 209-215. doi:10.3189/S0022143000015860
- Narcisi, B., Petit, J.R., Delmonte, B., Batanova, V., Savarino, J. Multiple sources for tephra from AD 1259 volcanic signal in Antarctic ice cores. *Quaternary Science Reviews*, Elsevier, 2019, 210, pp.164-174. Doi: 10.1016/j.quascirev.2019.03.005
- Nassar, R., Bernath, P. F., Boone, C. D., Gettelman, A., McLeod, S. D. and Rinsland, C. P. (2007), Variability in HDO/H₂O abundance ratios in the tropical tropopause layer, *J. Geophys. Res.*, 112 (D21), D21305, doi: 10.1029/2007JD008417.
- NEEM community Members (2013), Eemian interglacial reconstructed from a Greenland folded ice core, *Nature*, 493(7433), 489–494, https://doi.org/10.1038/nature11789
- Neumann, T. A. and Waddington, E. D. (2004), Effects of firn ventilation on isotopic exchange, *J. Glaciol.*, 50 (169), 183–194. doi.org/10.3189/172756504781830150
- Parrenin, F., S. Barker, T. Blunier, J. Chappellaz, J. Jouzel, A. Landais, V. Masson-Delmotte, J. Schwander, and D. Veres (2012), On the gas-ice depth difference (Δ depth) along the EPICA Dome C ice core, *Clim. Past*, 8 (4), 1239–1255, doi:10.5194/cp-8-1239-2012.
- Petit, J., Jouzel, J., Raynaud, D. et al. (1999), Climate and atmospheric history of the past 420,000 years from the Vostok ice core, Antarctica. *Nature* 399, 429–436, doi.org/10.1038/20859
- Ritter, F., Steen-Larsen, H. C., Werner, M., Masson-Delmotte, V., Orsi, A., Behrens, M., Birnbaum, G., Freitag, J., Risi, C. and Kipfstuhl, S. (2016), Isotopic exchange on the diurnal scale between near-surface snow and lower atmospheric water vapor at Kohnen station, East Antarctica, *The Cryosphere*, 10 (4), 1647–1663, doi: 10.5194/tc-10-1647-2016
- Röthlisberger, R., Hutterli, M., Wolff, E., Mulvaney, R., Fischer, H., Bigler, M., Steffensen, J. (2002). Nitrate in Greenland and Antarctic ice cores: A detailed description of post-depositional processes. *Annals of Glaciology*, 35, 209-216. doi:10.3189/172756402781817220

- Ruth, U., Wagenbach, D., Bigler, M., Steffensen, J., Röthlisberger, R., & Miller, H. (2002). High-resolution microparticle profiles at NorthGRIP, Greenland: Case studies of the calcium–dust relationship. *Annals of Glaciology*, 35, 237–242. doi:10.3189/172756402781817347
- Schaller, C. F., Freitag, J., Kipfstuhl, S., Laepple, T., Steen-Larsen, H. C., and Eisen, O. (2016), A representative density profile of the North Greenland snowpack, *The Cryosphere*, 10, 1991–2002, doi.org/10.5194/tc-10-1991-2016.
- Schwander, J., Stauffer, B. Age difference between polar ice and the air trapped in its bubbles. *Nature* 311, 45–47 (1984). <https://doi.org/10.1038/311045a0>
- Schwander, J., J.-M. Barnola, C. Andrie, M. Leuenberger, A. Ludin, D. Raynaud, B. Stauffer (1993), The age of the air in the firn and the ice at Summit, Greenland, *J. Geophys. Res.*, 98 (D2), 2831–2838.
- Schwander, J., T. Sowers, J.-M. Barnola, T. Blunier, A. Fuchs, and B. Malaize (1997), Age scale of the air in the summit ice: Implication for glacial-interglacial temperature change, *J. Geophys. Res.*, 102 (D16), 19,483–19,493, doi:10.1029/97JD01309.
- Severi, M., Becagli, S., Traversi, R., Udisti, R. (2015), Recovering Paleo-Records from Antarctic Ice-Cores by Coupling a Continuous Melting Device and Fast Ion Chromatography, *Anal. Chem.* 2015, 87, 22, 11441–11447, doi.org/10.1021/acs.analchem.5b02961
- Sowers, T., M. Bender, D. Raynaud, and Y. S. Korotkevich (1992), $\delta^{15}\text{N}$ of N_2 in air trapped in polar ice: A tracer of gas transport in the firn and a possible constraint on ice age-gas age differences, *J. Geophys. Res.*, 97 (D14), 15,683–15,697, doi:10.1029/92JD01297
- Steen-Larsen, H. C., Masson-Delmotte, V., Sjolte, J., Johnsen, S. J., Vinther, B. M., Bréon, F.-M., Clausen, H. B., Dahl-Jensen, D., Falourd, S., Fettweis, X., Gallée, H., Jouzel, J., Kageyama, M., Lerche, H., Minster, B., Picard, G., Punge, H. J., Risi, C., Salas, D., Schwander, J., Steffen, K., Sveinbjörnsdóttir, A. E., Svensson, A. and White, J. (2011), Understanding the climatic signal in the water stable isotope records from the NEEM shallow firn/ice cores in northwest Greenland, *J. Geophys. Res.*, 116 (D6), D06108, doi: 10.1029/2010JD014311.
- Steen-Larsen, H. C., Masson-Delmotte, V., Hirabayashi, M., Winkler, R., Satow, K., Prié, F., Bayou, N., Brun, E., Cuffey, K. M., Dahl-Jensen, D., Dumont, M., Guillevic, M., Kipfstuhl, S., Landais, A., Popp, T., Risi, C., Steffen, K., Stenni, B. and Sveinbjörnsdóttir, A. E. (2014), What controls the isotopic composition of Greenland surface snow?, *Clim. Past*, 10 (1), 377–392, doi: 10.5194/cp-10-377-2014

- Steinhage, D., Kipfstuhl, S., Nixdorf, U., & Miller, H. (2013), Internal structure of the ice sheet between Kohnen station and Dome Fuji, Antarctica, revealed by airborne radio-echo sounding. *Annals of Glaciology*, 54(64), 163-167. doi:10.3189/2013AoG64A113
- Stenni, B., Scarchilli, C., Masson-Delmotte, V., Schlosser, E., Ciardini, V., Dreossi, G., Grigioni, P., Bonazza, M., Cagnati, A., Karlicek, D., Risi, C., Udisti, R., and Valt, M. (2016), Three-year monitoring of stable isotopes of precipitation at Concordia Station, East Antarctica, *The Cryosphere*, 10, 2415–2428, doi.org/10.5194/tc-10-2415-2016.
- Stenni, B., Curran, M. A. J., Abram, N. J., Orsi, A., Goursaud, S., Masson-Delmotte, V., et al. Neukom, R., Goosse, H., Divine, D., van Ommen, T., Steig, E. J., Dixon, D. A., Thomas, E. R., Bertler, N. A. N., Isaksson, E., Ekaykin, A., Werner, M., and Frezzotti, M. (2017). Antarctic climate variability on regional and continental scales over the last 2000 years, *Climate of the Past*, 13, 1609–1634, doi:10.5194/cp-13-1609-2017
- Talalay, P. (2016). "Mechanical Ice Drilling Technology". Springer, Singapore. isbn:978-981-10-0559-6. doi: 10.1007/978-981-10-0560-2.
- Thomas, E. R., van Wessem, J. M., Roberts, J., Isaksson, E., Schlosser, E., Fudge, T. J., Vallelonga, P., Medley, B., Lenaerts, J., Bertler, N., van den Broeke, M. R., Dixon, D. A., Frezzotti, M., Stenni, B., Curran, M., Ekaykin, A. A. (2017), Regional Antarctic snow accumulation over the past 1000 years. *Climate of the Past*, 13, 1491-1513, doi: 10.5194/cp-13-1491-2017
- Touzeau, A., Landais, A., Stenni, B., Uemura, R., Fukui, K., Fujita, S., Guilbaud, S., Ekaykin, A., Casado, M., Barkan, E., Luz, B., Magand, O., Teste, G., Le Meur, E., Baroni, M., Savarino, J., Bourgeois, I. and Risi, C. (2016), Acquisition of isotopic composition for surface snow in East Antarctica and the links to climatic parameters, *The Cryosphere*, 10 (2), 837–852, doi: 10.5194/tc-10-837-2016.
- Town, M. S., Warren, S. G., Walden, V. P., and Waddington, E. D. (2008). Effect of atmospheric water vapor on modification of stable isotopes in near-surface snow on ice sheets. *Journal of Geophysical Research*, 113, D24303, doi:10.1029/2008JD009852
- Traufetter, F., Oerter, H., Fischer, H., Weller, R., & Miller, H. (2004), Spatio-temporal variability in volcanic sulphate deposition over the past 2 kyr in snow pits and firn cores from Amundsenisen, Antarctica. *Journal of Glaciology*, 50(168), 137-146, doi:10.3189/172756504781830222

- Van den Broeke, M. R., & van Lipzig, N. P. M. (2003). Factors Controlling the Near-Surface Wind Field in Antarctica, *Monthly Weather Review*, 131(4), 733-743. doi.org/10.1175/1520-0493(2003)131
- Vaughn, B.H., J.W.C. White, M. Delmotte, M. Troler, O. Cattani, and M. Stievenard (1998), An Automated System for Hydrogen Isotope Analysis of Water, *Chem. Geol.* 152, 309.
- Weinhart, A. H., Freitag, J., Hörhold, M., Kipfstuhl, S., and Eisen, O. (2020), Representative surface snow density on the East Antarctic plateau. *The Cryosphere* 14, 3663–3685. doi:10.5194/tc-14-3663-2020
- Weißbach, S., Wegner, A., Opel, T., Oerter, H., Vinther, B. M., and Kipfstuhl, S. (2016), Spatial and temporal oxygen isotope variability in northern Greenland – implications for a new climate record over the past millennium, *Clim. Past*, 12, 171–188, doi.org/10.5194/cp-12-171-2016.
- Werner, M., Langebroek, P. M., Carlsen, T., Herold, M. and Lohmann, G. (2011), Stable water isotopes in the ECHAM5 general circulation model: Toward high-resolution isotope modeling on a global scale, *J. Geophys. Res. Atmos.*, 116, doi:10.1029/2011JD015681
- Whillans, I. (1975). Effect of Inversion Winds on Topographic Detail and Mass Balance on Inland Ice Sheets. *Journal of Glaciology*, 14(70), 85-90. doi:10.3189/S0022143000013423
- Whillans, I. M. and Grootes, P. M. (1985), Isotopic diffusion in cold snow and firn, *J. Geophys. Res.*, 90 (D2), 3910–3918, doi: 10.1029/JD090iD02p03910.
- Wiener, N. (1949). Extrapolation, interpolation, and smoothing of stationary time series. MIT press. isbn: 978-0-262-23002-5.
- Winski, D. A., Fudge, T. J., Ferris, D. G., Osterberg, E. C., Fegyveresi, J. M., Cole-Dai, J., Thundercloud, Z., Cox, T. S., Kreutz, K. J., Ortman, N., Buizert, C., Epifanio, J., Brook, E. J., Beaudette, R., Severinghaus, J., Sowers, T., Steig, E. J., Kahle, E. C., Jones, T. R., Morris, V., Aydin, M., Nicewonger, M. R., Casey, K. A., Alley, R. B., Waddington, E. D., Iverson, N. A., Dunbar, N. W., Bay, R. C., Souney, J. M., Sigl, M., McConnell, J. R. (2019), The SP19 chronology for the South Pole Ice Core – Part 1: volcanic matching and annual layer counting. *Climate of the Past*, 15(5), 1793—1808, doi: 10.5194/cp-15-1793-2019
- Wolff, E., Fischer, H., Fundel, F. et al. (2006), Southern Ocean sea-ice extent, productivity and iron flux over the past eight glacial cycles. *Nature* 440, 491–496, doi.org/10.1038/nature04614

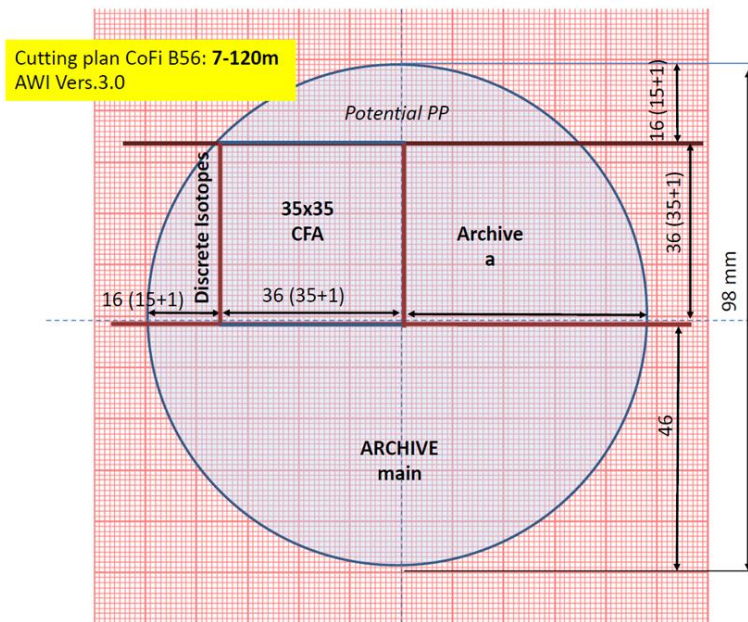
APPENDIX-A: SETUP OF THE CFA-SYSTEM FOR FIRN AND ICE CORES AT THE AWI



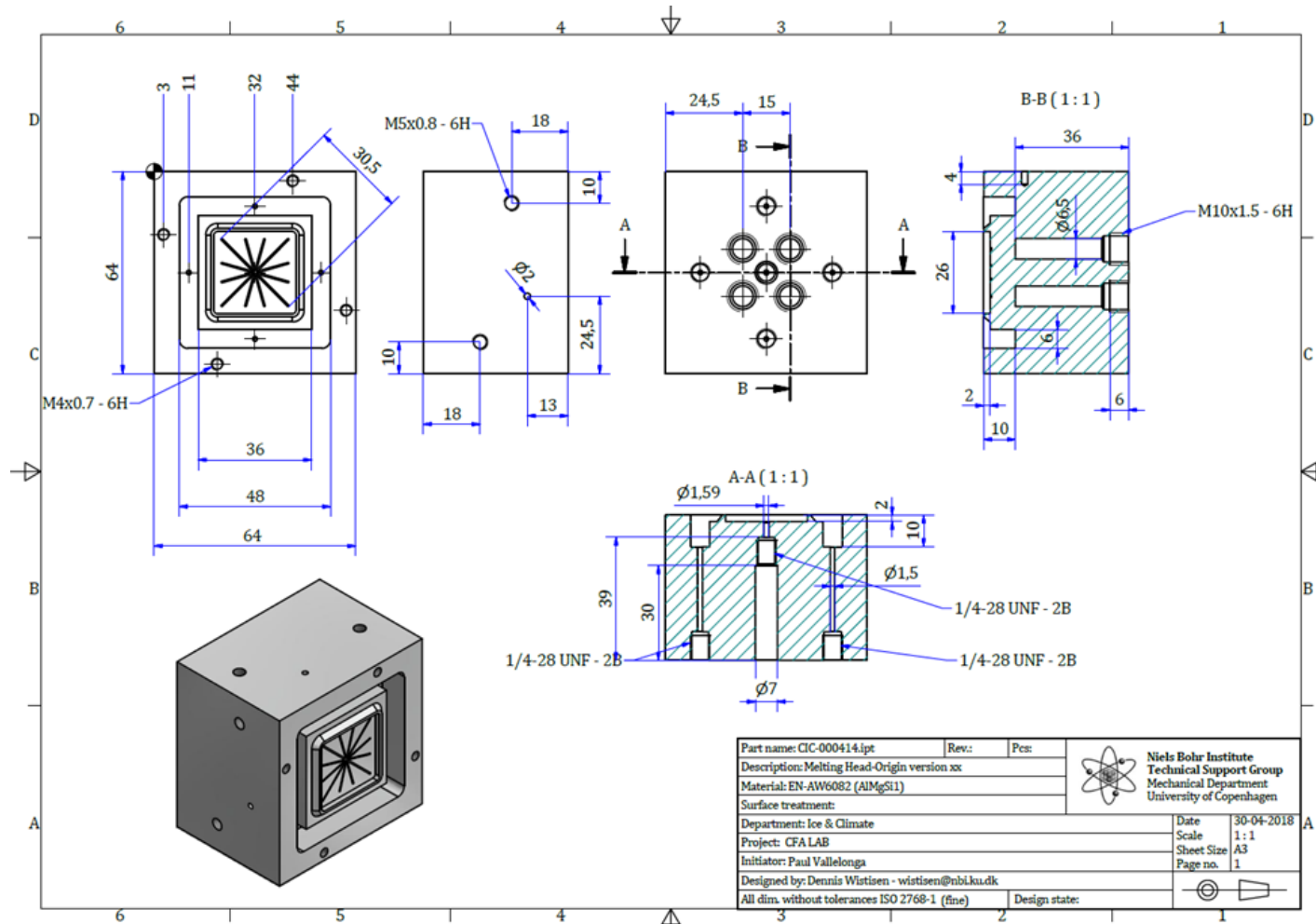
Flow chart of the AWI CFA-system as used for the analysis of firn core B56. The melt-speed is determined by a laser positioning sensor (PS). A weight is placed on the top of the snow core to stabilize the flow and reflect the laser beam. In the laboratory are the conductivity detectors for data synchronization (CC-i); an injection valve (Master IV) switching between MQ water and ice sample; a debubbling unit (DB); a manifold (MF); selection valves (SV) for analytical units switching between MQ, sample, and standards. In addition to the electrical conductivity, the various analytical units include a micro-particles detection unit, a water isotope mixing ratio unit (WI), and an inner-channel fraction collector. Liquid flow sensors (FM) monitor the good behavior of the system. Finally, detection of air bubbles takes place upstream (BD1) and downstream (BD2) of the DB. All flows values are expressed in ml/min.

APPENDIX-B: CUTTING PLAN OF A FIRN/ICE CORE

For comparative studies, cores must be cut lengthwise in several pieces according to a defined cutting-plan. Example of the cutting plan of the firm core B56, with parts for discrete isotope measurements, physical properties measurements, CFA measurements, and archive pieces separated and sealed.

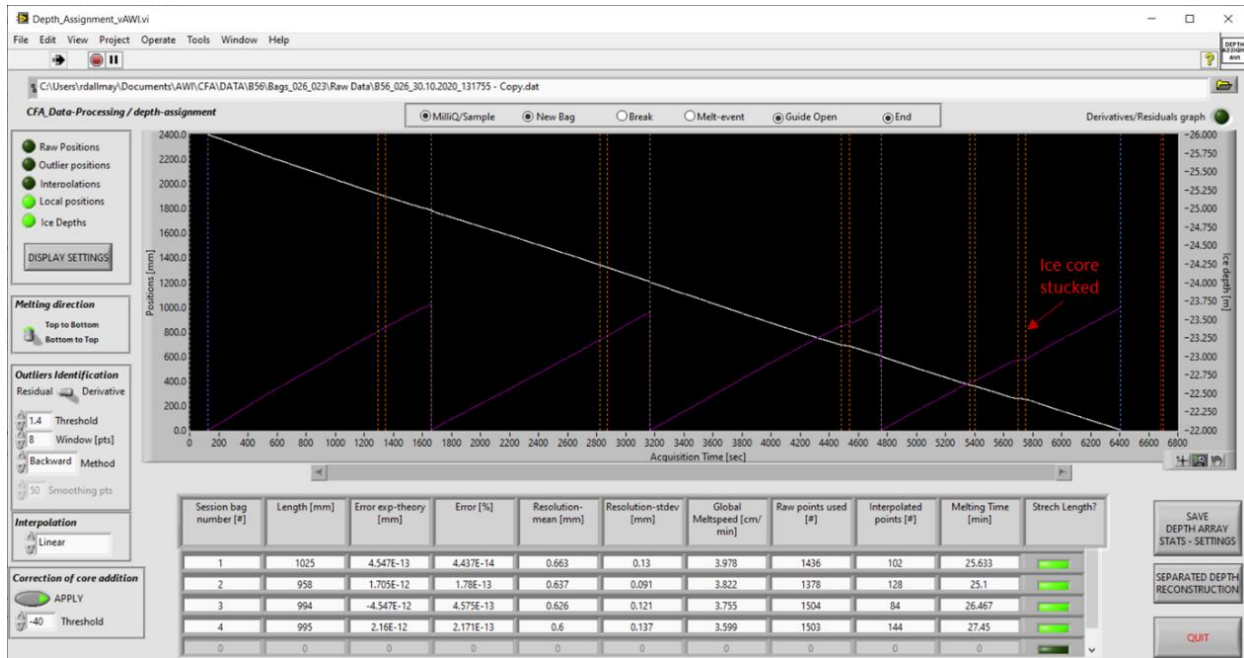


APPENDIX-C: MELT-HEAD FOR FIRN AND ICE CORE



Technical drawing of the Mel-Head developed at the Center for Physics of Ice, Climate and Earth (PICE), Niels Bohr Institute, University of Copenhagen

APPENDIX-D1: CFA-PROCESSING /DEPTH ASSIGNMENT

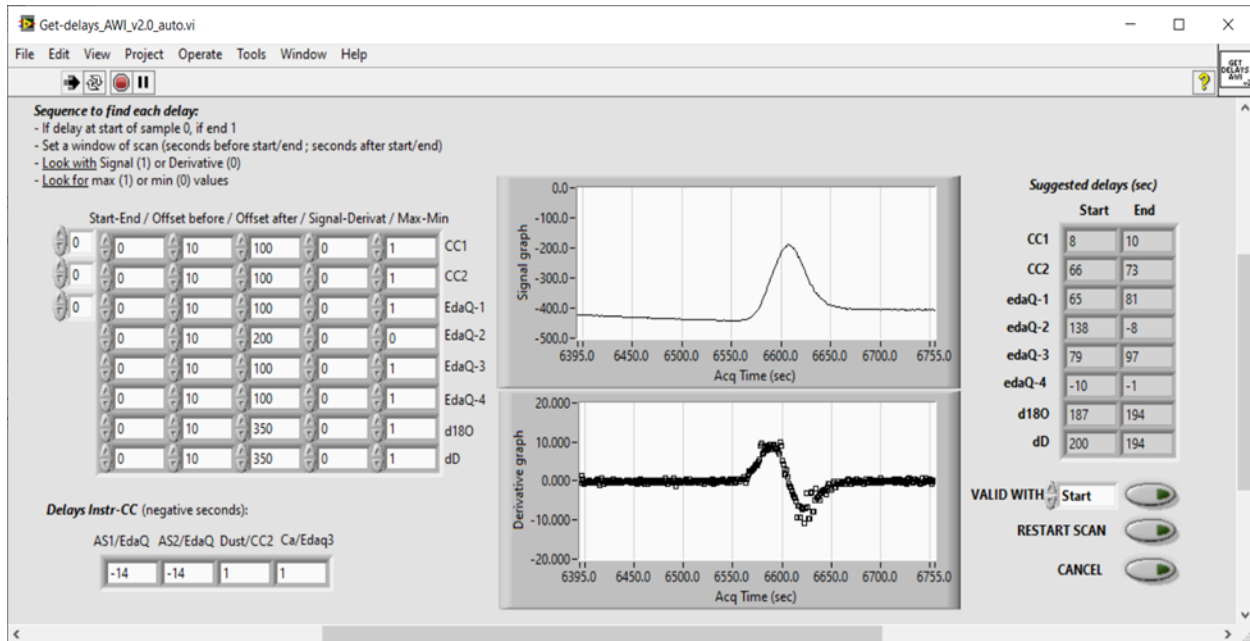


Screenshot of the depth-assignment routine with the example of the depths between 22-26 m. All vertical dashed lines show the recorded melting-events (blue: sample start-end, white; new core, orange: core-holder change of state, red: end of run). The purple line shows the reconstructed length of each core, and the white line the reconstructed depths along the run.

All settings (outlier identification window and method, type of interpolation, correction of added cores) can be tuned by the user. Statistics for each core reconstruction are indicated (theory-experiment error, resolution mean and standard-deviation, melting time and speed, proportion of interpolated points).

Once confirmed, all values, statistics, and settings are stored in the corresponding processing depth-assignment_output-file.

APPENDIX-D2: CFA-PROCESSING /DATASETS DELAYS



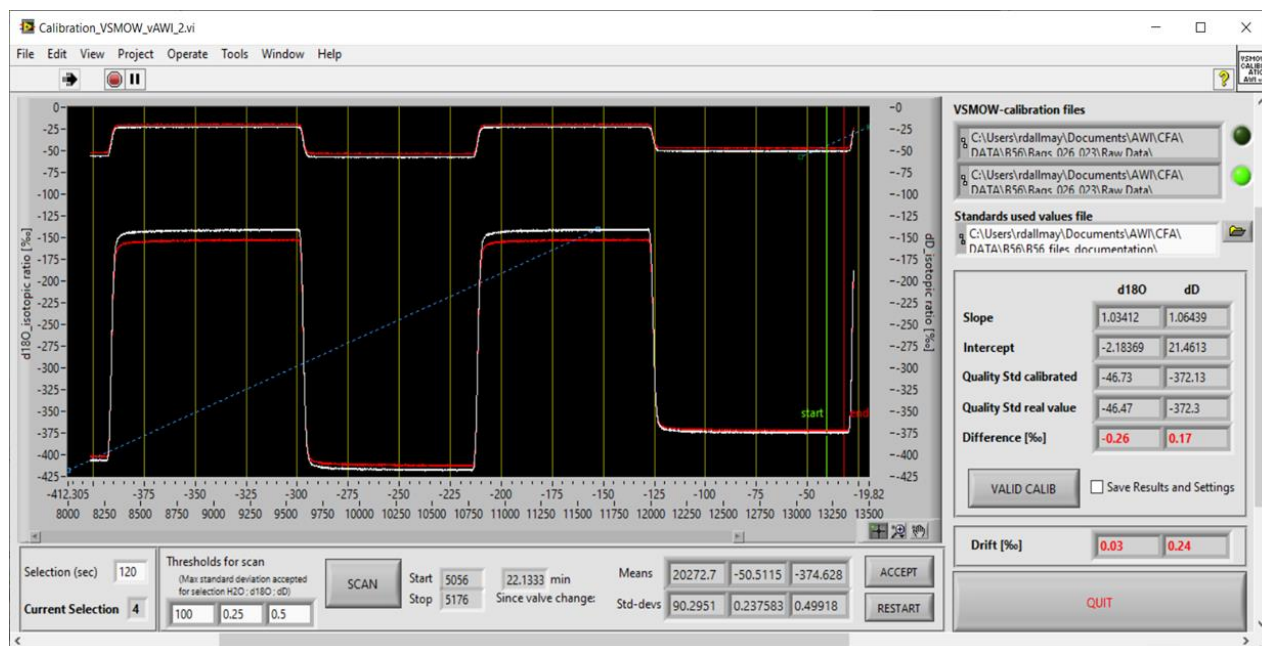
Screenshot of the get-delays routine (δD signal). For each signal the routine search for each delay at the start and end of the run. The user sets:

- (1) a window of acquisition-time to scan.
- (2) if the signal or its derivative is scanned.
- (3) if the scan searches a minimum or a maximum.

Once scanned, the routine suggests its computed delays. The user can choose if applying the delay from start, end, or a mean delay. The main processing software allows later for a visual optimization of the applied delays.

Once confirmed, all values and settings are stored in the corresponding processing_output-file.

APPENDIX-D3: AWI-CFA-PROCESSING /WATER-ISOTOPES CALIBRATION



Screenshot of the VSMOW-calibration routine, example with calibration after analysis of depths 22-26 m. A calibration run presents the high standard, low standard, high standard, and quality-check standard. White-lines are the raw data. The user sets:

(0) length of selection (120 s)

(1) the precision to scan for (i.e. selection with variabilities of (H_2O ; $\delta^{18}\text{O}$; δD) inferior to (100 ppm; 0.25 ‰; 0.5 ‰).

After 2 selection accepted, calibrated data are computed (red lines) and the user select the quality-check standard. Calibrated values are compared to true values to give the accuracy of the measurement. The values of quality-check standard of calibration before melting and after melting are compared and a drift-correction is applied to the calibration coefficients. Once confirmed, all values and settings are stored in the corresponding processing VSMOW_calibration_output-file.

APPENDIX-D4: AWI-CFA-PROCESSING /DATASET CLEANING

Clean_saved_datasets_2.0.vi

File Edit View Project Operate Tools Window Help

Melting Events Visual Cleaning

Clean saved data around melting events [cm] before - [cm] after ([0,0] = no cleaned data)

| | MQ-Sple event | | New-Bag event | | Breaks event | | other melting-events | | Column |
|-------------------------------|---------------|---|---------------|---|--------------|-----|----------------------|---|--------|
| Total counts [Counts / #1] | 5 | 3 | 4 | 2 | 3 | 1.5 | 0 | 0 | 10 |
| WI-H2O [ppm] | 0 | 0 | 0 | 0 | 0 | 0 | 0 | 0 | 11 |
| d18O [‰] | 5 | 2 | 0 | 0 | 0 | 0 | 0 | 0 | 12 |
| dD [‰] | 5 | 2 | 0 | 0 | 0 | 0 | 0 | 0 | 13 |
| Ca2+ [Voltage] | 5 | 3 | 5 | 2 | 3 | 1.5 | 0 | 0 | 14 |

Air in System
Clean data if bubbles are detected

MQ in System
Clean data if MasterValve is on MQ

Water-Isotopes
Clean data if H2O [ppm] level outside of range 17000 23000
Clean " [0,0] "

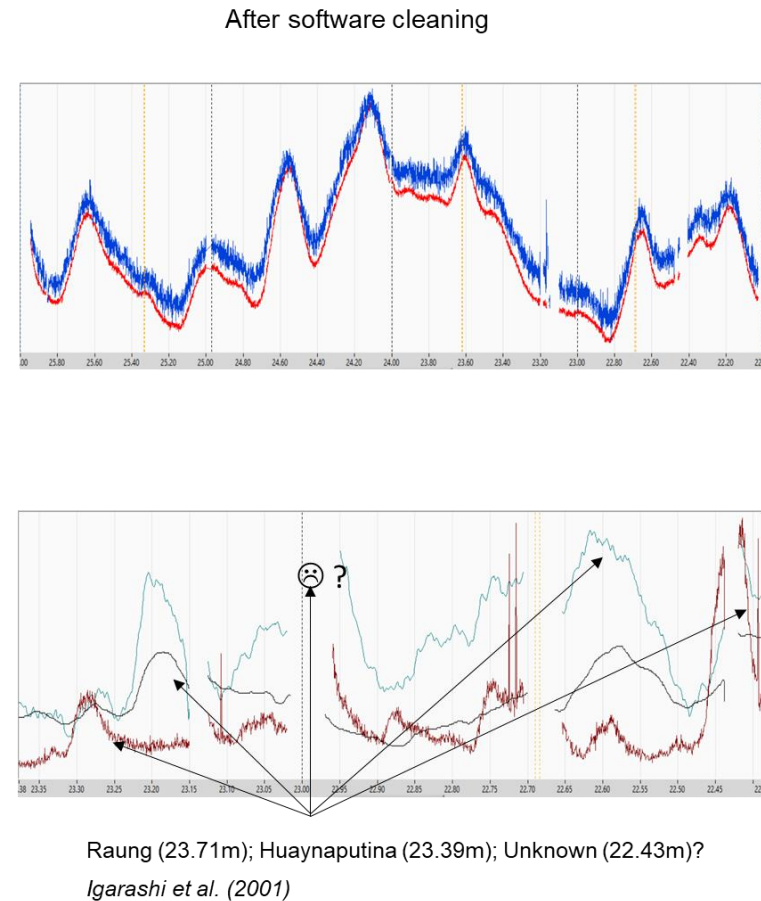
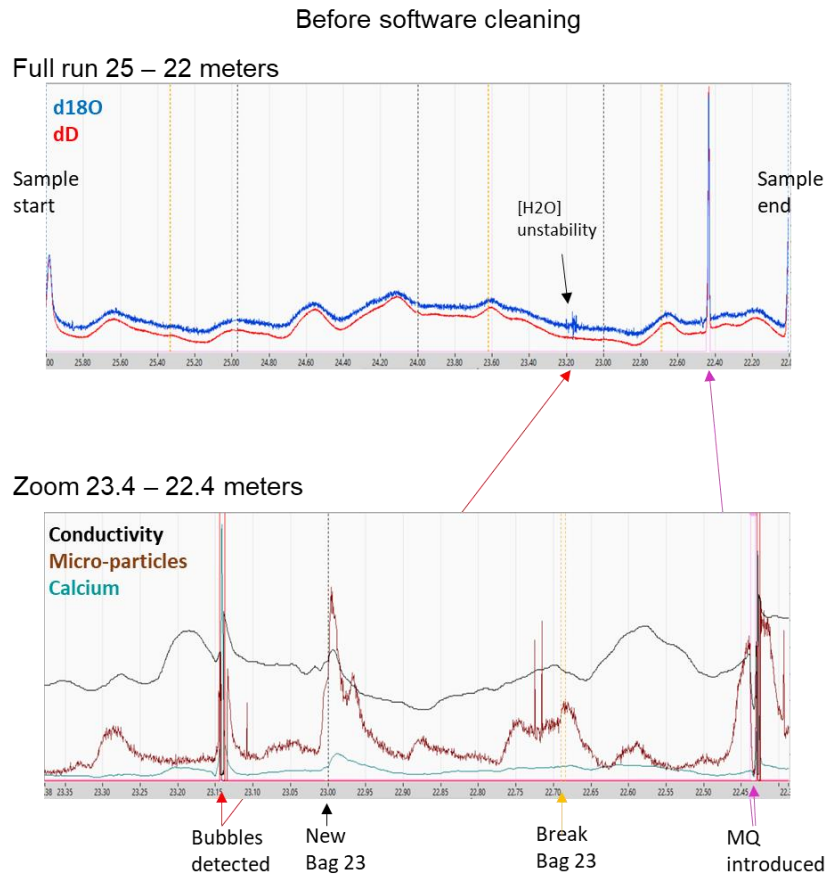
Dusts
Clean Abakus "wrong data "

CANCEL VALID

Screenshot of the Cleaning-datasets routine.

All cleaning setting parameters (for all datasets cleaning around melting-events; air-bubbles detection; MQ-introduced; specific cleaning for the water-isotopes and micro-particles datasets). Collected vials are flagged if potentially contaminated.

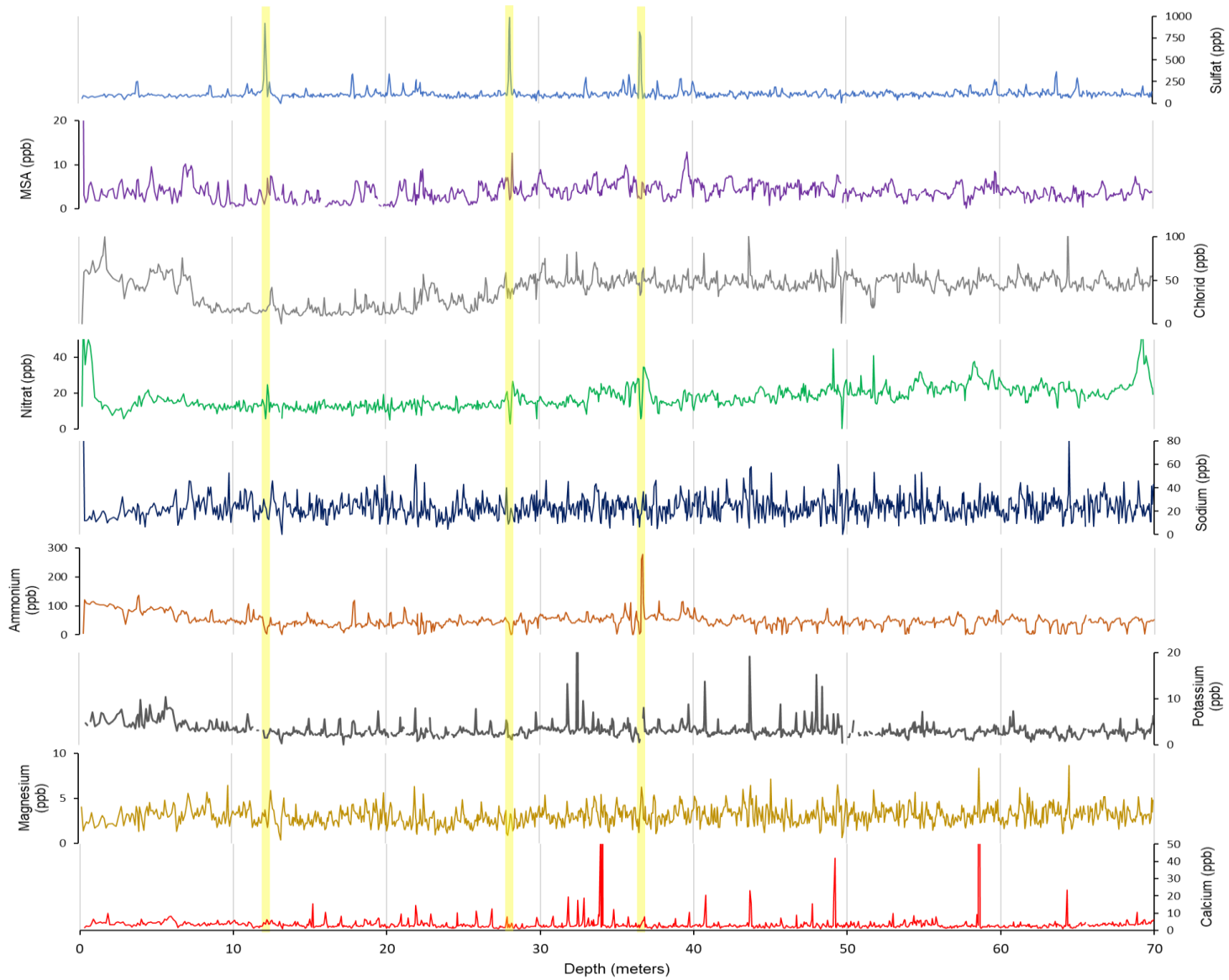
Once confirmed, all values and setting parameters are stored in the corresponding processing _output-file.



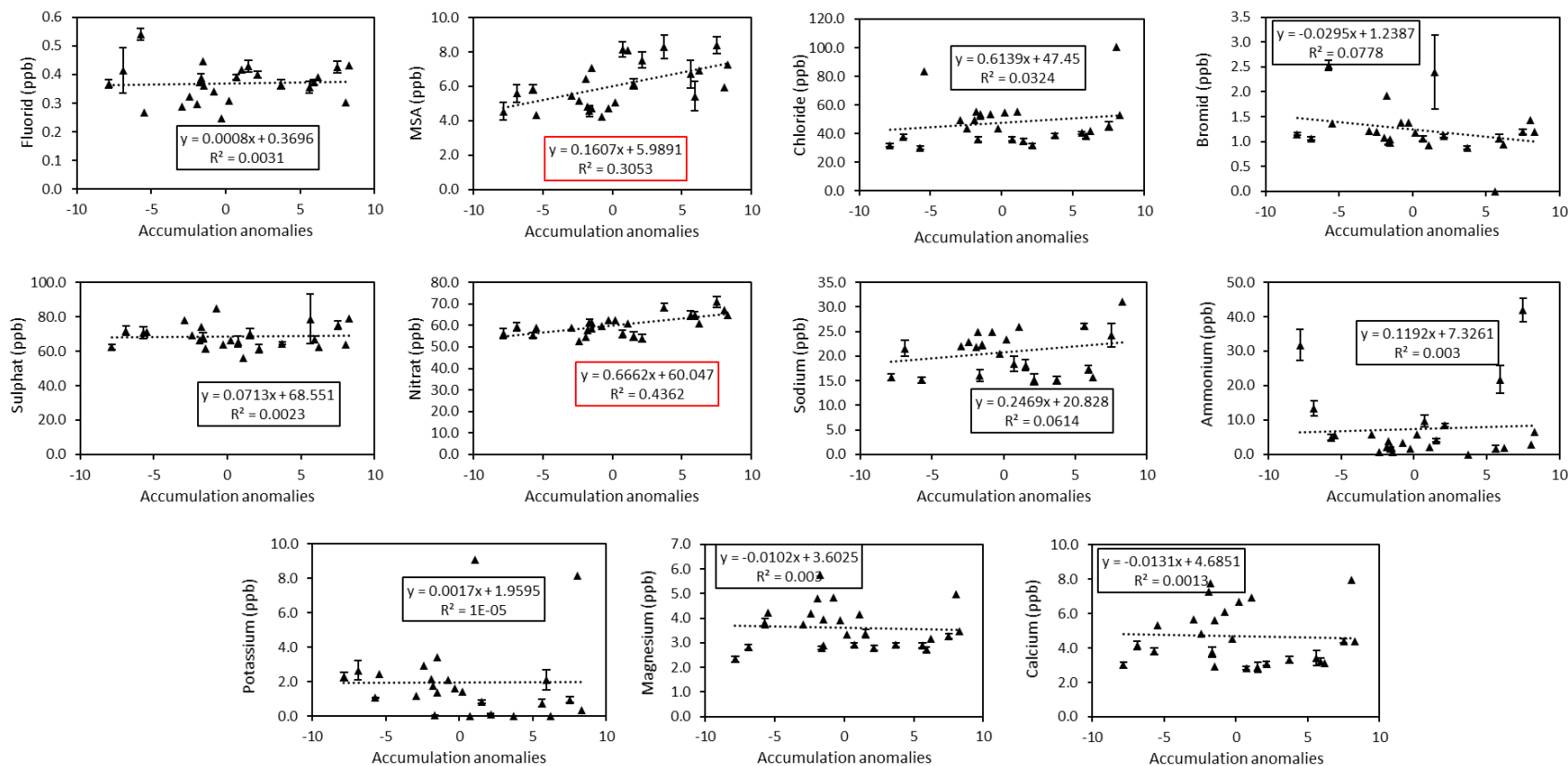
Screenshots of AWI-CFA-Processing software, run bags 026_023

Example of cleaning routine applied, showing the efficiency of the procedure and the potential danger of erasing volcanic records if located at boundaries (break in core, start of a core). It is thus recommended to generate both cleaned and non-cleaned processed datasets.

APPENDIX-E: IMPURITIES RECORDS ALONG THE B56 FIRN CORE

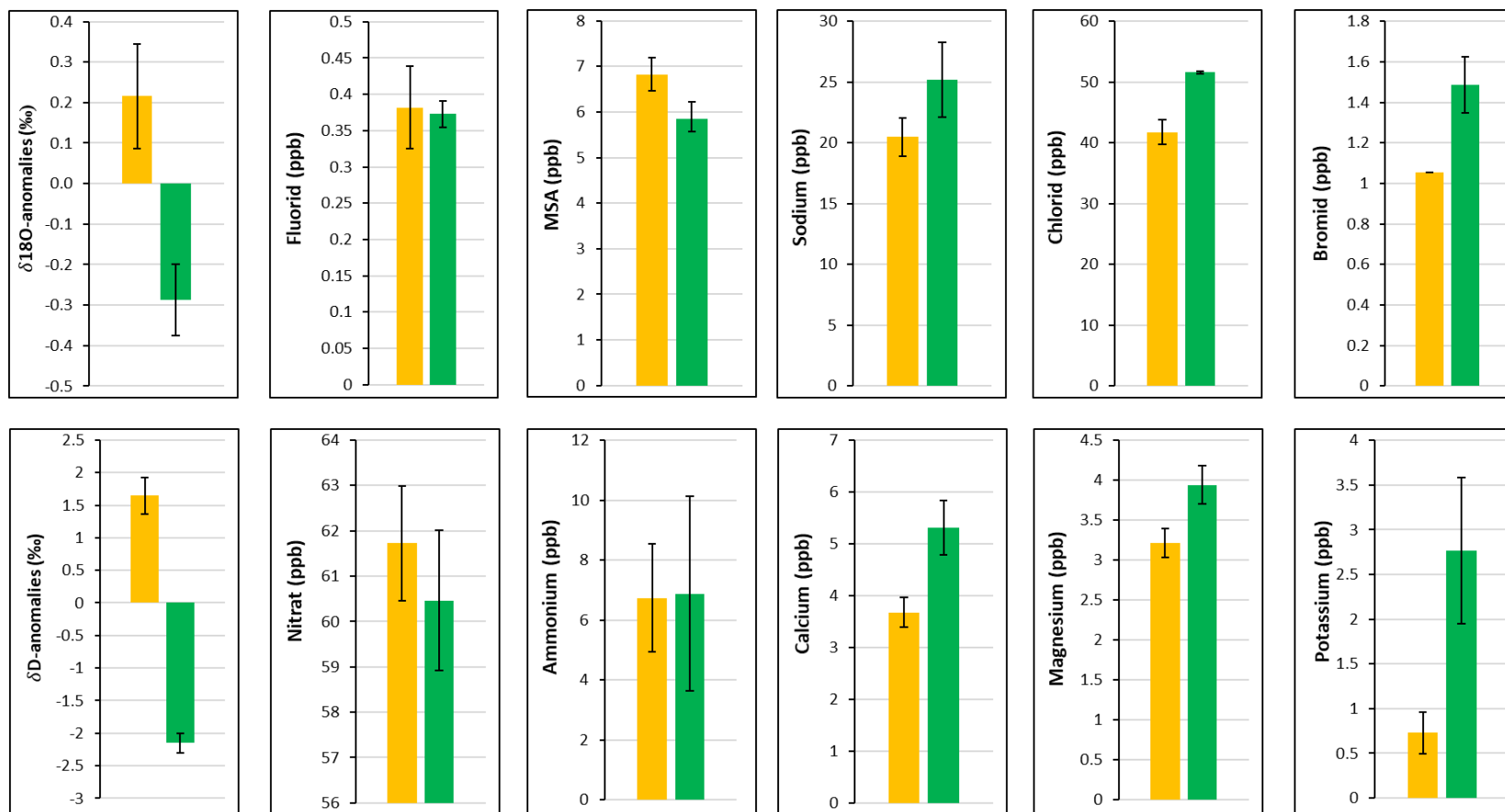


APPENDIX-F1: SPATIAL VARIABILITY OF IMPURITIES WITH RESPECT TO LOCAL ACCUMULATION RATE ALONG THE KOHNEN-QK TRAVERSE



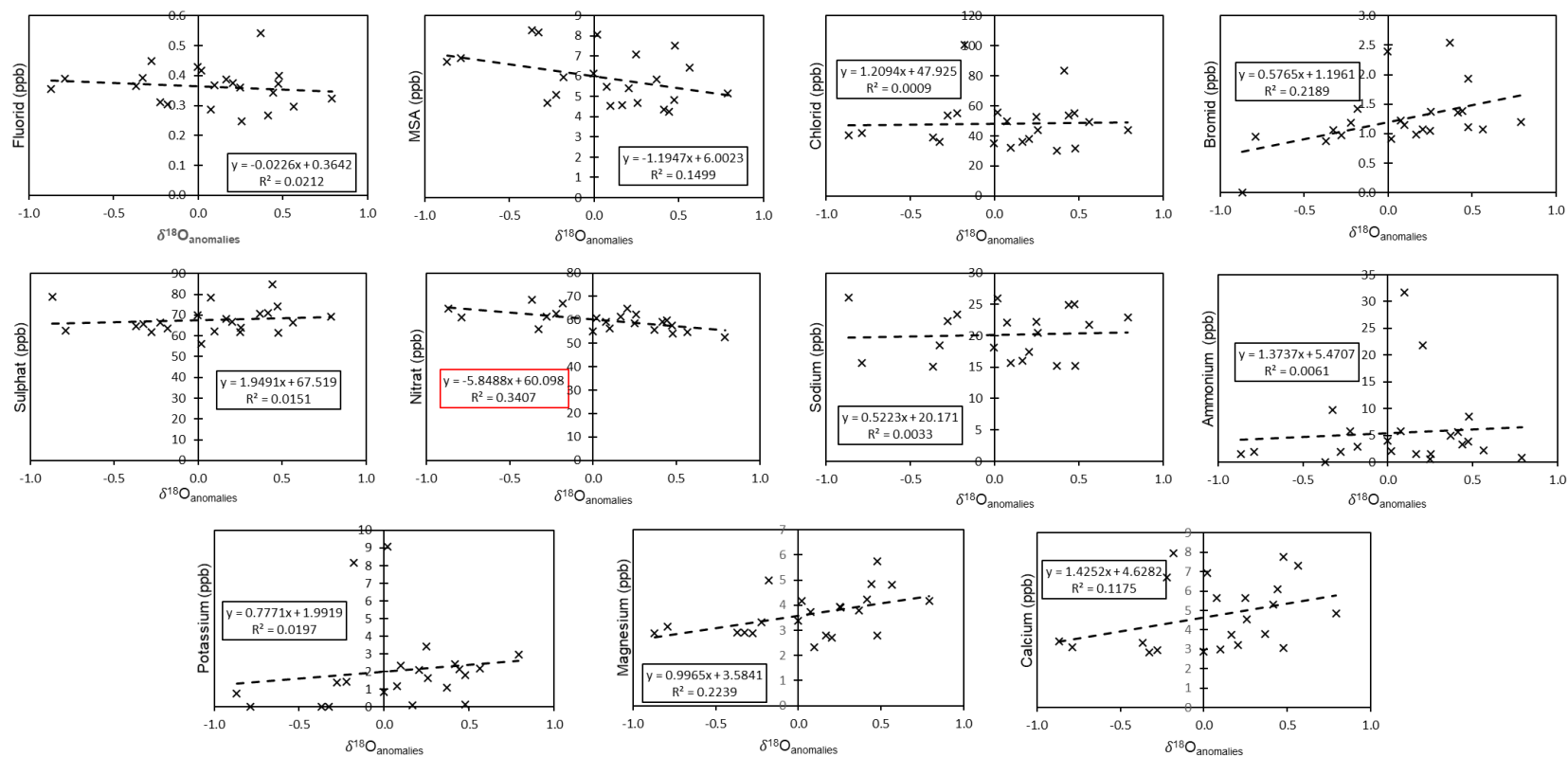
Regression analyzes of impurity concentrations versus accumulation rate anomalies. N=27 sites. Error-bars represent the 90 m spatial variability at single sampling sites (independent cores, dual-tubes technique). Similarly to Publication-II, the Accumulation anomalies are 100 m averages of the local accumulation rate at site (mean standard-error of 0.04) and are expressed in $\text{kg m}^{-2} \text{yr}^{-1}$.

APPENDIX-F2: SPATIAL VARIABILITY OF IMPURITIES THROUGH SITES-GROUP ALONG THE KOHNEN-QK TRAVERSE



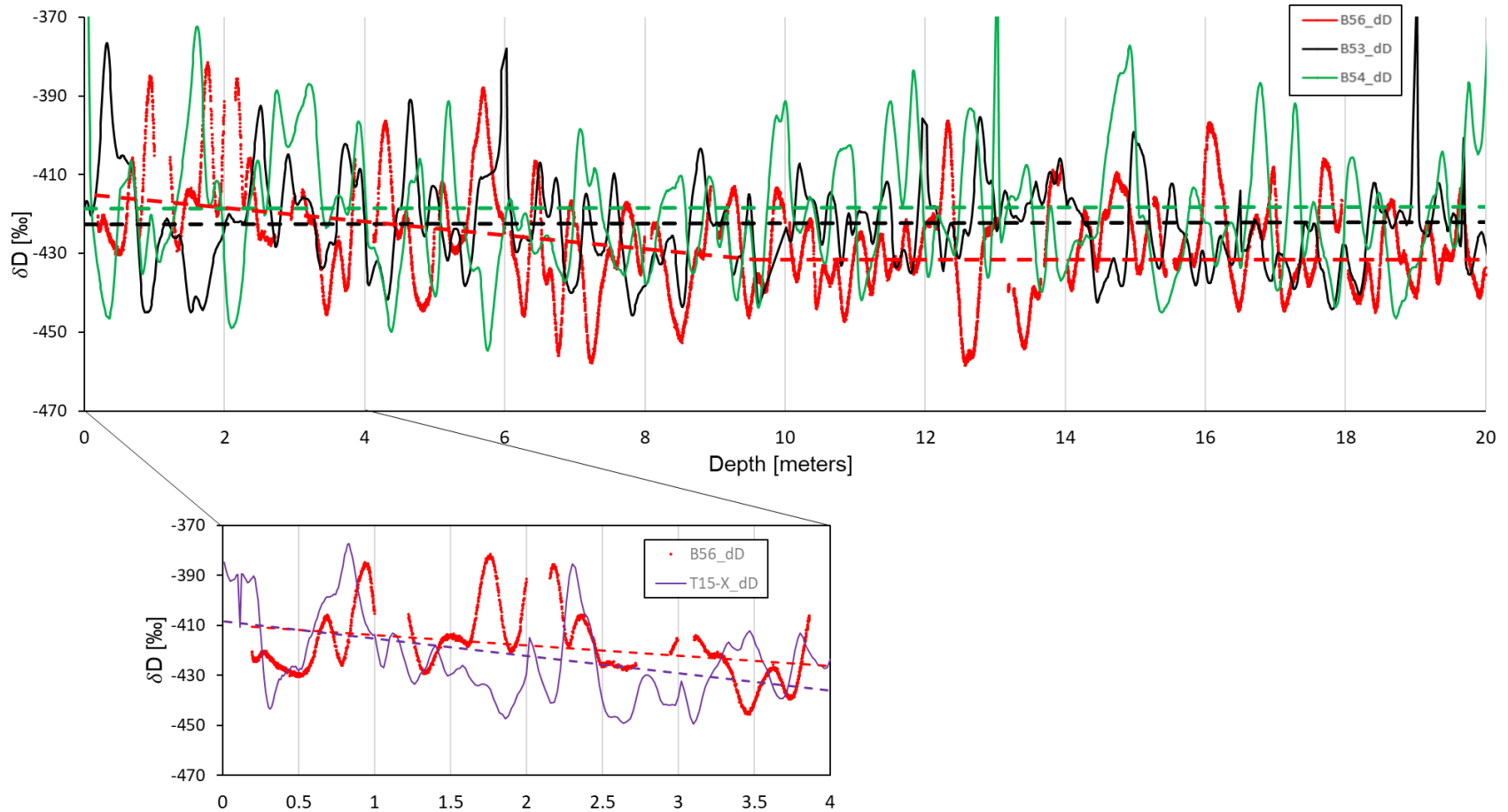
Impurities concentrations of site-groups with positive (green, 15 sites) or negative (orange, 12 sites) accumulation rate anomalies. The error-bars represent the standard error of the mean within each group.

APPENDIX-F3: IMPURITIES AGAINST $\delta^{18}\text{O}_{\text{anomalies}}$ ALONG THE KOHNEN-QK TRAVERSE



Regression analyzes of impurity concentrations versus isotopic composition anomalies (expressed in ‰). N=27 sites.


APPENDIX-G: TOP-20M PROFILES OF δD FOR FIRN CORES B56, B53, B54, AND TOP-4M LINER T15-X (AT B56)




(Top) Top 20-meter of δD records; cores B56, B53, and B54. The green, black, and red dashed lines shows the trends over depth-sections [20 to 10m], and [10 to 0m], respectively.

(Bottom) Top 4-meter of δD records; core B56 and the 4 m long liner T15-X. The red and purple dashed lines shows the trend over the 4-meter section.


APPENDIX-H: EGU21/PRESENTATION OF THE DUAL-TUBE SAMPLING TECHNIQUE




A dual-tube sampling technique for snowpack studies - Remi Dallmayr, J.F., M.H., T.L., J.L., F.W., D.D-L. - 28.04.2021




December 2018, near Kohnen-station (75.0°S, 0.1°E, 2892 m.a.s.l.) on the East-Antarctic plateau.
Scientists of the Alfred-Wegener Institut are collecting a maximum number of upper-meter samples...




Ok I finished the pit! Now we can take the 1-meter core out.
pfff I'm tired..




Tired of digging?!
Haha so you should use the new dual-tube sampling device!
Come and look!!





First, let's push the sampler down!



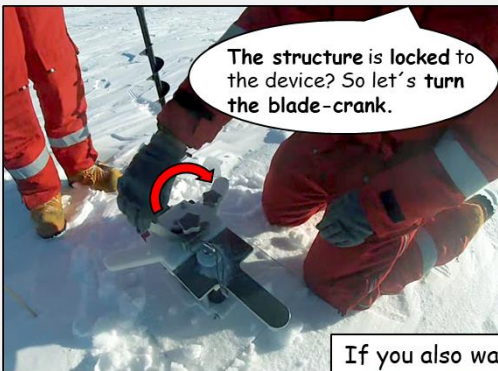
Is the cap covering the sampling-tube? So we can remove the snow in the second tube with the Auger.









Now we can insert the core-cutting structure, it has a 180° rotating blade at the bottom.



The structure is locked to the device? So let's turn the blade-crank.



We pull everything out and..



..Voilà!!
In few minutes, we have an exact 1-meter core, safely covered at its top and bottom. 😊

Great! But now how do you Collect the samples?
What about Contamination?
Are there Results?

If you also want to know more:
→ <https://doi.org/10.1017/jog.2020.85>
→ live presentation



Article

*Formerly Alfred-Wegener-Institut, Bremerhaven.

Cite this article: Dallmayr R, Freitag J, Hörhold M, Laepple T, Lemburg J, Della-Lunga D, Wilhelms F (2021). A dual-tube sampling technique for snowpack studies. *Journal of Glaciology* 67(261), 84–90. <https://doi.org/10.1017/jog.2020.85>

Received: 11 May 2020

Revised: 9 September 2020

Accepted: 10 September 2020

First published online: 9 October 2020

Key words:

Efficiency; isotopic composition and topography; sampling; snowpack

Author for correspondence:

Remi Dallmayr, E-mail: remi.dallmayr@awi.de

A dual-tube sampling technique for snowpack studies

Remi Dallmayr^{1,2}, Johannes Freitag¹ , Maria Hörhold¹ ,

Thomas Laepple^{3,4} , Johannes Lemburg¹ , Damiano Della-Lunga^{1,*}

and Frank Wilhelms^{1,2}

¹Alfred-Wegener-Institut Helmholtz-Zentrum für Polar- und Meeresforschung, Bremerhaven, Am Handelshafen 12, 27570 Bremerhaven, Germany; ²GZG Abt. Kristallographie, University of Göttingen, Göttingen, Germany;

³Alfred-Wegener-Institut Helmholtz-Zentrum für Polar- und Meeresforschung, Potsdam, Telegrafenberg A45, 14473 Potsdam, Germany and ⁴University of Bremen, MARUM – Center for Marine Environmental Sciences and Faculty of Geosciences, 28334 Bremen, Germany

Abstract

The validity of any glaciological paleo proxy used to interpret climate records is based on the level of understanding of their transfer from the atmosphere into the ice sheet and their recording in the snowpack. Large spatial noise in snow properties is observed, as the wind constantly redistributes the deposited snow at the surface routed by the local topography. To increase the signal-to-noise ratio and getting a representative estimate of snow properties with respect to the high spatial variability, a large number of snow profiles is needed. However, the classical way of obtaining profiles via snow-pits is time and energy-consuming, and thus unfavourable for large surface sampling programs. In response, we present a dual-tube technique to sample the upper metre of the snowpack at a variable depth resolution with high efficiency. The developed device is robust and avoids contact with the samples by exhibiting two tubes attached alongside each other in order to (1) contain the snow core sample and (2) to access the bottom of the sample, respectively. We demonstrate the performance of the technique through two case studies in East Antarctica where we analysed the variability of water isotopes at a 100 m and 5 km spatial scales.

Introduction

Polar ice sheets are considered a unique paleo-climatic archive spanning up to 800 ka before present (EPICA Community Members, 2004). They are most prominently used to analyse in situ greenhouse gas concentrations (Nakazawa and others, 1993), impurities (Gfeller and others, 2014) which are used as a proxy for atmospheric transport and biogeochemical activity and stable water isotopes which are used as a proxy for temperature (Jouzel and others, 1997). However, a reliable interpretation of all analysed records is based on a profound understanding of the mechanisms involved in the transfer of climatic signals from the atmosphere into the snowpack and their modification during the exposure of surface snow to the atmosphere. Among several (post-) depositional processes the re-distribution and erosion of snow by wind hampers the consecutive burial of the topmost snow layer, introducing stratigraphic noise into the time series of any proxy record used for paleo climate reconstruction (Fisher and others, 1985). However, firn- and ice core drill campaigns usually do not recover the uppermost metre(s), as the snow is soft and fragile hampering the handling and storage of the snow cores in the same manner as ice. Hand-corers enable the drilling of the first metres, but the irregular shapes and volume of the retrieved pieces are not suitable for comparative statistical studies of the spatial distribution of paleo proxies in snow. Dedicated sampling efforts to retrieve ambiguous snow samples have therefore been conducted in the recent past. First results have shown that sampling more than one profile, for example, a row of profiles such as a trench wall, substantially improves the signal-to-noise ratio of the proxy record (Laepple and others, 2016; Münch and others, 2016). The corresponding sampling campaigns used tubes made of carbon fibre which was pushed into the snow and subsequently excavated. We will hereafter refer to the application of these tubes (100 mm diameter, 1 mm thickness and 1 m length) as the liner technique, offering sampling an exact 1 m long high-quality cylinder of preserved snow. Nevertheless, digging each full-length tube out of the snowpack is exhausting and time-consuming, and thus extending such an attempt to larger spatial scales remains a logistical challenge. In addition, the amount of snow sampled with the liner technique is adapted for firn-densification studies by means of X-ray computer tomography (Freitag and others, 2004), but the amount of snow sampled can be significantly reduced for proxy measurement sampling of the snowpack. We upgraded the liner technique to propose the following dual-tube technique (Fig. 1) that meets the following requirements: (a) is fast and effortless, (b) mechanically simple, (c) collects a minimal but representative amount of snow with an accurate and reproducible depth/sampling interval and (d) obtains 1 m of snow with separation of its subsections at each location.

After describing the newly developed device and the associated sampling procedure, we present two applications related to the isotopic composition of the snowpack in Dronning



Fig. 1. Dual-tube sampler in action.

Maud Land on the East Antarctic plateau. This first small-scale study allows us to validate our device by comparing our stable water isotope variability measurements with similar results from published studies in the same area. As a second example, a 5 km transect delivers the results of a first large-scale application of the sampling device.

Description of the technique

Philosophy and challenges

Polar ice sheets are isolated areas with extreme conditions. In addition to the reliability and reproducibility of sampling an exact

amount of snow in a contamination-free way in such an extreme environment, the key points to a successful technique are convenience and simplicity of use, together with easy repairs. Based on this philosophy, we adapted and implemented the liner technique to a higher degree of efficiency:

- To avoid digging we attached alongside the sampling tube a second tube, where the snow is removed using a hand auger. Once emptied, the bottom of the sampling tube is accessible and a custom-designed core-cutting structure can be inserted to cut the bottom of the sample core, cover it and retrieve the core from the snowpack.
- With the aim of only collecting small sample amounts of dry snow zone, we conducted preliminary tests with different sampling tubes and determined as an optimal combination a 1 mm sharp edge with a minimum sampling diameter of 50 mm. Regarding the targeted analysis, only a fraction of the tube diameter is needed; however, using a smaller diameter would lead to compaction when pushing the tool into the dry snow. Therefore, the technique must also offer the ability of splitting the 1 m long core longitudinally before final collection of sample bags, in addition, to be able to precisely separate the subsections along the core axis.

Description of the implemented snow-sampling device

Sampler

We chose to use carbon fibre tubes (Carbon-Werke GmbH) as they have a low thickness/solidity ratio, are chemically inert and are lightweight. The sampler (see Fig. 2, panel A) features two tubes of 1.2 m length. One with a 50 mm diameter (hereafter referred to as the sampling tube) to contain the snow core sample and one with a 100 mm diameter (hereafter referred to as the auger tube) to insert the cutting structure. The diameter of the auger tube was chosen to fit the 90 mm diameter auger (conventional soil auger, Fig. 2, panel B). The two tubes are mounted in the body of the device at both the top of the device and at the snow surface level (e.g. the snow surface plate, Fig. 2, panel A). With

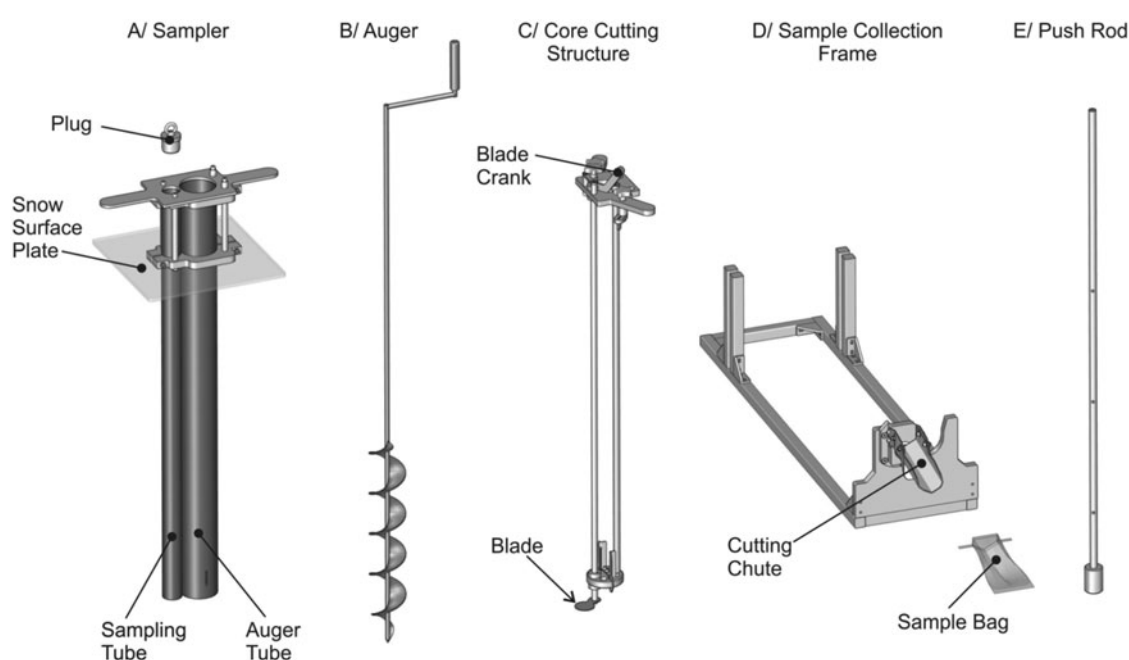


Fig. 2. All components of the sampling device in the order of use. Panel A: the core sampler body featuring handles, a snow surface plate and the two parallel tubes; panel B: the hand auger; panel C: the core cutting structure featuring the crank and blade; panel D: the sample collection frame featuring the V-shape cutting chute (with associated sampling bag); and panel E: the pushing rod, featuring 0.33 m depth intervals made for this study.

this set-up, the top 0.2 m of the tubes stays above the snow surface to maintain and ensure the vertical alongside alignment of both tubes and the remaining 1 m sits within the snowpack.

Core cutting structure

The cutting structure, which is as long as the tubes and designed to fit the diameter of the auger tube, features two parallel stainless steel mechanical shafts (see Fig. 2, panel C). At its top, the main shaft is connected to a 180° crank with a 50 mm diameter stainless steel circular blade at its bottom. To distribute the mechanical stress of torsion and maintain its position while cutting the snow via rotating the blade, the main shaft is connected at its top and bottom to a slightly smaller fixed rod. Finally, two fasteners to fix the structure to the sampler, in addition to a blade rotation locker.

Sample collection frame

A custom-built collection frame has also been developed (Fig. 2, panel D). Once the sampler is placed on the frame, the end of the sampling tube is connected to a cutting chute with a V-shaped stainless steel blade. The snow core is pushed out of the tube against the blade. At the end of the blade, sample bags can be mounted to catch the snow out of the tube. Only a fraction of the snow core is sampled into the bag, the rest falling to the ground during the splitting process. The height of the blade can be changed manually depending on the preferred amount of snow to be sampled.

Push rod

The stick used to push the snow core out of the tube is a 1.35 m long aluminium stick, with a 50 mm diameter and 100 mm long cylinder head. The push rod exhibits a series of holes along its length at defined intervals (0.33 m for our study) to accommodate end-stop pins if needed. Being wider than the tube, the push is paused at each pin for a precise sub-sampling of the 1 m long snow core.

Sampling procedure (Fig. 3)

- (1) The sampler (Fig. 2, panel A) is pushed into the snow vertically and straight, and the top of the sampling tube is covered with the plastic cap to prevent collecting surrounding snow.
- (2) The auger tube is emptied from snow (Fig. 2, panel B).
- (3) The core cutting structure (Fig. 2, panel C) is lowered into the empty auger tube until it reaches the bottom of both tubes, where it is aligned to the bolts of the sampler and locked by turning the fasteners.
- (4) The rotating blade turns below the sampling tube, cutting off the snow inside the tube from the snow below and closes the tube at the bottom. The rotating shaft is locked to disable any further motion. The whole device (tubes and cutting structure) can then be pulled out of the snow. Whereas the larger tube contains the cutter, the smaller tube is filled with the 1 m snow core that is held in place by the fixed circular blade at the bottom and covered by the cap at the top.
- (5) (a,b) The sampler is placed on the sample collection frame (Fig. 2, panel D), the cutting chute blade set for the desired amount of sample, and the desired length of snow is then pushed with the rod out of the sampling liner and into the corresponding sample bag. After each sampling interval, the filled sample bag is removed and closed, and a new sample bag is placed on the cutting chute.

Pushing the device into the snow and pulling out the 1 m core takes a few minutes. Sampling the snow into bags (three different

depth levels) takes an additional ~10 min. Altogether, collecting and then sampling the 1 m core into three subsamples takes <15 min. These timings depend on both the snow hardness and the weather conditions.

Applications of the sampling tool

Sampling sites and measurement methodology

Sampling campaigns were conducted during the austral summer 2018/19 field season near Kohnen station, Antarctica. Kohnen station is situated in the Atlantic sector of the East Antarctic Plateau (75.0°S, 0.1°E, 2892 m.a.s.l.) and has an annual mean temperature of -41 °C and an annual accumulation rate of 75 mm w.e.a⁻¹ (Wesche and others, 2016). In previous years, firn cores were drilled and several snow trench studies were conducted near the station (see Fig. 4). Analysing the water isotope variations in several 50 m long and 1–3 m deep trenches, it was shown that stratigraphic noise in water isotopes (Münch and others, 2016) and density (Laepple and others, 2016) in this region has a horizontal decorrelation scale of <10 m. However, given the limited spatial extent of the trenches, it was unclear if additional isotopic variations exist over larger spatial scales, for example, on the kilometre scale. As a first test and application of the dual-tube device, we thus performed two sampling campaigns; a series of cores along a 100 m transect with a 0.33 m depth resolution to create a dataset comparable to the existing trench studies and a 5 km long transect with a 1 m depth resolution to study the variability between the 100 m and the kilometre scales. Samples in both datasets were collected along a straight line from NW to SE (Fig. 4).

After collection, all samples were kept frozen at Kohnen station, as well as during their shipment back to the Alfred-Wegener-Institut Helmholtz-Zentrum für Polar-und Meeresforschung (AWI) in Bremerhaven, Germany, for their measurement of stable water isotopes ($\delta^{18}\text{O}$, δD). The stable water isotopes ratios were measured by means of cavity ring-down spectroscopy (I2130-i, Picarro Inc.) and calibrated to the international VSMOW/VSLAP scale. The procedure of Schaller and others (2016) was used and single measurements are provided with an accuracy of 0.1 per mil for $\delta^{18}\text{O}$ and 1.5 per mil for δD .

Small-scale 100 m study, technique validation

We first performed a 100 m scale study to test and validate our sampling tool against previous trench data. Near the B52 drilling site (74.9327°S, 0.4313°E) nine 1 m long snow cores were taken every 10 m. In order to demonstrate and validate our sampling device, we compared the spatial variability of this dataset (hereafter ST-B52) with the four trench datasets of similar spatial scale published by Münch and others (2017). For both $\delta^{18}\text{O}$ and δD isotopes, all datasets were averaged over a 1 m depth interval and we calculated each spatial standard deviation (SD) added to its 90% confidence intervals to ensure unbiased estimation of each variability (Bonett, 2006; Pishro-Nik, 2014, section 8.3.3). The results (Table 1) show considerable variations in the mean values of the different 1 m samples, thus demonstrating the role of stratigraphic noise even on large samples. The resulting $\delta^{18}\text{O}$ variability (SD = 0.7‰, 90% CI 0.5‰–1.1‰) from the new samples is fully consistent with the earlier trench studies undertaken in the same region.

Our dataset further allows an investigation into the number of profiles needed to obtain a robust estimate for the mean isotopic value of the area. Assuming independent samples, the standard

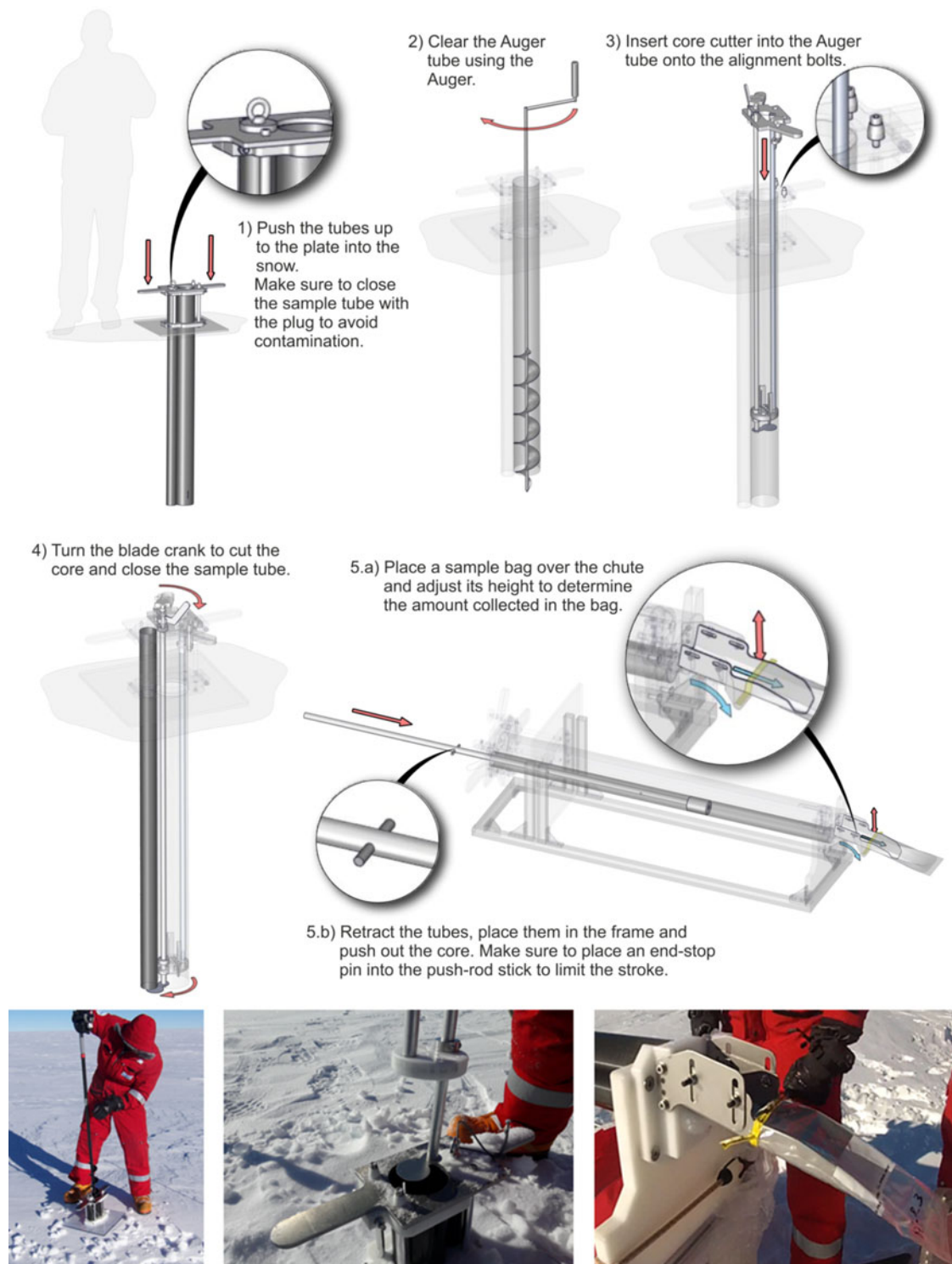


Fig. 3. Top: schematic of the sampling procedure. Bottom: photos corresponding to steps (2), (3), (5).

error of the mean is defined as:

$$\text{Standard error of the mean} = \frac{\sigma_0}{\sqrt{N}} \quad (1)$$

where σ_0 is the standard deviation of the area observed and N is the number of samples included. In our case, the 10 m distance is beyond the decorrelation length of the stratigraphic noise and thus we can assume independence. The required number of profiles depends on the sampling depth and the required accuracy (Fig. 5). For example, to obtain an accuracy (1SD) of 0.28 ‰

for $\delta^{18}\text{O}$, six 1 m profiles would have to be stacked. Obtaining the same 1SD level of accuracy for $\delta^{18}\text{O}$ by sampling only the first 0.67 m requires 15 samples or 21 samples for only the first 0.33 m. The results thus confirm the intuitive result that longer and thus larger snow samples result in less variability.

Kilometre scale study

To study the isotopic variability on the hundred metre to kilometre scale, we performed a sampling transect from trench T19 until the firn core drilling site B49 (Fig. 4, 75.04600° S,

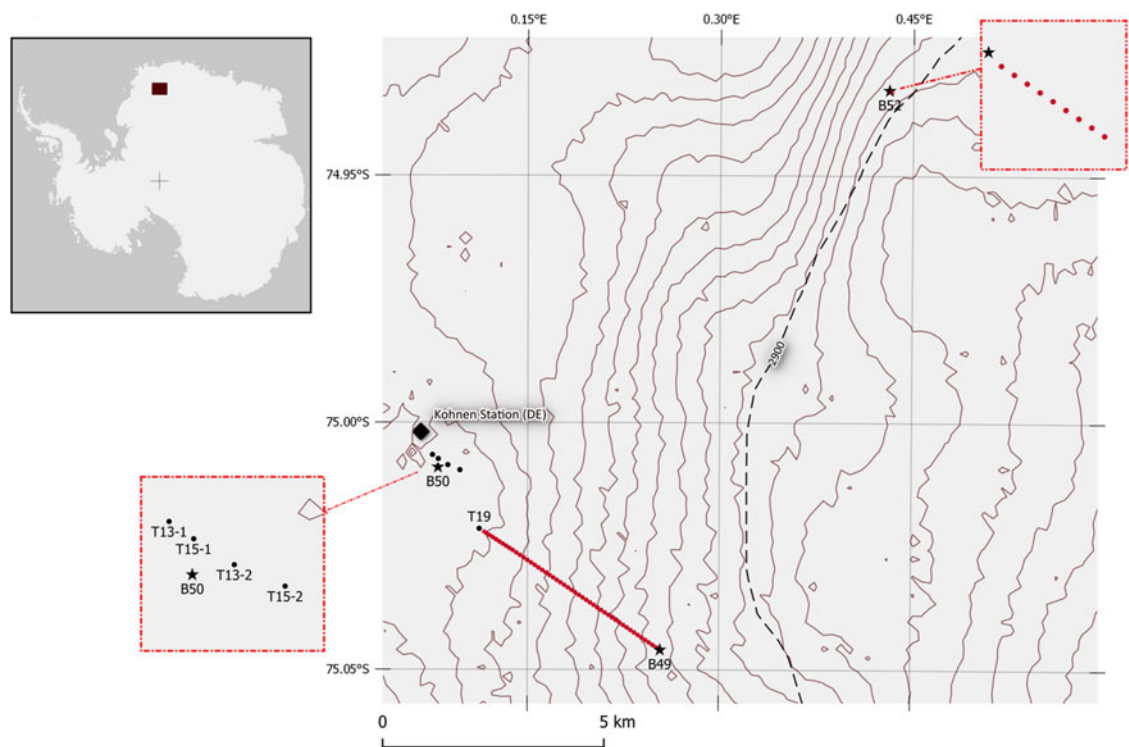


Fig. 4. Study area around Kohnen station, Dronning Maud Land. The 1 m elevation lines show the local topography of the area (The Reference Elevation Model of Antarctica, Howat et al., 2019, hereafter REMA). The sampling sites are indicated with red dots for both the 5 km long transect and the transect near the B52 drilling site (top-right detailed overview). Trenches T13-1 and T13-2 were excavated during the 2012/13 season and trenches T15-1 and T15-2 were excavated during the 2014/15 season (Münch and others 2017) and are shown in the bottom-left overview. The firn core drilling sites are marked by black stars.

Table 1. Comparison of variability on the 100 m scale observed with the sampling tool and published trench records (Münch and others, 2017)

| Dataset | ST-B52 (this study) | T13-1 | T13-2 | T15-1 | T15-2 |
|-------------------------------------|---------------------|---------------|----------------|----------------|----------------|
| Number of profiles | 9 | 38 | 4 | 11 | 11 |
| Profile distance (m) | 10 | ~0.1–2.5 | 10, 20 | 5 | 5 |
| SD $\delta^{18}\text{O}$, 90% (CI) | 0.7 (0.5–1.1) | 0.8 (0.7–1.0) | 0.6 (0.4–1.4) | 1.0 (0.8–1.6) | 1.0 (0.8–1.6) |
| SD δD , 90% (CI) | 5.4 (3.9–8.8) | 6.3 (5.3–7.8) | 4.2 (2.7–10.0) | 8.3 (6.2–12.8) | 7.6 (5.7–11.8) |

For all datasets, the number of profiles included and their adjacent sampling distance are indicated ($\delta^{18}\text{O}$, δD). The standard deviations (SD) and their 90% confidence interval (CI) were calculated using the chi-squared distribution and are expressed in per mil (‰).

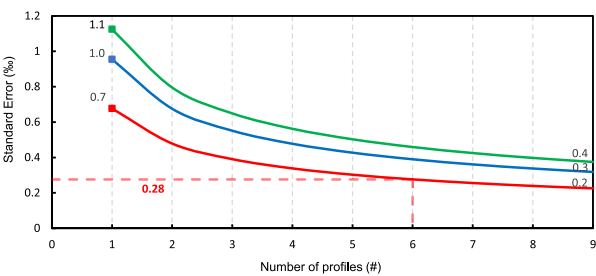


Fig. 5. Standard error of the mean for the top 0.33 m (green line), top 0.67 m (blue line) and top 1.0 m (red line) of the snowpack versus the number of profiles used (N) for $\delta^{18}\text{O}$. For each section of the top meter, the initial and final standard errors values are displayed.

0.25396° E). During this study, two 1 m long snow cores were taken 10 m apart from each other, every 100 m. The REMA high-resolution elevation model reveals a net elevation difference of 8 m between the two sites, 5 km apart. Furthermore, comparing the snow depth of volcanic signals in two firn cores B50 (close to Kohnen) and B49 revealed a 10–15% difference in the accumulation rate (Master thesis Alexandra Zuhr, table 4.3, not published) between the two sites.

The sampling transect revealed a small but statistically significant ($p < 0.05$) trend from trench T19 to site B49 with an increase in the isotopic composition of $\sim +0.5$ ‰ for $\delta^{18}\text{O}$ (i.e. trend of $+0.1$ ‰ km^{-1}) when increasing elevation and decreasing accumulation rate (Fig. 6a). As expected from the small-scale variability observed in the 100 m sampling study, this trend is overlaid by strong sample-to-sample variation. We thus average over multiple samples to reduce this stratigraphic noise. Indeed, when averaging over six samples, on a 300 m scale (Fig. 6b) the noise is reduced and reveals a stronger linear trend in $\delta^{18}\text{O}$ ($R^2 = 0.632$), supporting this correlation.

Discussion

We present a new device that allows for fast and highly efficient sampling of the snow surface with a well-defined depth assignment while minimizing possible contamination. We further present two applications studying the variability of water isotopes on different spatial scales. They demonstrate that our device not only allows for the study of stratigraphic noise at the local (metre) scale but also the investigation of the interplay among local topography, changes in elevation and accumulation at the kilometre scale. Initial results of the kilometre scale study indicate that both increasing elevation and decreasing accumulation may

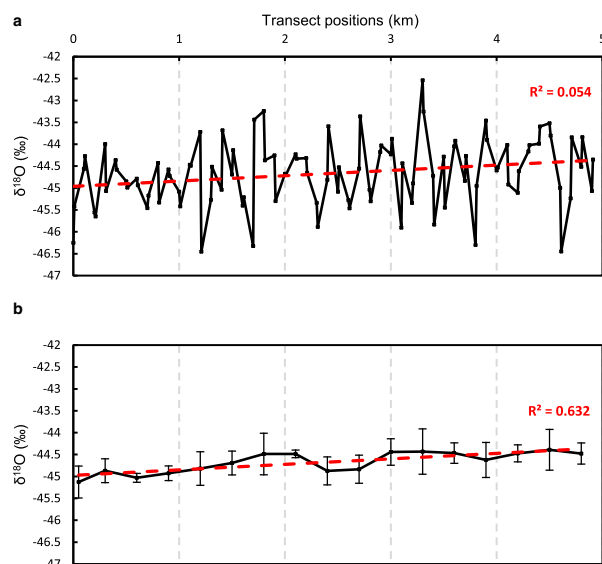


Fig. 6. Evolution of the $\delta^{18}\text{O}$ isotopic composition in the top meter of the snowpack along the 5 km transect. The black points show (a) the raw data of the transect (two profiles every 100 m) and (b) the 300 m averaged results, with error bars representing one standard error of the spatial averaging. The best linear fit is shown as a dashed red line.

lead to an enrichment in stable water isotopic composition, confirming specific effects of local post-depositional alteration of the initial isotopic composition of the snow (Ekaykin and others, 2002, 2016).

The presented device performed very well in the first field application in Antarctica; however, experience gained during the field season also suggest limitations and possible technical improvements.

- The 1 mm wall thickness of the tubes appears to limit the smoothness of pushing down the sampler into the snowpack when hard layers are encountered. Consequently, the effectivity of the device depends highly on the snow condition. Moreover, during the field season, several auger tubes were destroyed due to the repeated use of the auger. To improve this issue, we propose the use of thinner tubes (≤ 0.5 mm wall thickness) made of stainless steel; to compensate for the recognizable addition of weight we suggest using a 50 mm diameter hand auger (Kovacs Ice Drilling Equipment) to greatly reduce the diameter of the auger tube.
- Pushing the core out of the sampling tube compresses the snow core, which is problematic when sampling is conducted at a high resolution. We also observed that the tubes absorb incoming solar radiation, leading to a melting and refreezing of the snow core inside, which worsens the snow compression, as it takes more force to push the core out. Using a larger sampling tube combined with shadowing from direct sunlight will improve the issue.
- Modifying the sampler and allow for exchanging the sampling tube in a quick-connect way will permit to ship full tubes to laboratories for detailed analysis. Larger sampling tubes (e.g. 100 mm diameter) would ease firn-densification process studies (Freitag and others, 2013). However, using a sampling tube of such size requires an auger tube with a minimum diameter of 100 mm. In this case, to optimize the total weight of the device, a carbon fibre sampling tube can be combined with a stainless steel auger tube.
- The sampling technique can be extended down to a depth of 2 m simply by adapting the length of the different components. However, sampling further down (e.g. 4–5 m deep) without changing the approach requires the device to be

extendable, for example, through several 1 m extensions of the sampler, the core cutting structure and the auger. After each depth increment, the next extension is added with a quick and solid connection system, such as bayonet couplings. Ensuring a straight vertical alignment for sampling can be fostered by implementing a spirit level on the device's plate. Finally, a winch-system at the surface could ease both the removal of deep snow out of auger tube and the core extraction out of the snowpack.

Conclusion

We presented a new dual-tube sampling technique that allows for efficient sampling of the topmost metre of the snowpack with a variable depth resolution. In addition to demonstrating the device's merit in characterizing stratigraphic noise on the sub 100 m spatial scale, we successfully applied the described technique to document the potential effect of local topography on water isotopic composition. The present work focused on the composition of stable water isotopes, but the sampling device exhibits the advantage of noncontact sampling, which is essential for contamination-prone chemical investigations. Adding extension units to our new device in order to sample the snowpack down to 5 m will possibly replace the excavation of trenches, thus avoiding excavation machines and their exhaust fumes. Thus, this new sampling technique is ideal for extensive sampling missions such as surface traverses and will actively benefit the glaciological community through the provision of laterally highly resolved profiles with many sample positions to improve the quality of snowpack characterization. Initially designed for climatological purposes on the East Antarctica plateau snowpack, this technique can be adapted to a variety of snowpack research.

Data. The isotopic datasets of the both small and kilometre scale transects presented in this study are archived at the PANGAEA database, under <https://doi.pangaea.de/10.1594/PANGAEA.921928> and <https://doi.pangaea.de/10.1594/PANGAEA.921930>, respectively. PANGAEA is hosted by the Alfred Wegener Institute Helmholtz Centre for Polar and Marine Research (AWI), Bremerhaven, and the Center for Marine Environmental Sciences (MARUM), Bremen, Germany.

The technical drawings of all the components of the dual-tube sampling device and their assembly are available at the digital library Zenodo, under <https://doi.org/10.5281/zenodo.4001469>.

Acknowledgements. We thank all the scientists, technicians and logistic support who worked at Kohnen station during the austral 2018/19 summer, especially Klaus Trimborn for his resourcefulness, warm company and skilfulness. We also thank Jan Tell for initial investigations addressing the optimal tube combination. In the name of Matthias Littmann, we gratefully acknowledge the AWI-workshop for the successful realization of the complete sampling device. We further thank Melanie Behrens and York Schlomann for conducting the isotopic measurements in Bremerhaven. This project was supported by Helmholtz funding through the Polar Regions and Coasts in the Changing Earth System (PACES) programme of the Alfred Wegener Institute. TL was supported by the European Research Council (ERC) under the European Union's Horizon 2020 Research and Innovation Programme (grant agreement no. 716092). We gratefully acknowledge the work of three anonymous reviewers and the editor, Alec Van Herwijnen.

Author contributions. JF actively contributed to this work by participating in the design of the technique, the fieldwork, regularly discussed preliminary results and provided guidance to the first author. In addition to motivating and enabling the device development, TL suggested relevant insights, comments and statistical calculus for this manuscript. Via AWT's technical services, JL contributed to the device realization and provided the technical illustrations for the manuscript. MH participated during different stages of the study (philosophy, fieldwork, paper preparation). DDL helped with sampling the presented datasets. FW contributed to the results and discussion sections and edited the language of the paper. RD designed and coordinated the realization

of the sampling device, led its use in the field, analysed the results and prepared this manuscript. The manuscript has been reviewed by all co-authors.

References

- Bonett D** (2006) Approximate confidence interval for standard deviation of nonnormal distributions. *Computational Statistics & Data Analysis* **50**(3), 775–782. doi:[10.1016/j.csda.2004.10.003](https://doi.org/10.1016/j.csda.2004.10.003)
- Ekaykin A and 6 others** (2016) Non-climatic signal in ice core records: lessons from Antarctic megadunes. *The Cryosphere* **10**, 1217–1227. doi: [10.5194/tc-10-1217-2016](https://doi.org/10.5194/tc-10-1217-2016).
- Ekaykin A, Lipenkov V, Barkov N, Petit J and Masson-Delmotte V** (2002) Spatial and temporal variability in isotope composition of recent snow in the vicinity of Vostok station, Antarctica: implications for ice-core record interpretation. *Annals of Glaciology* **35**, 181–186. doi:[10.3189/172756402781816726](https://doi.org/10.3189/172756402781816726)
- EPICA Community Members** (2004) Eight glacial cycles from an Antarctic ice core. *Nature* **429**(6992), 623–628. doi:[10.1038/nature02599](https://doi.org/10.1038/nature02599)
- Fisher D, Reeh N and Clausen H** (1985) Stratigraphic noise in time series derived from ice cores. *Annals of Glaciology* **7**, 76–83. doi:[10.3189/S0260305500005942](https://doi.org/10.3189/S0260305500005942)
- Freitag J, Kipfstuhl S, Laepple T and Wilhelms F** (2013) Impurity-controlled densification: a new model for stratified polar firn. *Journal of Glaciology* **59** (218), 1163–1169. doi:[10.3189/2013JoG13J042](https://doi.org/10.3189/2013JoG13J042)
- Freitag J, Wilhelms F and Kipfstuhl S** (2004) Microstructure-dependent densification of polar firn derived from X-ray microtomography. *Journal of Glaciology* **50**(169), 243–250. doi:[10.3189/172756504781830123](https://doi.org/10.3189/172756504781830123)
- Gfeller G and 5 others** (2014) Representativeness and seasonality of major ion records derived from NEEM firn cores. *The Cryosphere* **8**(5), 1855–1870. doi:[10.5194/tc-8-1855-2014](https://doi.org/10.5194/tc-8-1855-2014)
- Howat IM, Porter C, Smith BE, Noh MJ and Morin P** (2019) The reference elevation model of Antarctica. *The Cryosphere* **13**, 665–674. doi:[10.5194/tc-13-665-2019](https://doi.org/10.5194/tc-13-665-2019)
- Jouzel J and 12 others** (1997) Validity of the temperature reconstruction from water isotopes in ice cores. *Journal of Geophysical Research* **102**(C12), 471–487. doi: [10.1029/97JC01283](https://doi.org/10.1029/97JC01283).
- Laepple T and 5 others** (2016) Layering of surface snow and firn at Kohnen station, Antarctica: noise or seasonal signal? *Journal of Geophysical Research* **121**(10), 1849–1860. doi:[10.1002/2016JF003919](https://doi.org/10.1002/2016JF003919)
- Münch T, Kipfstuhl S, Freitag J, Meyer H and Laepple T** (2016) Regional climate signal vs. Local noise: a two-dimensional view of water isotopes in Antarctic firn at Kohnen station, Dronning Maud Land. *Climate of the Past* **12**, 1565–1581. doi:[10.5194/cp-12-1565-2016](https://doi.org/10.5194/cp-12-1565-2016)
- Münch T, Kipfstuhl S, Freitag J, Meyer H and Laepple T** (2017) Constraints on post-depositional isotope modifications in East Antarctic firn from analysing temporal changes of isotope profiles. *The Cryosphere* **11**, 2175–2188. doi:[10.5194/tc-11-2175-2017](https://doi.org/10.5194/tc-11-2175-2017)
- Nakazawa T and 6 others** (1993) Measurements of CO₂ and CH₄ concentrations in air in a polar ice core. *Journal of Glaciology* **39**(132), 209–215. doi:[10.3189/S0022143000015860](https://doi.org/10.3189/S0022143000015860).
- Pishro-Nik H** (2014) Introduction to probability, statistics, and random processes, available at <https://www.probabilitycourse.com>, Kappa Research LLC, 2014.
- Schaller CF and 5 others** (2016) A representative density profile of the North Greenland snowpack. *The Cryosphere* **10**(5), 1991–2002. doi:[10.5194/tc-10-1991-2016](https://doi.org/10.5194/tc-10-1991-2016)
- Wesche C and 6 others** (2016) Neumayer III and Kohnen station in Antarctica operated by the Alfred Wegener Institute. *Journal of Large-Scale Research Facilities JLSRF* **2**(0), 85. doi: [10.17815/jlsrf-2-152](https://doi.org/10.17815/jlsrf-2-152).

Topographic effect creates non-climatic variations in ice-core based temperature records of the last millennium

Remi Dallmayr^{1,4}, Johannes Freitag¹, Thomas Laepple^{2,3}, Frank Wilhelms^{1,4}, Daniela Jansen¹, Melanie Behrens¹ and Maria Hörhold¹

¹ Alfred-Wegener-Institut Helmholtz-Zentrum für Polar-und Meeresforschung, Bremerhaven, Am Handelshafen 12, 27570 Bremerhaven, Germany

² Alfred-Wegener-Institut Helmholtz-Zentrum für Polar-und Meeresforschung, Potsdam, Telegrafenberg A45, 14473 Potsdam, Germany

³ University of Bremen, MARUM – Center for Marine Environmental Sciences and Faculty of Geosciences, 28334 Bremen, Germany

⁴ GZG Abt. Kristallographie, University of Göttingen, Göttingen, Germany

Corresponding author: remi.dallmayr@awi.de

Key points:

- The isotopic composition in surface snow is anti-correlated to local accumulation rate anomalies, driven by the local surface topography.
- Spatial variability is advected into an ice-core site by ice-flow, inducing millennial scale non-climatic variation in the isotopic record.
- Map of time scales variations due to topography effect in East Antarctica for consideration in the interpretation of records from ice-cores.

Key words:

Antarctic isotope record, surface topography, accumulation rate, spatial and temporal variability, paleoclimate reconstructions

Abstract

Past temperature reconstructions from polar ice sheets are commonly based on stable water isotope records in ice-cores. However, despite major efforts in the understanding of the ice-core signal formation, the temperature reconstructions of the last millennium in Antarctica remain highly uncertain. Here, using a 100 km scale representative surface water isotope dataset, we show that the spatial variability of local surface topography and accumulation rate anomalies influences the isotopic composition of the upper-meter snowpack. The magnitude of this non-temperature effect on water isotopes is similar to changes of the last millennium. We demonstrate that these spatial anomalies are advected into the deeper firn and ice column, and are translated into an artificial centennial to millennial scale variability in the isotope record. Additionally, we provide an estimation of areas where this effect is relevant for last millennium temperature reconstructions.

Plain Language Summary

Stable water isotopes measured in ice-cores are commonly used as a paleo-thermometer. However, these records can be affected by multiple processes and their reliability is unclear, particularly for centennial to millennial time scales in Antarctica. We demonstrate that in low accumulation rate regions, the local topography can create significant spatial variability in water

isotopes. This can create temporal variability in ice-core records as these anomalies are advected into the core by ice-flow. This mechanism creating non-temperature related water isotope variations on time-scales from centuries to millennia is likely omnipresent within the continent, potentially affecting numerous ice-cores. We estimate relevant areas with respect to this effect to assist future coring efforts, as well as the careful interpretation of existing records.

1. Background and motivation

Stable water isotopes in ice are commonly used as a proxy for paleotemperatures (Jouzel et al., 1997) and allow reconstructions of past temperature from ice-cores (PAGES 2k Consortium, 2013, Steig et al., 2013). Despite major advances in the analysis methods and field studies to understand signal formation of the isotope signal preserved in the firn and ice (Casado et al., 2018; Münch et al., 2017; Münch & Laepple, 2018), temperature reconstructions from East-Antarctic ice cores are still highly uncertain on centennial to millennial scale and often show a low correlation with observations and simulations (Jones et al., 2016; Klein et al., 2019; Stenni et al., 2017).

Stratigraphic noise (Fischer et al., 1985, Münch et al., 2017) masks climate signals from interannual to multi-decadal scales but can be minimized by averaging multiple records or taking temporal averages (Münch et al., 2016). Post-depositional effects near the surface might affect the isotopic composition (Neumann & Waddington, 2004; Town et al., 2008) but their importance for ice-core records is under discussion (Münch et al., 2017). Precipitation intermittency acts on longer spatial scales and leads to strong noise in water isotope records but is generally well understood and averages out on long-timescales (Casado et al., 2020).

While these processes create a strong non-climatic variability, they cannot explain observed differences in the nearby ice-core isotope records that can last for several centuries. One example is the ice-core site B31 in Dronning Maud Land, with a drop in stable water isotopic composition accompanied by a sudden increase in accumulation rate (Oerter et al., 2004). The nearby core B32 does not confirm these changes. Radar-data within the ~100 km distance between sites show strong local variations of accumulation rate within short distances (up to $\sim 30 \text{ kg m}^{-2} \text{ a}^{-1}$, i.e. ~50%, Rotschky et al., 2004). Precipitation varying only slightly on such scale, these variations were related to surface undulations caused by bedrock topography (Eisen et al., 2004; Rotschky et al., 2004), providing a first hint to a relation of topography, accumulation and isotopic composition.

A relationship between these variables has been suggested by previous studies. First, surface undulations were found to lead to spatial changes in deposition of snow (Arcone et al., 2005; Black & Budd, 1964; Eisen et al., 2005; Frezzotti et al., 2002a, 2004; Fujita et al., 2011; Rotschky et al., 2004, 2007; Whillans, 1975). Second, Ekaykin et al. (2016) observed significant variations of the upper-meter isotopic composition along the slopes of a surface undulation within a megadune area near Vostok station. They proposed that the spatial variability can lead to temporal non-climatic variations of the record (Ekaykin et al., 2016), due to the upwind drift of the dune (Frezzotti et al., 2002a). This situation is limited to particular areas covering only small parts of the Antarctica ice sheet (Fahnestock et al., 2000), but raises the question to what extend variations in paleo-climate records may be biased by local topography-induced variations in accumulation rate.

Motivated by these findings we designed a specific study to evaluate the effect of surface topography on the stable-water-isotopic composition. Strongly replicated sampling of the top

meter of snow, together with Ground Penetrating Radar (GPR) and Global Positioning System (GPS) data on a 115 km traverse including the B31 site allowed us for the first time a representative characterization of the near-surface isotopic composition on a large-scale and its relationship with the local topography.

2. Methods and data

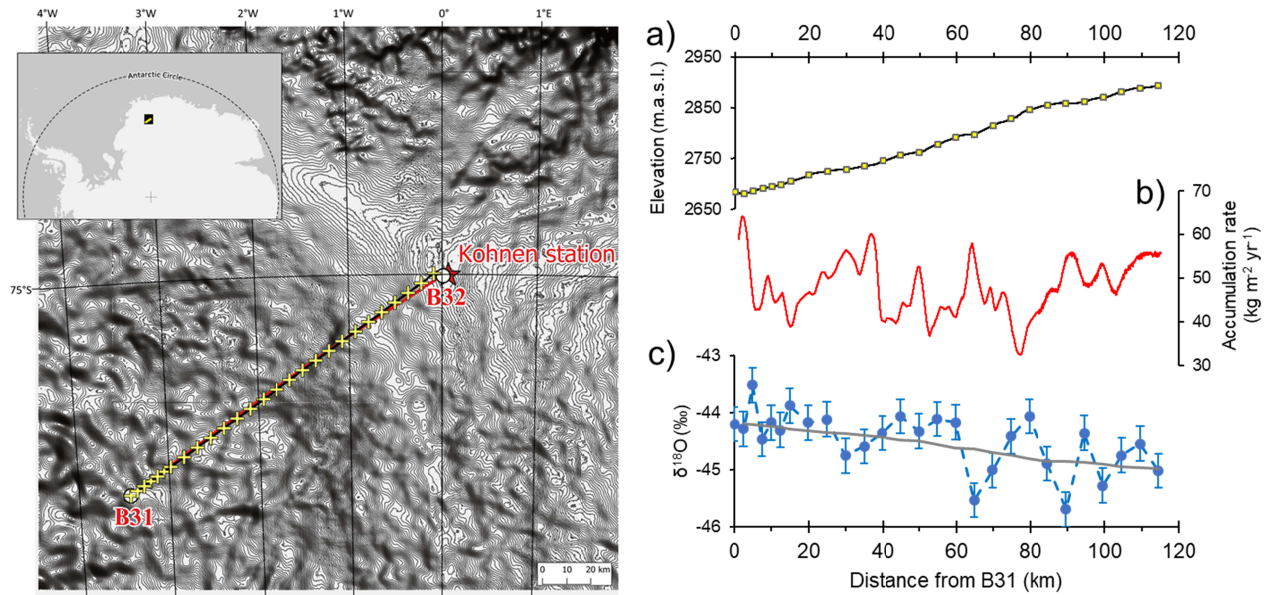


Figure 1. The area of investigation (left) and the field work results (right).

Left panel: Traverses -00/01 (red line) and -18/19 (this study, black line) in between the B31 and B32 sites (white circles). The sampling sites of season 18/19 are indicated with yellow crosses. The topography is shown as 1m elevation contours (Howat et al., 2019). Right panel: a) The elevation along the traverse-18/19 (black line) with yellow points marking the sampling sites. b) Accumulation rate along the traverse-00/01 (red line, Rotschky et al., 2004). c) $\delta^{18}\text{O}$ at sites, (blue markers connected by dashed line) with the error-bars indicating the estimated remaining

uncertainty (1 standard-error) from stratigraphic noise. The solid gray line represents the linear trend of $\delta^{18}\text{O}$ versus elevation.

In the austral field season 2018/2019 we performed a 115 km long traverse (hereafter traverse-18/19) in the interior of Dronning Maud Land, East Antarctica (Fig. 1) connecting the B31 ice-core site ($3^{\circ}25.82'\text{W}$ $75^{\circ}34.890\text{ S}$, 2680 m.a.s.l.) to the B32 ice-core site ($0^{\circ}00.42'\text{E}$ $75^{\circ}00.14'\text{S}$, 2892 m.a.s.l) and Kohnen station (EDML deep ice-core site, $0^{\circ}04\text{E}$ $75^{\circ}00\text{ S}$, 2892 m.a.s.l.).

A post-processed kinematic (PPK) global positioning system mounted at the living container sampled geodetic positions at 1 Hz (i.e. $\sim 3.5\text{ m}$), and allowed to derive the surface elevation profile of the traverse (Fig. 1).

We further make use of accumulation data based on GPS and GPR measurements (Eisen et al., 2004; Rotschky et al., 2004) from a traverse in 2000/2001 (hereafter traverse-00/01) to estimate the surface mass-balance profile (Fig. 1). For this, we use the internal radar reflection horizon corresponding to $\text{AD}1817 \pm 5\text{ a}$ (i.e. $\pm 2.5\%$ on accumulation rate) (Rotschky et al. 2004).

2.1 Stable water isotopes sampling positions and strategy

Along the route-18/19, 27 sampling sites were chosen with regard to the decorrelation length of the topographic anomalies, i.e. 2.5 km distance between sites for the first 15 km of the traverse, and 5 km later on (Fig. 1). With the knowledge gained from trench studies (Laepplé et al., 2016; Münch et al., 2016) and the use of a newly developed fast sampling tool (Dallmayr et al., 2020), we extracted and averaged at each site 10 upper-meter samples with 10 m distance to minimize the uncertainty from stratigraphic noise (Fisher et al., 1985). The mean value of uncertainty is

estimated as 0.3 ‰, (1 standard-error) from the remaining variability of the replicated one-meter averages. (see Text S1 and Table S1, supporting information).

2.2 Measurement of stable water isotopes

All samples were kept frozen during shipment and storage until measurement at the Alfred-Wegener-Institut Helmholtz-Zentrum für Polar-und Meeresforschung (AWI) in Bremerhaven and Potsdam, Germany. The stable water isotope ratios of ^{18}O and D were measured by means of cavity ring-down spectroscopy (Picarro Inc. L-2120-i, and L-2140-i in AWI-Bremerhaven, L-2130-i in AWI-Potsdam.) and calibrated to the international VSMOW/VSLAP scale. Single measurements are provided with a precision of 0.1 and 1.0 ‰ (1sd) for $\delta^{18}\text{O}$ and δD . The accuracy of the measurement determined by a quality standard in each measurement run is ≤ 0.16 ‰ for $\delta^{18}\text{O}$ and ≤ 1.1 ‰ for δD .

2.3 Data processing – Small-scale anomalies

The heavy stable water isotopes exhibit a depletion along the traverse with increasing altitude (Dansgaard, 1964) (Fig. 1 c). The observed relationship (-0.0037 ‰ per meter of elevation, Fig. 1c) is consistent to the magnitude of trends expected from isotope enabled climate models within the studied area (ECHAM5-wiso model; Münch & Werner, 2020). Thus, to study the effect of local topography on water isotopic composition, we removed the observed linear trend of $\delta^{18}\text{O}$ against elevation along the route.

We derived the local heights (i.e. local topography) by first removing the long-term trend by subtracting a 20 km running mean and then reducing the noise and the small-scale variations

from sastrugis by applying a 1 km running mean (Fig.2a). The local surface slope (Fig. 2b) is computed as the spatial derivative of the local heights. Similarly, local variations of accumulation rate (accumulation rate anomalies, Fig. 2) are derived as the residuals of the accumulation rate and its 20 km running mean.

3 Results and discussion

3.1 Small-scale spatial variability of accumulation rate and isotopic composition

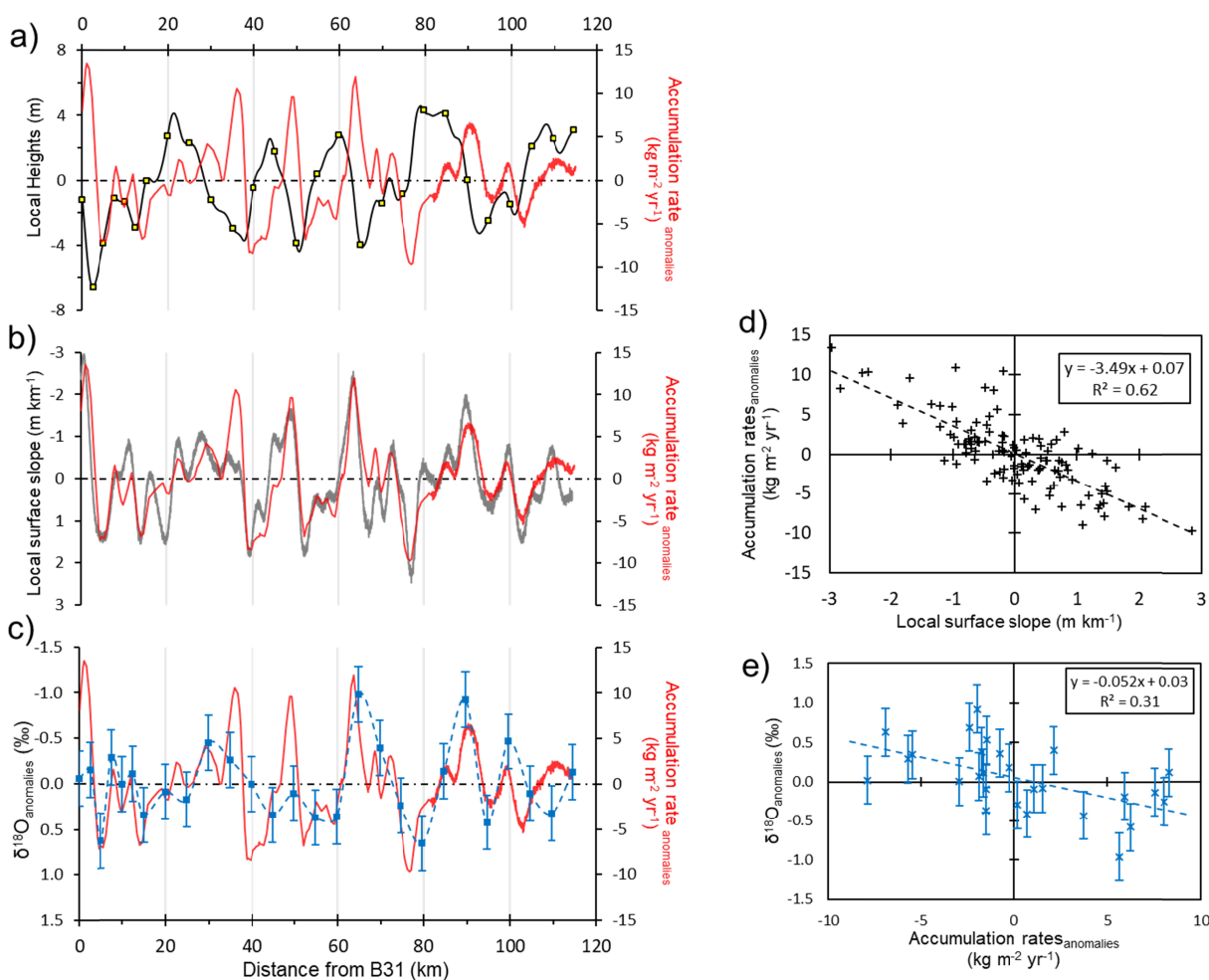


Figure 2. Small-scale anomalies of accumulation rate related to local topography (a, b, d) and to isotopic composition anomalies (c, e).

The variation of local accumulation (red lines) is superposed to the local height of surface undulations (a, black line, left axis) and the surface slope (b, grey line, left axis reversed). Regression of local accumulation against local slope (d) ($N=115$, 100 m average every kilometer, standard-errors of 0.1 m km^{-1} and $0.05 \text{ kg m}^{-2} \text{ yr}^{-1}$, respectively). The local topography at sampling sites is shown (a, yellow markers). The derived $\delta^{18}\text{O}$ anomalies along the route (c, left axis reversed, blue points connected by dashed line) are superposed to the local accumulation. Error bars in c) and d) indicate 1 standard error. Regression of $\delta^{18}\text{O}$ anomalies ($N=27$) against the 100 m average of the local accumulation at sites (e) (standard-error of $0.04 \text{ kg m}^{-2} \text{ yr}^{-1}$).

3.1.1 Relation of local accumulation rate and local surface topography

Extrema of local accumulation rate (maxima at kilometers 1.5, 36, 50, 64, 91, minima at kilometers 5, 40, 52, 77) surround the four distinct topographic features along the route (Fig. 2a) within a range of variation of $18.4 \text{ kg m}^{-2} \text{ yr}^{-1}$. With a prevailing wind in the area from North East to South West (Fujita et al., 2011), the deposition of drifted snow follows the pattern of increased and reduced accumulation rate in the hollows and bumps, a relationship that is well established (King et al., 2004).

Moreover, we find a strong relationship between the local surface slope and the accumulation rate anomalies ($R^2 = 0.62$, p-value <0.001 , Fig. 2b, Fig. 2d). This observation underlines the sensitivity of deposition to the slope of the surface (Fujita et al., 2011) as visible in the well-

spread intervals of increased and reduced accumulation rate along the windward- and leeward-slopes of the surface, respectively (Arcone et al., 2005; Whillans, 1975).

3.1.2 Relation of local accumulation rate and isotopic composition of snow

The $\delta^{18}\text{O}$ anomalies along the traverse show strong variations ($>2\text{‰}$) that seem to be coupled to the local accumulation. Negative anomalies of $\delta^{18}\text{O}$ were generally found in regions with positive local accumulation rate anomalies and vice versa (Fig. 2c). A linear regression analysis (Fig. 2e) shows a statistically significant negative linear relationship ($R^2 = 0.31$, p-value 0.0029) between both variables. We note that the remaining stratigraphic noise on our isotopic anomalies likely explains the relatively low correlation and the true underlying relationship is likely stronger. Our finding implies that a change in accumulation rate of $+10\text{ kg m}^{-2}\text{ yr}^{-1}$ leads to a depletion of -0.52‰ in $\delta^{18}\text{O}$ (i.e. a sensitivity of -0.052‰ per $\text{kg m}^{-2}\text{ yr}^{-1}$). This sensitivity is furthermore fully consistent with the enrichment of $\delta^{18}\text{O}$ composition ($+0.5\text{‰}$ per kilometer) towards a reduced accumulation rate site ($-8\text{ kg m}^{-2}\text{ yr}^{-1}$) observed over a 5 km transect in the vicinity of Kohnen station (Dallmayr et al., 2020).

Importantly, the range of spatial variations in $\delta^{18}\text{O}$ is similar to the temporal variations observed in Antarctic ice-cores over the last millennium (Stenni et al., 2017) but has the opposite direction to the temporal climatic relationship between precipitation and temperature, with more precipitation linked to warmer temperatures (Frieler et al., 2015).

There are several hypotheses to explain this spatial relationship:

(a) Seasonal redistribution of snow: a larger redistribution during winter due to higher wind speeds (Birnbaum et al., 2010) and smaller snow crystal sizes would lead to more isotopically depleted winter summer snow in the hollows and enriched summer snow in the bumps, respectively. (Ekaykin et al., 2002).

(b) Post-depositional effects: as a consequence of the reduced accumulation, the surface snow is subject to longer and stronger post-depositional modifications, which are characterized by an enrichment in heavier isotopes as described by Town et al. (2008). Evidence for this hypothesis was found by Ekaykin et al., (2016) interpreting the change in deuterium excess and $\delta^{17}\text{O}$. This idea is further supported by recent studies (Hughes et al., 2021; Ma et al., 2020a, 2020b).

While the data here doesn't allow to distinguish between both hypotheses, in either case the relationship of isotopes and local accumulation rate anomalies would have direct implications for the interpretation of ice-core records if the spatial changes also affect the downcore ice-core records. Ekaykin et al. (2016) suggested that a changing topography induced by moving megadunes together with an influence of topography on isotopes could create isotopic variations in ice-core records. While this only applies particularly to megadune areas, even stationary surface conditions (topography, accumulation rate, isotopic composition) will irremediably be advected by the ice flow over time and thus translate spatially varying surface conditions into temporal variations in ice-cores.

3.2 The B31-core: a spatial to temporal transfer induced by flowing ice

As an example, we study the B31 ice-core site. Here, the analysis of available radar profiles (Eisen et al., 2004; Rotchky et al., 2004) suggests that the topography of the study area was stationary over the last millennium, as constrained by bedrock topography (Steinhage et al., 1999). The ice sheet slowly flows towards South West at a velocity $\geq 3 \text{ m yr}^{-1}$ at the B31 site (satellite measurement, Fig. S1 in supporting information), and the topography upstream of the location exhibits a hollow with the lowest point $\sim 2.5 \text{ km}$ from the core-site (Fig. 3a). We independently estimated the ice-flow velocity from the GPR data (Arcone et al., 2005) by tracking the position of the lowest point over the last millennium in five dated internal reflection horizons (Eisen et al., 2004) (Fig. 3b). We find 3.8 m yr^{-1} ($\pm 0.6 \text{ m yr}^{-1}$, 1sd) towards SW, consistent with the satellite data. Considering the uncertainties of both methods, we assume a velocity of 3.5 m yr^{-1} to estimate the original position of the dated horizons (Fig. 3b). The results show that the recent horizons are advected into the B31 column from the windward slope and older horizons from the leeward slope $> 2.5 \text{ km}$ upstream.

In the 1500 years old B31 record, (Oerter et al., 2004), the accumulation rate shows a steep increase around 1000AD followed by a stable accumulation rate with a broad local maximum at 1500AD (Fig. 3c). The $\delta^{18}\text{O}$ record shows the inverse behavior; a decrease of around 2.5 ‰ from 500AD to 1000AD and more stable, slightly increasing values afterwards (Fig. 3d).

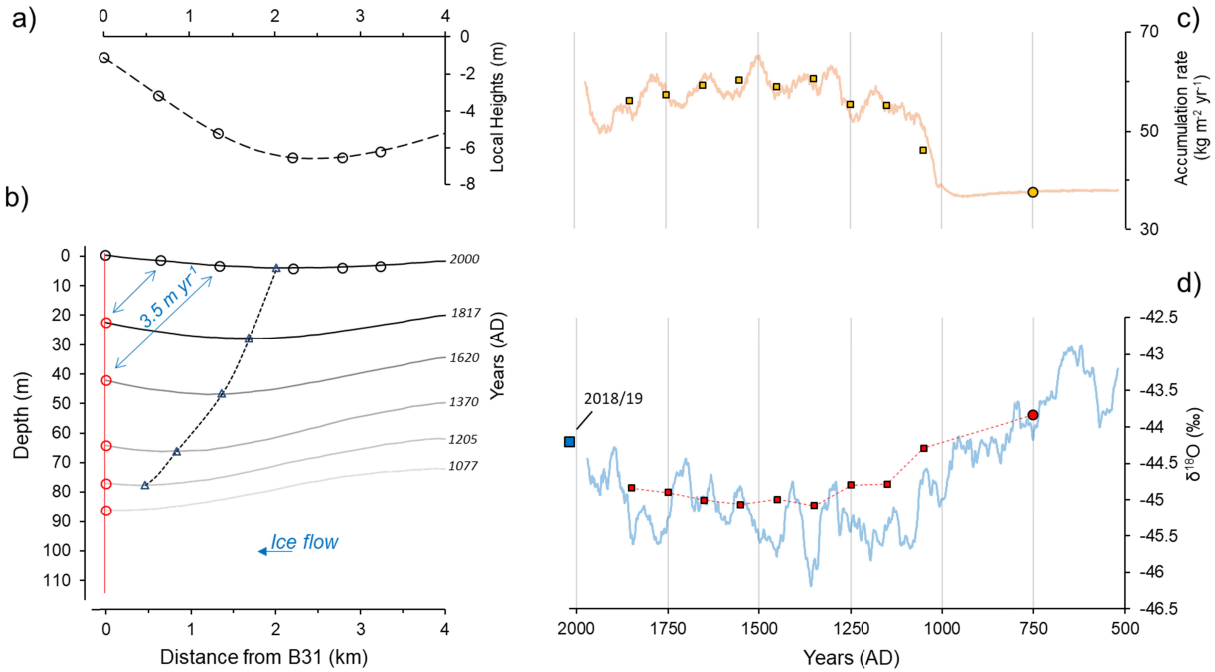


Figure 3. The B31 case: (a, b) upstream surface topography advected into the column at site, and records of (c) accumulation rate and (d) $\delta^{18}\text{O}$ composition.

a) the surface origins related to the local heights. b) The 114 m long B31-core (red line) and the depth profiles of the five internal reflection horizons with their age estimate (Eisen et al., 2004). The dotted black line connects the nearest bottom of the upstream hollow (triangle) used for estimation of flow velocity. The black circles indicate the original surface positions of each age horizon along the core (red circles) assuming a constant flow of 3.5 m yr^{-1} towards SW. c) 50 yr running mean of accumulation-rate record (orange line). The mean of the period 500-1000AD is marked with a circle, and the means of the nine 100 yr periods as squares. d) 50 yr running mean $\delta^{18}\text{O}$ record (blue line) and measurement of snow value of season 18/19 (blue marker). The predicted 100 yr $\delta^{18}\text{O}$ composition as induced by topography are shown by red squares (connected by dashed red line), with the mean of period 500-1000AD (red circle).

3.3 $\delta^{18}\text{O}$ record compared to the expected variations from the topographic effect

To predict the effect of the temporal $\delta^{18}\text{O}$ variations from the advection of the spatial variability, we assume that in first order, the accumulation rate at the site was constant over time. This assumption is supported by the analysis of B32 near Kohnen station that shows a nearly constant accumulation rate over time (Table S2, supporting information). This allows us to use the derived empirical relationship between isotopic anomalies and accumulation rate anomalies (i.e. $-0.052 \text{ ‰ per kg m}^{-2} \text{ yr}^{-1}$, section 3.1.2) together with the changes in accumulation rate to estimate the $\delta^{18}\text{O}$ anomalies induced by the topography ($\delta^{18}\text{O}_{topo}$)

$$\delta^{18}\text{O}_{topo}(t) = -0.052 * \Delta A(t - t_0) + \delta^{18}\text{O}(t_0) \quad (1)$$

$\Delta A(t-t_0)$ (in $\text{kg m}^{-2} \text{ yr}^{-1}$) refers to the accumulation rate anomaly between time (t) and the initial period (t_0) and $\delta^{18}\text{O}(t_0)$ is the initial isotopic composition. We choose 500–1000AD as the initial time period and perform the analysis on 100 yr mean values.

The resulting dataset is superposed to the 50 yr smoothed $\delta^{18}\text{O}$ temporal variations (Fig. 3c). The similar 1000-years trend between signals supports the hypothesis that this slow variation might be predominantly generated by the effect of topography, and not climate driven. This is further supported by comparing the B31 and B32 records over the last 1500 years (Fig. S2, supporting information). Being on the divide, the B32 site is not expected to be affected by the topography effect on millennial time-scales (as we show later, see Fig. 4) but due to their proximity (100km distance) we can assume similar climatic imprints. In contrast to B31, the isotope and accumulation time-series of B32 are rather constant but feature similar decadal to centennial variability, and the offset between both isotopic records can be explained by the difference in elevation between sites ($\sim 0.8 \text{ ‰}$ based on the depletion-elevation trend, Fig. 1c). This supports

that the 1000-yr variation observed in the B31 record are consistent to the expected upstream topographic anomaly.

4. Implications for other ice-cores and temperature reconstructions of the last millennium

To study how this interaction of spatial isotope variations linked to the local topography and ice-flow may affect other ice-core records, we derive a spatial map of the time scales that might be affected by this topographic effect. Assuming that a significant relationship between local topography and $\delta^{18}\text{O}$ anomalies also exists beyond our study area, and the ideal cases of stationary topography and constant ice-flow during the time period of interest, the affected time scales are the product of the length scale of surface undulations and the ice-flow velocity. We use the surface velocity distribution available across the continent (Mouginot et al., 2019) together with an estimated average 5 km length scale of surface undulation computed from Howat et al. (2019) (Text S2, supporting information).

The resulting map of the time scales potentially affected by the topographic-effect (Fig. 4) shows a wide range of affected timescales from several thousand years on the ice-divides down to centuries in regions with higher ice-flow. At the B32 site, the map predicts that the topographic effect does not act on millennial and faster time scales, whereas the map indicated time scale of around 1000 years at the B31 site, consistent with our detailed analysis.

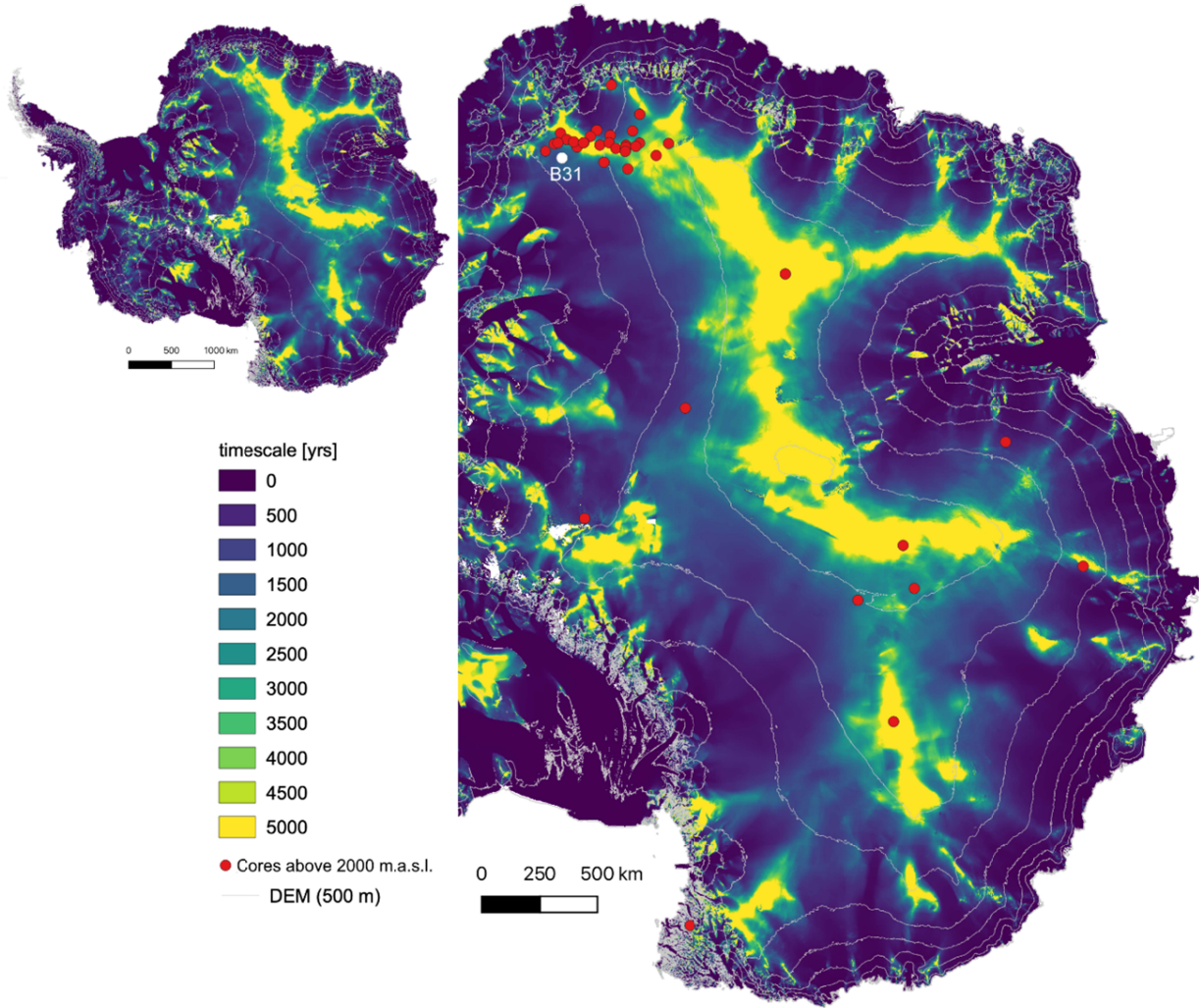


Figure 4. Map of estimated time scale variations in the records due to the topographic effect induced by ice flow in Antarctica (left), and overview of East-Antarctica (right). Ice cores from plateau sites > 2000 m.a.s.l. used in the Antarctica 2k temperature reconstruction (Stenni et al., 2017) are indicated as red points, including the B31 site (white point). The grey contours show the 500 m elevation lines (Howat et al., 2019).

The core B31 was used in the community temperature reconstruction of the last millennium (Antarctica 2k) (Stenni et al., 2017) without special consideration of its non-climatic variability

in the lowermost section. We can identify several additional cores included in the database located in similar ~1000 years scale variability estimation (red points in Fig. 4). For these cores, an analysis of the relationship between accumulation rate and isotopic records can provide further insight, as a negative relation might be a signature of the topographic effect (section 3.1.2). In such case using the records for climate reconstruction should be avoided, carefully apprehended by an adequate upstream correction (beyond the scope of this study), or filtered by interpreting only the safe time scales. Finally, if the topographic effect that we propose here is confirmed by other studies, it should be also considered in the choice of future drilling sites.

5. Conclusions

We performed a 115 km traverse on the plateau of Dronning Maud Land with representative snow sampling (10 x 1 m snow liner per site) on 27 sites resolving the small-scale topographic variations combined with GPR and GPS. The high precision of the mean $\delta^{18}\text{O}$ snowpack values from averaging out stratigraphic noise allowed us to identify a significant negative relationship between the local anomalies of $\delta^{18}\text{O}$ and deposition driven by the topography ('topographic effect'). We propose and demonstrate on the example of the B31 site that ice-flow advects these spatial anomalies into centennial to multi-millennial isotopic anomalies in ice cores and the topographic effect is thus highly relevant for the interpretation of ice-core. Confronting the estimated 'topographic effect' for the B31 core with the measured isotope record demonstrates that most of the millennial changes in this core can be explained without invoking climatic changes. As in many regions the topography on millennial scales is linked to the bedrock and thus stationary in time, we extrapolate our findings and provide a map of the potential topographic effect on ice-cores. This suggests that several ice-cores used in the reconstruction of

the last millennium might be also affected by these non-climatic variations. Further studies on the physical origin of this relationship and its strength beyond our study region will help to refine our understanding, potentially allow for a correction of affected records and thus a more robust reconstruction of the Antarctic climate of the last millennia.

Data Availability

The GPR related data (traverse-00/01) is archived at <https://doi.pangaea.de/10.1594/PANGAEA.935129> and <https://doi.pangaea.de/10.1594/PANGAEA.935031>, The traverse-18/19 data under <https://doi.pangaea.de/10.1594/PANGAEA.935030>, <https://doi.pangaea.de/10.1594/PANGAEA.935029>.

PANGAEA is hosted by the Alfred Wegener Institute Helmholtz Centre for Polar and Marine Research (AWI), Bremerhaven, and the Center for Marine Environmental Sciences (MARUM), Bremen, Germany.

Acknowledgment

This project was supported by Helmholtz funding through the Polar Regions and Coasts in the Changing Earth System (PACES) programme of the Alfred Wegener Institute. TL was supported by the European Research Council (ERC) under the European Union's Horizon 2020 Research and Innovation Programme (grant agreement no. 716092). We are grateful to the Kohnen 18/19 field season members, especially Klaus Trimborn for his decisive participation during the field

traverse. We thank Olaf Eisen for providing the necessary data from the traverse 2000/01, and Thomas Münch for his input with the ECHAM5/wiso model.

Authors contribution

T.L. and M.H. enabled the project. T.L. M.H. and J.F. designed the traverse, performed the field-work, and provided support and guidance to the first author for the preparation of the manuscript. M.H. supervised this part of the PhD project. F.W. contributed to the discussion sections and edited the language of the paper. D.J. provided the Figure 4 using the geographic information system Q-GIS, and MB conducted all isotopic measurements at AWI-Bremerhaven. R.D. performed the field-work, analyzed the data and prepared this manuscript, reviewed by all co-authors.

References

- Arcone, S., Spikes, V., & Hamilton, G. (2005). Stratigraphic variation within polar firn caused by differential accumulation and ice flow: Interpretation of a 400 MHz short-pulse radar profile from West Antarctica. *Journal of Glaciology*, 51(174), 407-422.
doi:10.3189/172756505781829151
- Birnbaum, G., Freitag, J., Brauner, R., König-Langlo, G., Schulz, E., Kipfstuhl, S., et al. (2010). Strong-wind events and their influence on the formation of snow dunes: Observations from Kohnen station, Dronning Maud Land, Antarctica. *Journal of Glaciology*, 56(199), 891-902.
doi:10.3189/002214310794457272

365 Black, H., & Budd, W. (1964). Accumulation in the Region of Wilkes, Wilkes Land, Antarctica.
 366 *Journal of Glaciology*, 5(37), 3-15. doi:10.3189/S0022143000028549

367 Casado, M., Landais, A., Picard, G., Münch, T., Laepple, T., Stenni, B., et al. (2018). Archival
 368 processes of the water stable isotope signal in East Antarctic ice cores. *The Cryosphere*, 12,
 369 1745–1766, doi:10.5194/tc-12-1745-2018.

370 Casado, M., Münch, T., and Laepple, T. (2020). Climatic information archived in ice cores:
 371 impact of intermittency and diffusion on the recorded isotopic signal in Antarctica, *Climate of*
 372 *the Past*, 16, 1581–1598. doi.org/10.5194/cp-16-1581-2020

373 Dallmayr, R., Freitag, J., Hörhold, M., Laepple, T., Lemburg, J., Della-Lunga, D., & Wilhelms,
 374 F. (2021). A dual-tube sampling technique for snowpack studies. *Journal of Glaciology*, 67(261),
 375 84-90. doi:10.1017/jog.2020.85

376 Dansgaard, W. (1964). Stable isotopes in precipitation, *Tellus*, 16:4, 436-468, doi
 377 10.3402/tellusa.v16i4.8993

378 Eisen, O., Nixdorf, U., Wilhelms, F., & Miller, H. (2004). Age estimates of isochronous
 379 reflection horizons by combining ice core, survey, and synthetic radar data. *Journal of*
 380 *Geophysical Research*, 109(B4), B04106. doi:10.1029/2003JB002858

381 Eisen, O., Rack, W., Nixdorf, U., & Wilhelms, F. (2005). Characteristics of accumulation around
 382 the EPICA deep-drilling site in Dronning Maud Land, Antarctica. *Annals of Glaciology*, 41, 41-
 383 46. doi:10.3189/172756405781813276

384 Ekaykin, A., Lipenkov, V., Barkov, N., Petit, J., & Masson-Delmotte, V. (2002). Spatial and
 385 temporal variability in isotope composition of recent snow in the vicinity of Vostok station,

386 Antarctica: Implications for ice-core record interpretation. *Annals of Glaciology*, 35, 181-186.
387 doi:10.3189/172756402781816726

388 Ekaykin, A., Eberlein, L., Lipenkov, V., Popov, S., Scheinert, M., Schröder, L., & Turkeev, A.
389 (2016). Non-climatic signal in ice core records: lessons from Antarctic megadunes. *The*
390 *Cryosphere*, 10, 1217–1227, doi:10.5194/tc-10-1217-2016

391 Fahnestock, M. A., Scambos, T. A., Shuman, C., Arthern, R. J., Winebrenner, D. P., & Kwok, R.
392 (2000). Snow megadune fields on the East Antarctic Plateau: Extreme atmosphere-ice
393 interaction, *Geophysical Research Letters*, 27(20), 3719– 3722. doi:10.1029/1999GL011248

394 Fisher, D., Reeh, N., & Clausen, H. (1985). Stratigraphic noise in time series derived from ice
395 cores. *Annals of Glaciology*, 7, 76–83. doi:10.3189/S0260305500005942

396 Frezzotti, M., Gandolfi, S., & Urbini, S. (2002). Snow megadunes in Antarctica: Sedimentary
397 structure and genesis. *J. Geophys. Res.*, 107(D18), 4344, doi:10.1029/2001JD000673

398 Frezzotti, M., Pourchet, M., Flora, O., Gandolfi, S., Gay, M., Urbini, S., et al. (2004). New
399 estimations of precipitation and surface sublimation in East Antarctica from snow accumulation
400 measurements. *Climate Dynamics*, 23, 803–813, doi:10.1007/s00382-004-0462-5

401 Frieler, K., Clark, P., He, F., Buizert, C., Reese, R., Ligtenberg, S.R.M., et al. (2015). Consistent
402 evidence of increasing Antarctic accumulation with warming. *Nature Climate Change*, 5, 348–
403 352. doi:10.1038/nclimate2574

404 Fujita, S., Holmlund, P., Andersson, I., Brown, I., Enomoto, H., Fujii, Y., et al. (2011). Spatial
405 and temporal variability of snow accumulation rate on the East Antarctic ice divide between
406 Dome Fuji and EPICA DML. *The Cryosphere*, 5, 1057–1081, doi:10.5194/tc-5-1057-2011

407 Howat, I. M., Porter, C., Smith, B. E., Noh, M.-J., & Morin, P. (2019). The Reference Elevation
408 Model of Antarctica. *The Cryosphere*, 13, 665–674, doi:10.5194/tc-13-665-2019

409 Hughes, A. G., Wahl, S., Jones, T. R., Zühr, A., Hörhold, M., White, J. W. C., & Steen-Larsen,
410 H. C. (2021). The role of sublimation as a driver of climate signals in the water isotope content
411 of surface snow: Laboratory and field experimental results. *The Cryosphere Discuss.*
412 doi:10.5194/tc-2021-87.

413 Jones, J.M., Gille, S.T., Goosse, H., Abram, N.J., Canziani, P.O., Charman, D.J. et al. (2016).
414 Assessing recent trends in high-latitude Southern Hemisphere surface climate. *Nature Climate*
415 *Change* 6, 917–926 (2016). doi.org/10.1038/nclimate3103

416 Jouzel J., Alley, R. B., Cuffey, K. M., Dansgaard, W., Grootes, P., Hoffmann, et al. (1997).
417 Validity of the temperature reconstruction from water isotopes in ice cores. *Journal of*
418 *Geophysical Research* 102(C12), 471–487 doi: 10.1029/97JC01283.

419 King, J. C., Anderson, P. S., Vaughan, D. G., Mann, G. W., Mobbs, S. D., & Vosper, S. B.
420 (2004). Wind-borne redistribution of snow across an Antarctic ice rise. *Journal of Geophysical*
421 *Research*, 109, D11104, doi:10.1029/2003JD004361.

422 Klein, F., Abram, N. J., Curran, M. A. J., Goosse, H., Goursaud, S., Masson-Delmotte, et al.
423 (2019). Assessing the robustness of Antarctic temperature reconstructions over the past
424 2 millennia using pseudoproxy and data assimilation experiments. *Climate of the Past*, 15, 661–
425 684, doi: 10.5194/cp-15-661-2019.

426 Laepple, T., Hörhold, M., Münch, T., Freitag, J., Wegner, A., Kipfstuhl, S. (2016). Layering of
427 surface snow and firn at Kohnen Station, Antarctica: Noise or seasonal signal?. *Journal of*
428 *Geophysical Research Earth Surface*, 121, 1849–1860, doi:10.1002/2016JF003919

429 Ma, T., Li, L., Li, Y., An, C., Yu, J, Ma, H., et al. Jiang, ~~S.~~, Shi, ~~G.~~ (2020). Stable isotopic
 430 composition in snowpack along the traverse from a coastal location to Dome A (East Antarctica):
 431 Results from observations and numerical modeling. *Polar Science*, 24, 1873-9652, doi:
 432 10.1016/j.polar.2020.100510.

433 Ma T., Li L., Shi G., & Li Y. (2020). Acquisition of Post-Depositional Effects on Stable Isotopes
 434 ($\delta^{18}\text{O}$ and δD) of Snow and Firn at Dome A, East Antarctica. *Water*, 12(6):1707.
 435 doi:10.3390/w12061707

436 Medley, B., McConnell, J. R., Neumann, T. A., Reijmer, C. H., Chellman, N., Sigl, M., &
 437 Kipfstuhl, S. (2018). Temperature and snowfall in western Queen Maud Land increasing faster
 438 than climate model projections. *Geophysical Research Letters*, 45, 1472–1480.
 439 doi:10.1002/2017GL075992

440 Mouginot, J., Rignot, E., & Scheuchl B. (2019). Continent-wide, interferometric SAR phase-
 441 mapping of Antarctic ice velocity. *Geophysical Research Letters*, 46, 9710-9718.
 442 doi:10.1029/2019GL083826

443 Münch T, Kipfstuhl S, Freitag J, Meyer H & Laepple T. (2016). Regional climate signal vs.
 444 Local noise: a two-dimensional view of water isotopes in Antarctic firn at Kohnen station,
 445 Dronning Maud Land. *Climate of the Past*, 12, 1565–1581. doi:10.5194/cp-12-1565-2016

446 Münch, T., Kipfstuhl, S., Freitag, J., Meyer, H., and Laepple, T. (2017). Constraints on post-
 447 depositional isotope modifications in East Antarctic firn from analyzing temporal changes of
 448 isotope profiles, *The Cryosphere*, 11, 2175–2188. doi:10.5194/tc-2017-35.

449 Münch, T., & Laepple, T. (2018). What climate signal is contained in decadal- to centennial-scale
 450 isotope variations from Antarctic ice cores? *Climate of the Past*, 14, 2053–2070, doi: 10.5194/cp-
 451 14-2053-2018

452 Münch T., & Werner, M. (2020). Antarctic time series of temperature, precipitation, and stable
 453 isotopes in precipitation from the ECHAM5/MPI-OM-wiso past1000 climate model simulation.
 454 DOT: 10.5281/zenodo.4001565

455 Neumann, T. A., & Waddington, E. D. (2004). Effects of firn ventilation on isotopic exchange.
 456 *Journal of Glaciology*, 50 (169), 183–194, doi:10.3189/172756504781830150

457 Oerter, H., Graf, W., Meyer, H., & Wilhelms, F. (2004). The EPICA ice core from Dronning
 458 Maud Land: First results from stable-isotope measurements. *Annals of Glaciology*, 39, 307-312.
 459 doi:10.3189/172756404781814032

460 PAGES 2k Consortium. (2013). Continental-scale temperature variability during the past two
 461 millennia, *Nature Geoscience*, 6, 339–346, Published online 21 April 2013,
 462 doi:10.1038/NGEO1797

463 Rotschky, G., Eisen, O., Wilhelms, F., Nixdorf, U., & Oerter, H. (2004). Spatial distribution of
 464 surface mass balance on Amundsenisen plateau, Antarctica, derived from ice-penetrating radar
 465 studies. *Annals of Glaciology*, 39, 265-270. doi:10.3189/172756404781814618

466 Rotschky, G., Holmlund, P., Isaksson, E., Mulvaney, R., Oerter, H., Van Den Broeke, M., &
 467 Winther, J. (2007). A new surface accumulation map for western Dronning Maud Land,
 468 Antarctica, from interpolation of point measurements. *Journal of Glaciology*, 53(182), 385-398.
 469 doi:10.3189/002214307783258459

470 Steinhage, D., Nixdorf, U., Meyer, U., & Miller, H. (1999). New maps of the ice thickness and
 471 subglacial topography in Dronning Maud Land, Antarctica, determined by means of airborne
 472 radio-echo sounding. *Annals of Glaciology*, 29, 267-272. doi:10.3189/172756499781821409

473 Steinhage, D., Kipfstuhl, S., Nixdorf, U., & Miller, H. (2013). Internal structure of the ice sheet
 474 between Kohnen station and Dome Fuji, Antarctica, revealed by airborne radio-echo sounding.
 475 *Annals of Glaciology*, 54(64), 163-167. doi:10.3189/2013AoG64A113

476 Stenni, B., Curran, M. A. J., Abram, N. J., Orsi, A., Goursaud, S., Masson-Delmotte, V., et al.
 477 (2017). Antarctic climate variability on regional and continental scales over the last 2000 years,
 478 *Climate of the Past*, 13, 1609–1634, doi:10.5194/cp-13-1609-2017

479 Steig, E., Ding, Q., White, J. W.C., Küttel, M., Rupper, S. B., Neumann, T. A., et al. (2013).
 480 Recent climate and ice-sheet changes in West Antarctica compared with the past 2,000 years.
 481 *Nature Geoscience*, 6, 372–375. doi: 10.1038/ngeo1778

482 Town, M. S., Warren, S. G., Walden, V. P., & Waddington, E. D. (2008). Effect of atmospheric
 483 water vapor on modification of stable isotopes in near-surface snow on ice sheets. *Journal of*
 484 *Geophysical Research*, 113, D24303, doi:10.1029/2008JD009852

485 Whillans, I. (1975). Effect of Inversion Winds on Topographic Detail and Mass Balance on
 486 Inland Ice Sheets. *Journal of Glaciology*, 14(70), 85-90. doi:10.3189/S0022143000013423

Supporting Information

Topographic effect creates non-climatic variations in ice-core based temperature records of the last millennium

Remi Dallmayr^{1,2}, Johannes Freitag¹, Thomas Laepple^{3,4}, Frank Wilhelms^{1,2}, Daniela Jansen¹, Melanie Behrens¹ and Maria Hörhold¹

TableS1: Sampling positions of survey 18/19

| Sample label | Sample type | <u>Geodetic sampling positions</u> | | | |
|--------------|-------------|------------------------------------|-----------------|----------------|------------------|
| | | Kilometres from B31 | Longitude (deg) | Latitude (deg) | Elevation (masl) |
| D2 | C | 0 | -3.43033 | -75.5815 | 2684.55 |
| D3 | S | 2.49 | -3.35479 | -75.56934 | 2680.60 |
| D4 | S | 4.98 | -3.27938 | -75.55715 | 2685.31 |
| D5 | M | 7.47 | -3.2041 | -75.54494 | 2690.89 |
| D6 | M | 9.96 | -3.12895 | -75.5327 | 2694.05 |
| D7 | C | 12.46 | -3.05392 | -75.52045 | 2697.14 |
| D8 | M | 14.95 | -2.97903 | -75.50816 | 2704.99 |
| D10 | S | 19.93 | -2.82962 | -75.48352 | 2716.90 |
| D12 | M | 24.91 | -2.68073 | -75.45878 | 2724.62 |
| D14 | S | 29.89 | -2.53234 | -75.43395 | 2728.25 |
| D16 | M | 34.87 | -2.38447 | -75.40903 | 2734.07 |
| D18 | S | 39.85 | -2.23711 | -75.38401 | 2745.06 |
| D20 | M | 44.83 | -2.09026 | -75.35889 | 2757.38 |
| D22 | S | 49.81 | -1.94392 | -75.33368 | 2763.51 |
| D24 | C | 54.79 | -1.79808 | -75.30838 | 2779.14 |
| D26 | M | 59.77 | -1.65276 | -75.28299 | 2793.12 |
| D28 | S | 64.75 | -1.50794 | -75.2575 | 2798.93 |
| D30 | M | 69.73 | -1.36362 | -75.23192 | 2815.19 |
| D32 | S | 74.71 | -1.21982 | -75.20625 | 2829.07 |
| D34 | M | 79.69 | -1.07651 | -75.18049 | 2847.11 |
| D36 | S | 84.67 | -0.93371 | -75.15465 | 2856.74 |

| | | | | | |
|-----|---|-------|----------|-----------|---------|
| D38 | C | 89.65 | -0.79141 | -75.12871 | 2860.02 |
| D40 | M | 94.63 | -0.64962 | -75.10268 | 2863.46 |
| D42 | S | 99.6 | -0.50832 | -75.07656 | 2871.40 |
| D44 | M | 104.6 | -0.36753 | -75.05036 | 2882.95 |
| D46 | S | 109.6 | -0.22723 | -75.02407 | 2889.87 |
| D48 | M | 114.5 | -0.08744 | -74.99769 | 2893.87 |

9

10 Geodetic positions derived from the Reference Elevation Model of Antarctica (Howat et al., 2019)
 11 of the 27 sampling sites of the traverse-18/19, and type of sampling applied at each site (Single,
 12 Camp sites, Mixed).

13

14 **TextS1: Sampling strategy of the survey 18/19**

15 Three types of sampling were applied to provide spatially representative values of the ~ upper-
 16 meter along the 115 km route:

17 1) Single sample sites (S): consist of 10 snow-cores extracted along a 90m long line using the dual-
 18 tube sampling technique developed by Dallmayr et al. (2020). Using Carbon-fiber tubes, the
 19 extracted cores are of 5 cm diameter and 100 cm length. Once withdrawn, each core is collected
 20 and packed into sealed plastic bags before measurement at the AWI-Bremerhaven.

21 The 10 samples at each site were analysed separately, with the mean value giving a statistical
 22 representative value of the upper-meter isotopic content in order to actively reduce the stratigraphic
 23 noise (Fisher et al., 1985). Further, the related standard-error of the mean (hereafter standard-error)
 24 allows estimating the remaining uncertainty due to the stratigraphic noise along each 90 m transect.
 25 Because the 10 m distance is beyond the decorrelation length of the stratigraphic noise (Münch et
 26 al., 2016), we can assume independence. The standard-error is then defined as:

$$\text{Standard error} = \frac{\sigma_0}{\sqrt{N}} \quad (1)$$

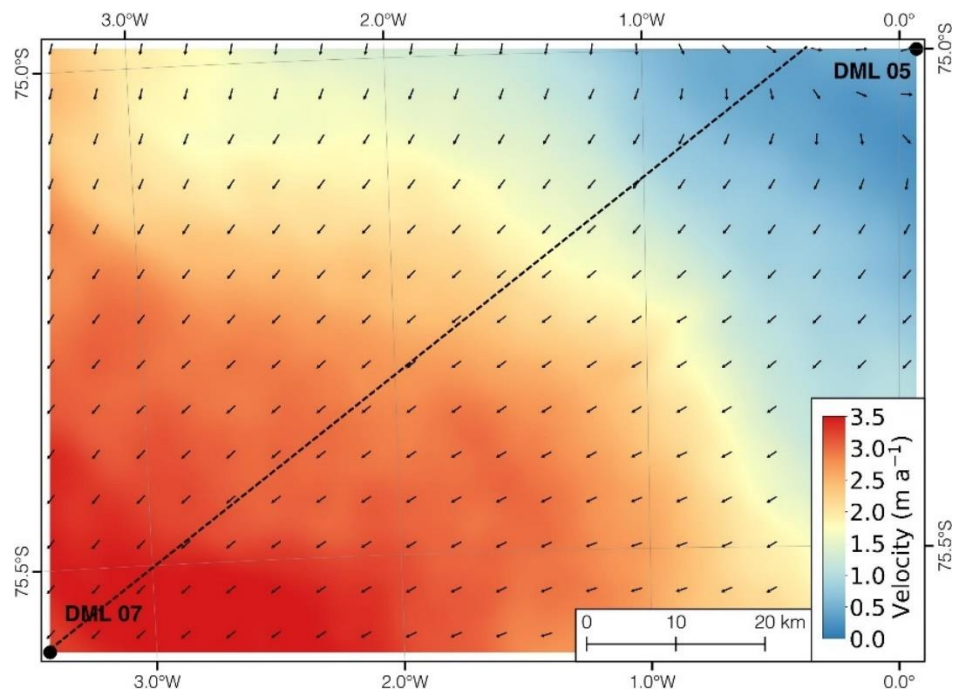
With σ_0 the standard deviation of the area, and N is the number of samples included.

Along the route, the mean value of standard-errors for the 11 sites considered is of 0.3‰.

2) Camp sites samples (C): consist of five liners (snow-cores of 10 cm diameter and 100 cm length, Schaller et al., 2016), extracted 10 meters apart along a trench created by a Pistenbully. Along each core discrete samples were cut on field and packed into sealed plastic bags and were analysed at the AWI-Potsdam. In addition, the estimated result at camp-sites D2 and D38 also include four single samples (S), two singles samples are added at the camp-site D24, and none at camp-site D7. At camp-each site the mean value of all profiles provided at each site is computed.

3) Mixed sample sites (M): consist of 10 snow cores along a 90m long trench created by a Pistenbully. Carbon-fiber tubes of 5 cm diameter, 1 mm thickness, and 120 cm long were pushed into the snow and dug-out using shovels. Once withdrawn, all snow-cores were manually mixed together, and one sample was collected and packed into sealed plastic bag and were measured at the AWI-Bremerhaven.

Figure S1. Ice flow of the studied area



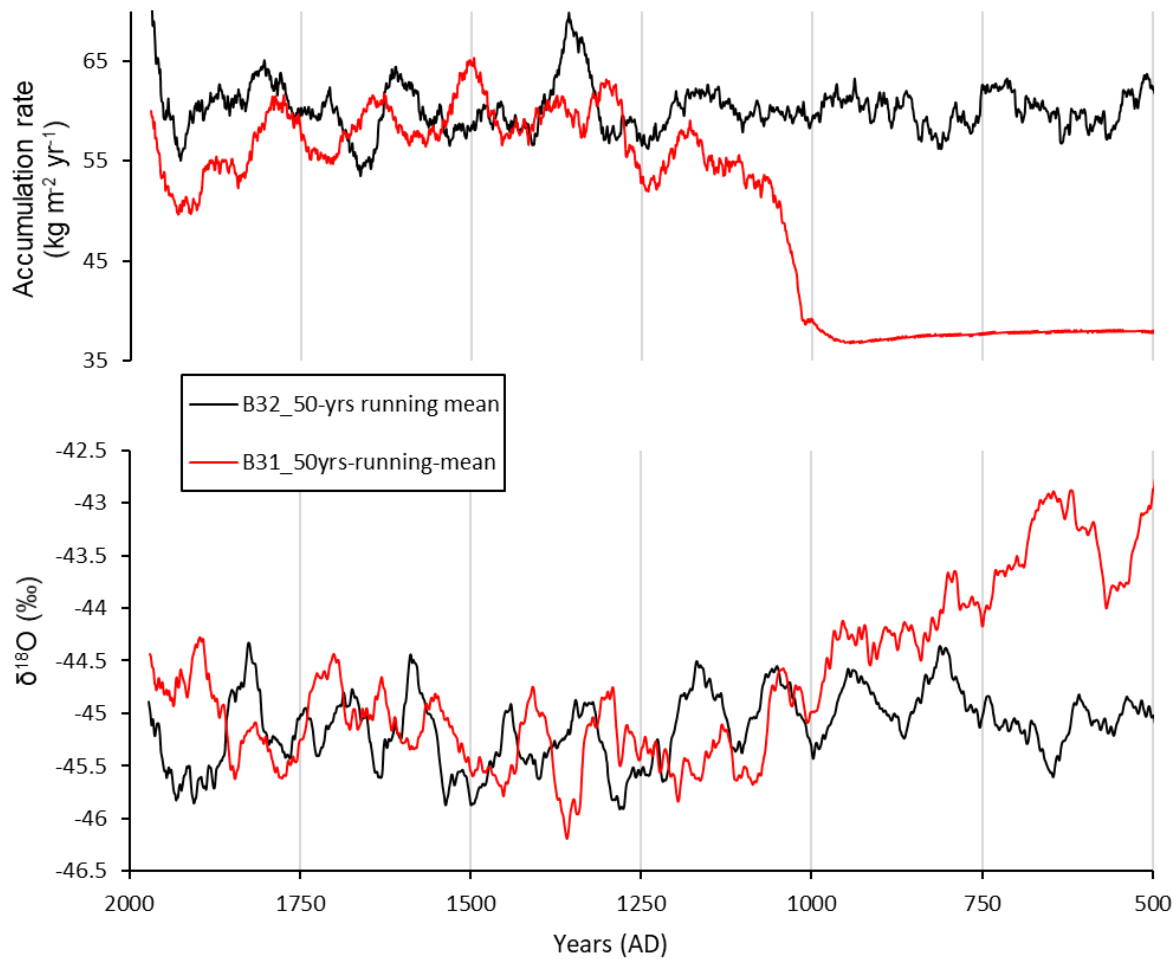
Direction (black arrows) and velocity (colour-scale) of the ice flow in of the studied area. Kohnen station is located 1.6 km westward of DML05, referring to the B32 site. DML07 refers to the site B31. Data are derived from Phase-Based Antarctica Ice Velocity Map (Mouginot et al., 2019).

TableS2: Long term accumulation rates at sites DML07 and DML05

| Time Interval | Annual accumulation rate (kg m ⁻² a ⁻¹) | |
|---------------|--|------------------|
| | Core B31 (DML07) | Core B32 (DML05) |
| 1249-1459 | 62.6 | 59.8 |
| 1459-1816 | 65.5 | 60.4 |
| 1816-1997 | 58.4 | 63.0 |

Annual accumulation rates for the firn cores B31 and B32 derived from the El Chichon, Kuwae, and Tambora volcanic eruption (Oerter et al., 2000) as analyzed by the DEP method (Wilhelms et al., 1998).

FigureS2: 50-years smoothed records from cores B31 and B32



(Top) 50 yr smoothed records of accumulation rate of cores B31 (red) and B32 (black), expressed in kg m⁻² yr⁻¹. (Bottom) 50 yr smoothed records of δ¹⁸O of cores B31 (red) and B32 (black), in ‰.

TextS2: Map of estimated time scale variations in the records due to the topographic-effect

In a first step, all slopes corresponding to the variations of surface elevation based on Howat et al. (2019) were computed across the continent. Further, profiles randomly selected along flow lines allowed to estimate an approximate mean undulation length of 5 km, which also fits to the observed surface undulation along the discussed traverse profile. Then, assuming the undulations to be perpendicular to the flow direction provided by Mouginot et al. (2019) comes

$$L = v \times t \quad (1)$$

With L referring to the length of undulation (5 km), v to the velocity field, and t to the time scale.

References used in Supporting Information

Dallmayr, R., Freitag, J., Hörhold, M., Laepple, T., Lemburg, J., Della-Lunga, D., & Wilhelms, F. (2021). A dual-tube sampling technique for snowpack studies. *Journal of Glaciology*, 67(261), 84-90. doi:10.1017/jog.2020.85

Fisher, D., Reeh, N., & Clausen, H. (1985). Stratigraphic noise in time series derived from ice cores. *Annals of Glaciology*, 7, 76–83. doi:10.3189/S0260305500005942

Graf, W.; Oerter, H.; Reinwarth, O.; Stichler, W.; Wilhelms, F.; Miller, H.; & Mulvaney, R. (2002). Calculated annual mean of $\delta^{18}\text{O}$ of firn core DML07C98_31 (B31). PANGAEA, <https://doi.org/10.1594/PANGAEA.104882>

Graf, W.; Oerter, H.; Reinwarth, O.; Stichler, W.; Wilhelms, F.; Miller, H.; & Mulvaney, R. (2002). Calculated annual mean of $\delta^{18}\text{O}$ and accumulation rate of firn core DML05C98_32 (B32). PANGAEA, <https://doi.org/10.1594/PANGAEA.104881>

103 Howat, I. M., Porter, C., Smith, B. E., Noh, M.-J., & Morin, P. (2019). The Reference Elevation
 104 Model of Antarctica. *The Cryosphere*, 13, 665–674, doi:10.5194/tc-13-665-2019
 105 Mouginot, J., E. Rignot, and B. Scheuchl. 2019. MEaSUREs Phase-Based Antarctica Ice Velocity
 106 Map, Version 1. [Indicate subset used]. Boulder, Colorado USA. NASA National Snow and Ice
 107 Data Center Distributed Active Archive Center. doi: <https://doi.org/10.5067/PZ3NJ5RXHR10>.
 108 [Date Accessed].
 109 Oerter, H., Wilhelms, F., Jung-Rothenhäusler, F., Göktas, F., Miller, H., Graf, W., & Sommer, S.
 110 (2000). Accumulation rates in Dronning Maud Land, Antarctica, as revealed by dielectric-profiling
 111 measurements of shallow firn cores. *Annals of Glaciology*, 30, 27-34.
 112 doi:10.3189/172756400781820705
 113 Schaller, C. F., Freitag, J., Kipfstuhl, S., Laepple, T., Steen-Larsen, H. C., & Eisen, O. (2016). A
 114 representative density profile of the North Greenland snowpack. *The Cryosphere*, 10, 1991–2002,
 115 doi.org/10.5194/tc-10-1991-2016
 116 Wilhelms, F., Kipfstuhl, J., Miller, H., Heinloth, K., & Firestone, J. (1998). Precise dielectric
 117 profiling of ice cores: a new device with improved guarding and its theory. *Journal of Glaciology*,
 118 44, 171–174, doi: 10.3189/S0022143000000246X

**High-precision profiles of water isotopes in snow-cores measured by CFA;
assessment of limitations and technical improvement**

Remi Dallmayr^{1,4}, Hannah Meyer^{1,2}, Johannes Lemburg¹, Vasileios Gkinis³, Thomas Laepple^{5,6},
Melanie Behrens¹, Frank Wilhelms^{1,4} and Maria Hörhold¹

¹ *Alfred-Wegener-Institut Helmholtz-Zentrum für Polar-und Meeresforschung, Bremerhaven, Am
Handelshafen 12, 27570 Bremerhaven, Germany*

² *Karlsruhe Institute of Technology, Kaiserstrasse 12, 76131 Karlsruhe, Germany*

³ *Niels Bohr Institute Physics of Ice, Climate and Earth, Tagensvej 16, 2200 Copenhagen, Denmark*

⁴ *GZG Abt. Kristallographie, University of Göttingen, Göttingen, Germany*

⁵ *Alfred-Wegener-Institut Helmholtz-Zentrum für Polar-und Meeresforschung, Potsdam,
Telegrafenberg A45, 14473 Potsdam, Germany*

⁶ *University of Bremen, MARUM – Center for Marine Environmental Sciences and Faculty of
Geosciences, 28334 Bremen, Germany*

Corresponding author: remi.dallmayr@awi.de

Key words: Stable water isotopes, CFA, Melt-Head, snowpack, diffusion

Due to the low Signal-to-Noise ratio, in areas with low accumulation rate of snow the climatic component of isotopic records in the upper-meters of the firn column is still poorly inferred.



Statistical studies via extended arrays of vertical profiles have however demonstrated improving the understanding of the formation, storage, and propagation of the isotopic signal in the snowpack. In order to cope with the numerous analyzes needed, in this study we modify a Continuous Flow Analysis system to analyze snow-cores. Such technique of analysis requires here a careful measurement strategy due to the low density of the samples considered. We quantify the smoothing of the isotope signal and develop correction approaches, such as an improved Melt-Head which allows to match the analytical challenge of percolation imposed by these highly porous cores. The observed diffusion within the snow-cores during storage time in cold facilities underlines the need of near-time analysis using such a development.

25

26 **1. Introduction**

27 Stable water stable isotopes ($\delta^{18}\text{O}$ and δD) in polar ice cores are commonly used to derive paleo-
28 temperatures (Jouzel et al., 1997). Combined to the low accumulation rate of the ice sheet in East
29 Antarctica, they enable reconstructing past climates over several interglacial periods, e.g. 420 000
30 years at Vostok (Petit et al., 1999), 720 000 years at Dome F (Kawamura et al., 2017). The
31 counterpart of low accumulation rate areas ($< 100 \text{ mm w.e. yr}^{-1}$) stands in difficulties to propose
32 records with reliable inter-annual to decadal climatic variabilities (Ekaykin et al., 2002; Hoshina
33 et al., 2014; Münch and Laepple, 2018). (Post-)depositional processes such as wind-redistribution

lead to spatial variability from stratigraphic noise (Fisher et al., 1985) and for these areas the signal is dominated by noise (Laepfle et al., 2018). However, recent small-scale studies (Münch et al. 2016, 2017) showed that stacking large number of independent vertical profiles allows for inferring the formation of the stable water isotope record and its propagation through the upper-meters of the firn column. Numerous high-resolution analyzes being required, the labor-intensive discrete analysis technique represent a limitation of the strategy.

By continuously melting a longitudinal section of a core sample on a chemically inert Melt-Head, the Continuous Flow Analysis technique (hereafter CFA) provides high-resolution measurements of stable water isotopes at high-pace (Gkinis et al., 2011; Dallmayr et al., 2016; Jones et al., 2017) in parallel with other proxies such as concentrations of chemical impurities (Osterberg et al., 2006; Bigler et al., 2011). However, such system is commonly not used with upper-firn cores due to the percolation occurring within the highly porous samples. A first approach to combine snow-cores with CFA is the LISA Box (Kjaer et al., 2021), where a snow-liner (core of 10 cm-diameter \times 1 m-length, Schaller et al., 2016) is melted on-site for conductivity and peroxide analysis. A quick estimation of age and accumulation rate with high quality is allowed as several liners of each site can be analyzed. Concerning water isotopes however, continuous analysis of snow-cores remains an analytical challenge.

In order to respond to this need, we modified the CFA-system developed at the Alfred-Wegener Institut (hereafter AWI) to analyze continuously snow-liners by using the proposed Melt-Head (Kjaer et al., 2021). We developed a method to characterize on a routine base the smoothing filter of the system by (1) means of isotopic standards, and (2) with respect to discrete records. Doing so, we find the major contributor to this smoothing to be the in-situ mixing due to the percolation within the snow-core while melting. We designed and implemented consequently an improved

Melt-Head that strongly limits the percolation, making our system suitable to analyze isotopic profiles in snow-cores for low accumulation rate areas.

2. Material and method

2.1. Experimental set-up

The system to analyze 1-meter snow-cores consists of a melting unit, a degassing unit, an electrical conductivity unit, a water isotope measurement unit, a micro-particles detection unit, a fraction collector module, and a datasets synchronization system (Fig. 1). From the Melt-Head, the potentially contaminated outer part of the snow sample is drained to the waste. The inner-line stream is driven to the degassing unit by a peristaltic pump (Ismatec IPC) through a perfluoroalkoxy (PFA) tubing with 1/16" outer diameter (OD) and 0.76 mm inner diameter (ID). Downstream of the debubbling unit (DB), a second peristaltic pump (Ismatec IPC) drives the bubble-free water stream to a polyether ketone (PEEK) manifold (P-150, IDEX), from where sub-streams are distributed to the different analytical units through PFA tubing (0.51mm ID). When the melting unit is not generating melted water, the analytical units are fed with ultrapure water (Millipore Advantage, Milli-Q $\geq 18.2 \text{ M}\Omega\cdot\text{cm}^{-1}$, hereafter MQ).

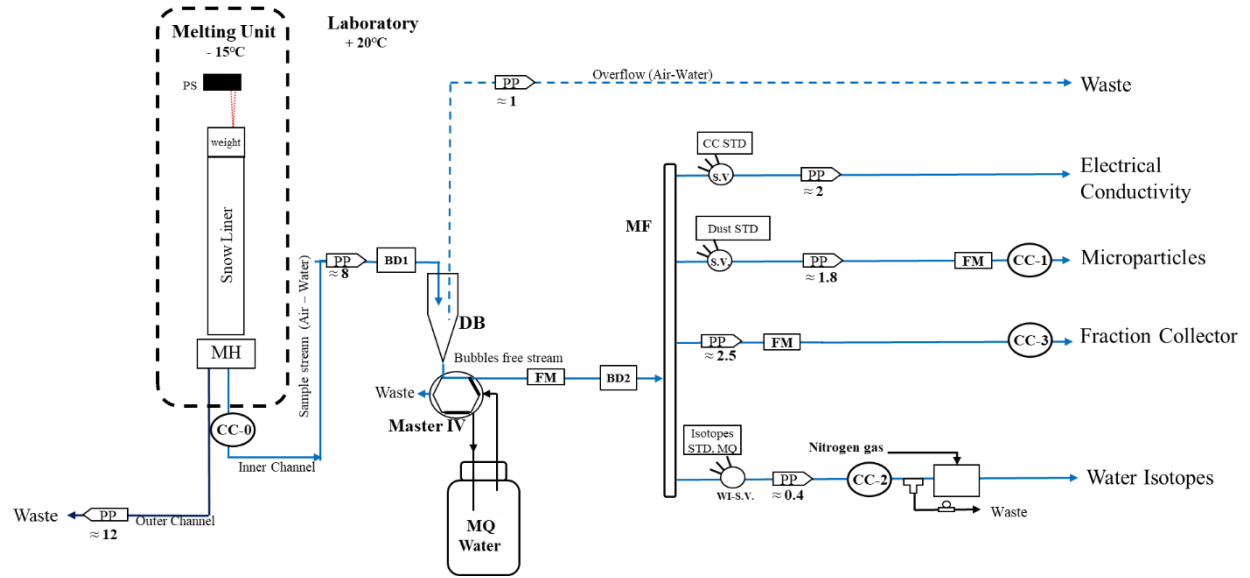


Figure 1. Setup of the AWI-CFA system used for snow cores. The snow-core is held in a snow sample holder (SSH) and melted on a Melt-Head (MH) in a -15°C environment. The laser positioning sensor (PS) determines the distance to the weight (W) placed on the top of the core. In the laboratory, the conductivity detectors for synchronization (CC-i); an injection valve (Master IV) switching between MQ water and ice sample; a debubbling unit (DB); a manifold (MF); selection valves (SV) for analytical units switching between MQ, sample, and standards. All analytical measurements are indicated. Liquid flow sensors (FM) monitor the flow behavior of the system. Finally, detection of air bubbles takes place upstream (BD1) and downstream (BD2) of the DB. All indicated flow values are expressed in $\text{ml}\cdot\text{min}^{-1}$.

Snow-core Melting unit

As illustrated in Fig. 2a, the melting unit features a 10 cm inner diameter and 120 cm long tube made of acrylic and positioned centrally above the Melt-head, guiding the sample during the experiment. A light weight (~ 150 g) is placed atop of the snow-core sample to stabilize the melt-flow, and is covered on both sides with a 1 mm thickness layer of PTFE to prevent contamination.

Following the work of Dallmayr et al. (2016), a high-accuracy laser positioning sensor (Way-con, LLD-150-RS232-50-H) determines the distance from the sensor and the top of the weight with a precision of 0.1 mm in order to derive accurate melt-speeds and to assign precise depths to the datasets generated.

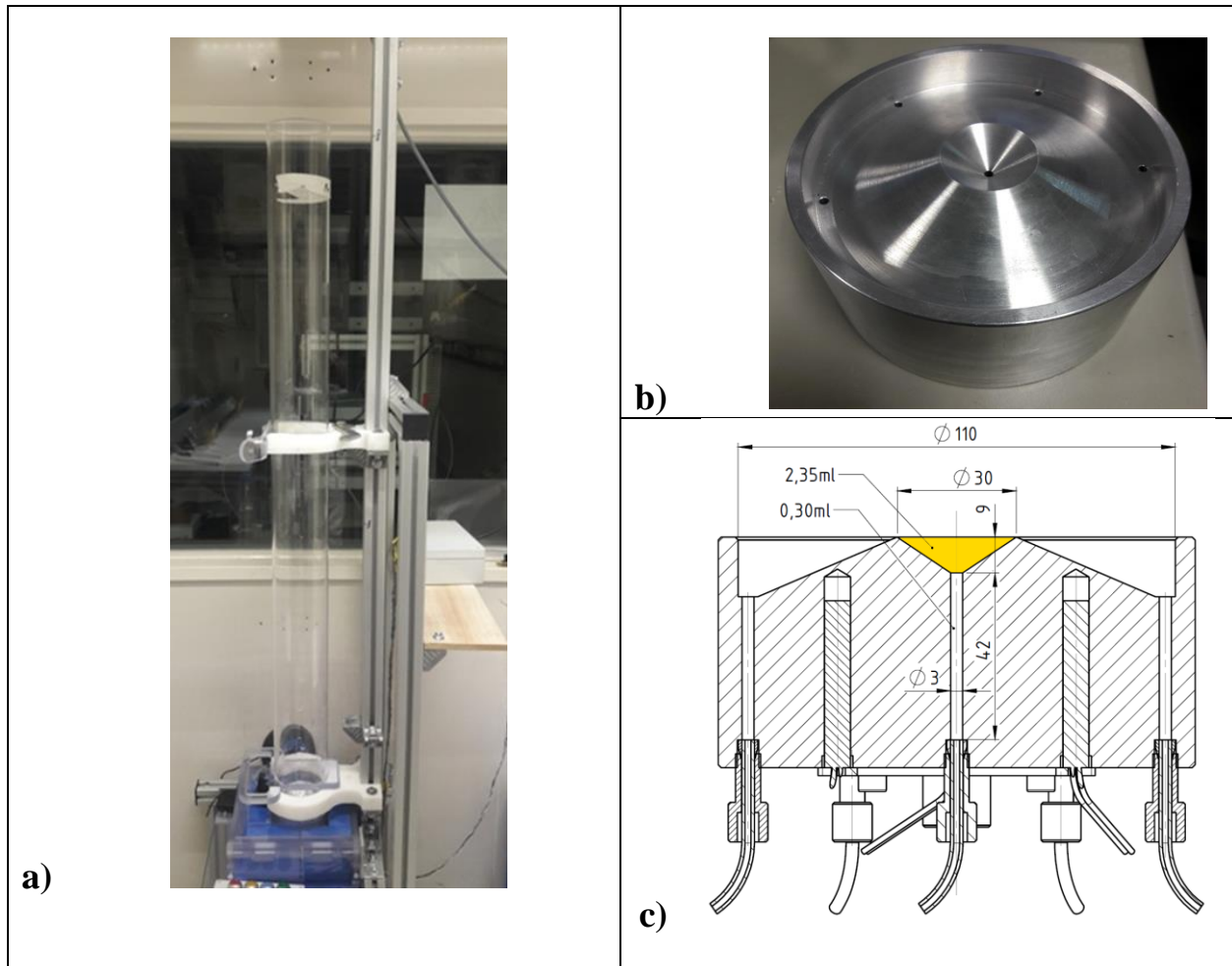


Figure 2. Melting Unit: a) Setup of the snow core melting unit. b) Illustration of the PICE-design Melt-Head. c) Sectional-view of the PICE-design Melt-Head, showing the dimension of the inner-channel concave volume (orange).

The Melt-Head for snow-cores (Fig. 2b) is based on the Physics of Ice, Climate and Earth, (Copenhagen, Denmark, hereafter PICE) design (Kjaer et al., 2021), made of aluminum, and manufactured at the AWI in Bremerhaven, Germany. Through a concave volume at the inner-channel (highlighted in Fig. 2c), the shape of the Melt-Head prevents mixing of clean inner-part with the potentially contaminated outer-part of the core sample. The temperature of the Melt-Head is regulated by a Proportional-Integrated-Derivative (PID) temperature controller (JUMO corporate, Germany) attached to eight 125W heating cartridges and a conventional thermocouple type J.

Debubbling Unit

Air in the sample stream leads to significant effects and interferences in the online liquid detectors, and a debubbling unit (hereafter debubbler, DB in Fig. 1) is required. The incoming flow drips into a micropipette opened to the air, releasing and the air bubbles to the atmosphere by buoyancy and leading to a bubble-free flow downstream. Regarding the distribution of air bubbles in the incoming flow, maintaining a safety volume of sample in the debubbler is essential. A tube connected to a peristaltic pump is continuously sucking air, or an overflow if the water-level within the pipette gets in contact. We set the height of this overflow-tube to a minimal safety volume of ~1 ml. A bubble detector located upstream of the unit (Fig. 1) monitors the variability of air in the incoming stream. A second bubble detector is located downstream of the unit (Fig. 1), monitoring, warning and recording the detection of air.

Analytical measurements

The CFA-system performs the online measurement of electrical conductivity (conductivity-cell model 3082, Amber Sciences Inc., USA, Breton et al., 2012) and micro-particles counting and sizing (Abakus, Klotz GmbH, Germany, Ruth et al., 2002). Meanwhile, fractions are carefully collected under a laminar flow bench for further offline measurements of chemical impurities by Ion Chromatography (normative precision of <10%, Göktas et al., 2002), and stable water isotopes ($\delta^{18}\text{O}$ and δD) mixing ratios are continuously measured by a Cavity Ring Down Spectrometer (CRDS, Picarro Inc, USA, Maselli et al., 2013). To obtain the continuity and stability of a micro-flow rate of vapor as required by the instrument, a stream vaporization module was made based on the original method of Gkinis et al. (2010). A micro-volume tee is used to split a micro-flow into a 50 μm ID fused-silica capillary from the incoming stream. The waste line featuring a smaller ID, a back-pressure is enabled and pushes the micro-flow through the capillary towards the oven where mixing with N_2 gas occurs before injection to the instrument. To control the back-pressure precisely and efficiently, we divided the waste line using a second tee and added to one sub-waste line a 10-turn micro-metering needle valve (Dallmayr et al., 2016). Schematic and technical details of the water isotope line are provided in Appendix-1.

Data synchronization system

Additional electrical conductivity measurements are performed at the melting unit outlet (CC0 in Figure 1, Amber Sciences model 1056, USA) as well as near the inlet of each detection unit (CC1 to 3 in Fig. 1, contactless conductivity measurement, Edaq, Australia). Such duplicated measurements allow for a straightforward and efficient synchronization of the different datasets during data processing (Dallmayr et al., 2016).

143

144 *Control and data acquisition, processing system, analysis of diffusion*

145 All devices are connected to the controlling computer, using a software developed with LabVIEW
146 2012. Drivers are either provided by manufacturers (pumps, flowmeters) or developed to suit the
147 purpose (Laser positioning, actuated valves, bubbles detectors, all analytical units). Analytical data
148 are recorded every second, and are processed after the experiment by using a second piece of
149 software also developed with LabVIEW 2012. The analyzes of isotopic diffusion are realized using
150 algorithms developed with the software R (R Core Team, 2018).

151

152 *2.2. Characterization of diffusion*

153 CFA-systems are known to diffuse and attenuate the original signal (Gkinis et al., 2011; Jones et
154 al., 2017). The resulting smoothing can be described as a mathematical convolution:

$$155 \quad \delta_m(t) = [\delta_0 \circledast G](t) = \int \delta_0(\tau)G(t - \tau)d\tau \quad (1)$$

156 With δ_m the measured data and δ_0 the original isotopic value of the sample. G is a smoothing filter
157 denoting the impulse response of the system and \circledast refers to the convolution operation. We address
158 the characterization of this smoothing by analyzing the impulse response of the system (i.e. the
159 derivative of the response of the system to an instantaneous isotopic change). In earlier works,
160 Gkinis et al. (2010; 2011) fit this so-called step response of the system to a scaled cumulative
161 distribution function (hereafter CDF) of a normal distribution, as:

$$162 \quad \delta_{normal}(t) = \frac{A}{2} \left[1 + \operatorname{erf} \left(\frac{t-t_0}{\sigma\sqrt{2}} \right) \right] + B \quad (2)$$

With A and B the isotopic values of the step scaled, t_0 the initial time, and σ the standard deviation. All parameters are determined by means of least square optimization. In this approach of normal distribution, the impulse response of the CFA-system is described by a Gaussian impulse probability density function (PDF):

$$G_{normal}(t) = \frac{1}{\sigma_{normal}\sqrt{2\pi}} e^{-\frac{(t-t_0)^2}{2\sigma_{normal}^2}} \quad (3)$$

Here, the standard deviation of the Gaussian PDF (σ_{normal}) characterizes the diffusion length of the system, expressed in seconds. Seconds are converted into millimeters by applying the considered melt-speed.

Because of the skewed shape of the impulse response, Jones et al. (2017) proposed an implementation from normal CDF to two multiplied lognormal CDFs ($\delta_{log-log}(t) = \frac{C}{2} \left[1 + \operatorname{erf} \left(\frac{t-t_1}{\sigma_1\sqrt{2}} \right) \right] \left[1 + \operatorname{erf} \left(\frac{t-t_2}{\sigma_2\sqrt{2}} \right) \right] + D$). This approach provides a slightly better fit to the signals, but the diffusion length is then retrieved using an additional function fitting the two lognormal CDFs. The derived diffusion length requires thus a careful interpretation due to these additional uncertainties. Our results differing of <10% between approaches, we present in this work the diffusion lengths and assessment of contributions computed with the straightforward Gaussian approach.

2.3 Snow-core samples

To evaluate the performances of the CFA-system, we compare continuous analysis with discrete samples via seven 1-meter long snow-cores (KF13 to KF18, and KF20). The samples correspond to the absolute depths 240-340 cm, are 5 meters spaced, and were taken in a trench excavated

during the 2014/2015 season (Münch et al., 2017), near from Kohnen station (0°04E 75°00 S, 2892 m.a.s.l.), Dronning Maud Land. This area is characterized by an accumulation rate of 74 mm w.e. yr⁻¹ (Steinhage et al., 2013), and the sampling procedure used liners (tubes made of carbon fiber of 1 mm thickness, Schaller et al., 2016) pushed into the snow and subsequently withdrawn.

On all cores, a width of 25 mm was cut lengthwise and discrete sample were analyzed with a 22 mm depth-resolution at AWI -Potsdam in 2015 (hereafter dataset discrete-15). In 2019, a second discrete dataset was cut lengthwise (20 mm wide) with a similar 22 mm depth-resolution (33 mm for the core KF20) before the continuous analysis of the remaining core (55 mm wide). For this second discrete dataset (hereafter discrete-19), isotopic measurement of five cores (KF13-16 and 20), and impurities measurements of two cores (KF17 and 18) were realized at the AWI - Bremerhaven. For both discrete datasets, single isotopic measurements are provided with an accuracy of 0.1 ‰ for $\delta^{18}\text{O}$, and 1.5 ‰ for δD .

3. Results

3.1 Stability of system

The stability is determined by Allan variance test (Allan, 1966) over a period longer than 12h by continuous injection of MQ water. Such a test allows the investigation of the behavior of the noise and drift of our system with respect to the integration time. The results are presented in Fig. 3 and show the linear decrease of the Allan deviation (square root of Allan variance) up to an optimal deviation for an integration time of ~6000 s. Instrumental drift starts slightly earlier than 10⁴ s with low deviation (0.01 ‰ for $\delta^{18}\text{O}$ and 0.1 ‰ for δD) up to 4*10⁴ s. Therefore, for our snow-cores study and the longest single analysis segment of <3000 s, a single calibration per core is necessary.

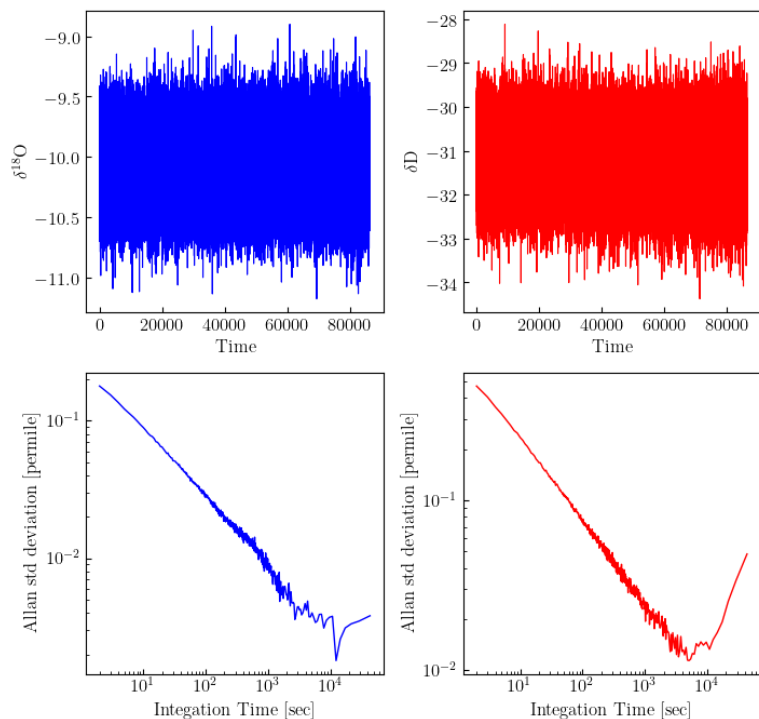


Figure 3. >12h of Allan deviation analysis for $\delta^{18}\text{O}$ (left panel, in blue), and δD (right panel, in red).

3.2 Calibration to the VSMOW-VSLAP scale, precision of continuous dataset

Calibrations of the raw data are performed using 3 laboratory-standards (Table 1) which are annually calibrated to the international VSMOW-VSLAP scale. The last 2 minutes of each >15 min laboratory-standard run are averaged. Based on the measured and real values of the standards, a linear regression fitting the 3-point is applied and defines the calibration coefficients (Fig. 4).

| | NZE | TD1 | JASE |
|-----------------------|--------|--------|--------|
| $\delta^{18}\text{O}$ | -19.85 | -33.85 | -50.22 |
| δD | -152.7 | -266.2 | -392.5 |

Table 1. Isotopic composition of the laboratory standards used for VSMOW calibrations, in ‰.

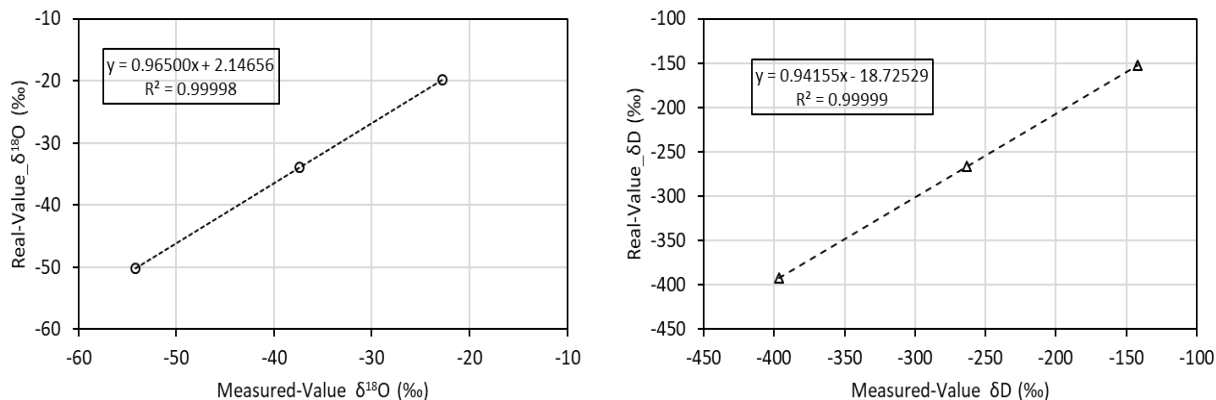


Figure 4. VSMOW three-points calibration with laboratory standards NZE, TD1, JASE (left: $\delta^{18}\text{O}$, right: δD).

In addition to the calibration, the laboratory-standards are used to infer the precision of our measurements, defined as the level of internal agreement among independent measures. The standard-deviation (1SD) of the last 2 minutes of each injected standard (N=18) is of $0.24 \pm 0.02 \text{ ‰}$ and $0.47 \pm 0.04 \text{ ‰}$ for $\delta^{18}\text{O}$ and δD , respectively.

3.3. Smoothing induced by the experimental CFA-system

Through a set of three experiments (Fig. 5), we estimate the diffusion length induced by the whole system and we differentiate the contributions of (1) the Melt-Head, (2) downstream of the Melt-Head to the water isotope selection valve (section dominated by the safety volume of the debubbler), and (3) downstream of the selection valve to the CRDS instrument (domination of the CRDS device).

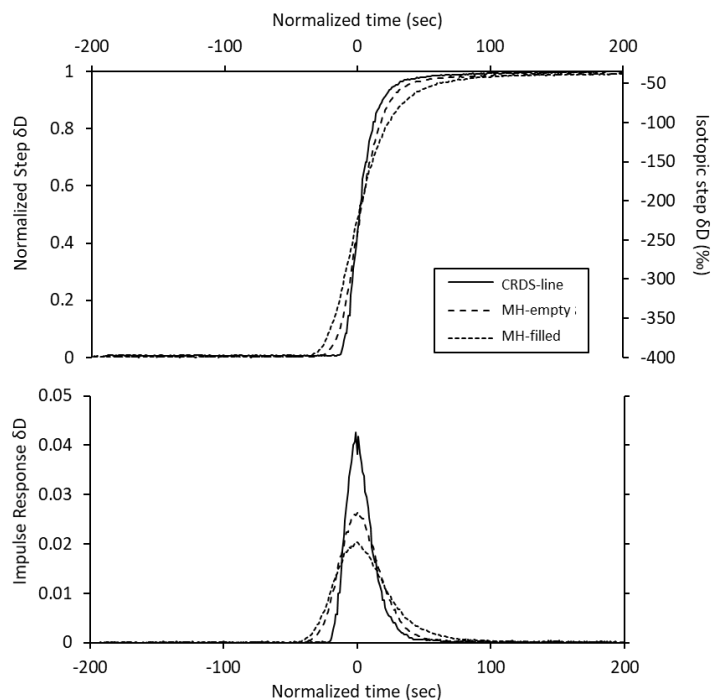


Figure 5. Isotopic step and impulse responses obtained for the three experiments realized: isotopic switch at the isotope selection valve (WI-SV in Fig. 1) or at the Melt-Head (MH, Fig. 1), concave volume filled or empty.

In a first experiment we applied a liquid isotopic step at the Melt-Head with its concave volume filled (dataset MH-filled). In a second experiment we applied the same liquid step in an empty concave volume (dataset MH-empty). For both experiments, 4-steps are considered. Abrupt isotopic changes are realized during each calibration procedure at the water isotopes selection valve (dataset CRDS-line), for which 15-steps are considered. Using equations (1) to (3), we compute the diffusion lengths (σ) of our set of experiments ($\sigma_{MH-filled}$, $\sigma_{MH-empty}$, $\sigma_{CRDS-line}$). The results for both isotopologues δD and $\delta^{18}O$ are very similar, and we focus our study on the results for δD .

| $\sigma_{MH-filled}$ | $\sigma_{MH-empty}$ | $\sigma_{CRDS-line}$ | σ_{MH} | $\sigma_{MH\ to\ WI-SV}$ |
|----------------------|---------------------|----------------------|---------------|--------------------------|
| <i>21.6 (2.4)</i> | <i>14.5 (1.2)</i> | <i>12.6 (1.8)</i> | | |
| 13.6 (1.5) | 9.2 (0.7) | 8.0 (1.1) | 10.0 | 4.5 |

Table 2. δD means diffusion length expressed in seconds (italic) and in mm (bold), derived from the normal PDF. Values in parenthesis represent 1SD. The conversion of seconds to mm is based on a melt-speed of 38 mm.min⁻¹. σ_{MH} and $\sigma_{MH\ to\ WI-SV}$ correspond to differences in quadrature between $\sigma_{MH-filled}$ and $\sigma_{MH-empty}$, and between $\sigma_{MH-empty}$ and $\sigma_{CRDS-line}$, respectively.

Assuming independent smoothing from the Melt-Head to the CRDS instrument, the total smoothing filter is the sum of the variances of each smoothing filter along the CFA-system based on our three experiments:

$$\sigma_{CFA-system}^2 = \sigma_{MH}^2 + \sigma_{MH\ to\ WI-SV}^2 + \sigma_{CRDS-line}^2 \quad (6)$$

We can evaluate the smoothing induced by the concave volume of the Melt-Head by quadrature difference ($\sigma_{MH} = \sqrt{\sigma_{MH-filled}^2 - \sigma_{MH-empty}^2}$), as well as the smoothing induced downstream of the Melt-Head to the isotopic selection valve ($\sigma_{MH\ to\ WI-SV} = \sqrt{\sigma_{MH-empty}^2 - \sigma_{CRDS-line}^2}$).

The Table 2 shows a diffusion length of the whole system of ~14 mm, and differentiating the contributions indicates that the majority of the instrumental smoothing is induced by the concave volume of the Melt-Head (10 mm diffusion length), closely followed by the CRDS-line (8 mm). The section dominated by the volume of the debubbler shows a significantly smaller contribution of 4.5 mm. While we address the Melt-Head contribution via a new design in section 3.5,

improving the smoothing induced by the CRDS-line requires modifications of the analytical unit itself (e.g. significant increase of volume at its inlet before a pressure-drop to the 40 Torr cavity).

3.4. Snow-core samples analysis

3.4.1. Continuous records versus discrete records

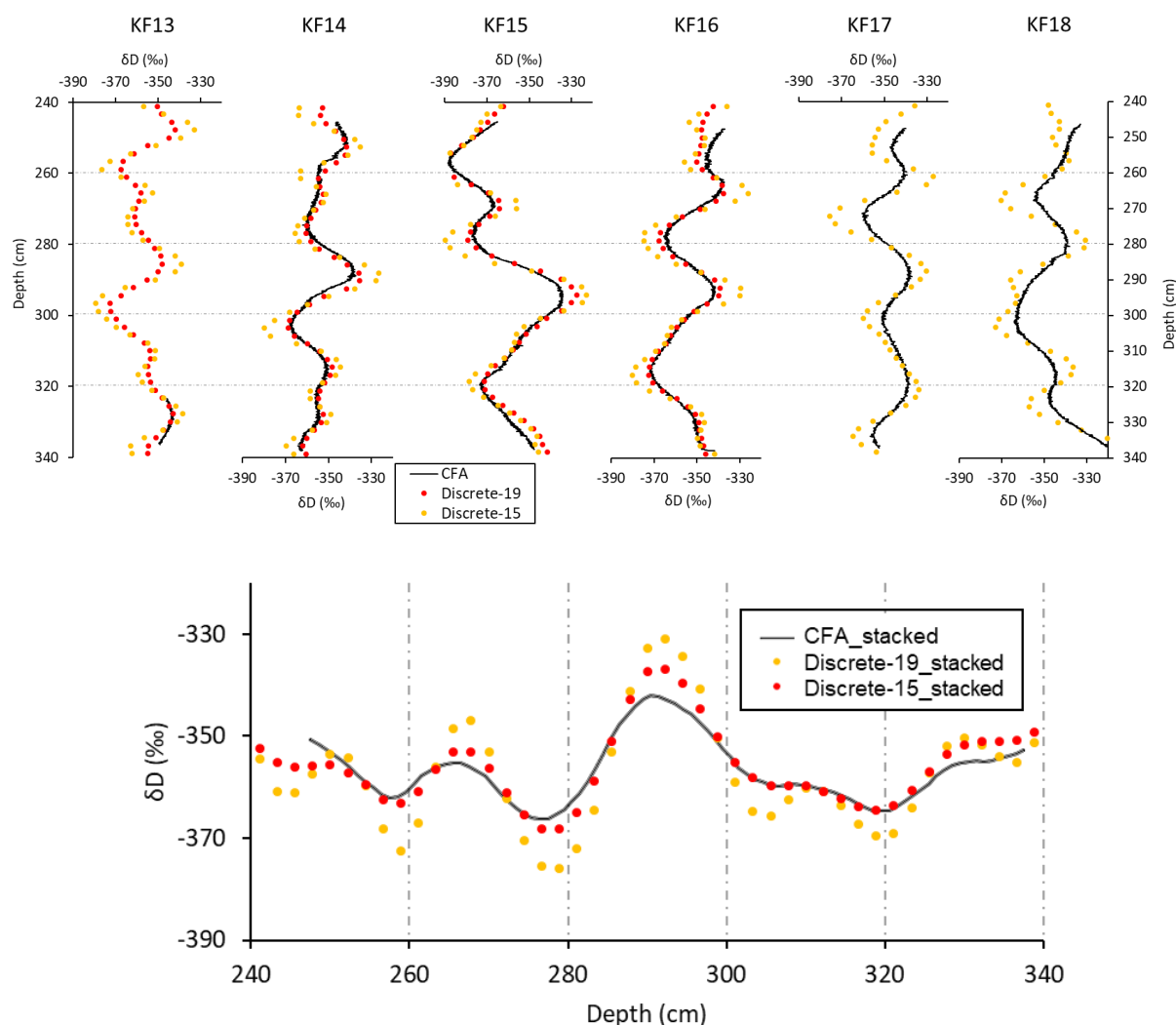


Figure 6. Top: 240-340 cm depth δD profiles of the six cores, 5 meters spaced. Datasets of continuous measurement (black lines), discrete-15 (orange markers) and discrete-19 (red markers) are shown. Because of the transition from MQ to sample and vice-versa, we removed the top-70

mm and bottom-20 mm of the continuous dataset. Note the small 150 mm portion of reliable continuous analysis for the core KF13, due to issues during the run. The averaged melt-speed of the 6 runs is 38 mm.min^{-1} ($1\text{SD} = 9 \text{ mm.min}^{-1}$). Bottom: Mean datasets of the stacked profiles KF-14, -15, -16.

The differences in the profiles (Fig. 6-top) show the spatial heterogeneity of the isotopic composition due to the stratigraphic noise (Fisher et al., 1985) and the necessity of stacking the profiles (Münch et al., 2016). The Fig. 6-bottom shows the mean stacked-profile of the three cores for which all datasets are available, and besides the relative high-quality of the depth-assignment (phase of the CFA and discrete datasets offset by $12.3 \pm 6.4 \text{ mm}$, due to the inhomogeneous density and rapid changes in the melt-speed), we see the difficulties-inability of our system to capture weak isotopic cycles (e.g. loss of cycle between 240-260 cm depth). Comparing the amplitudes between isotopic minima and maxima show that the continuous record attenuates on average $\sim 17\%$ of the discrete-19 record, and $\sim 48\%$ of the discrete-15 record. Such strong difference between both discrete datasets reveals a further and significant diffusional process occurring likely during the storage of the core samples (Van der Wel et al., 2011). As a result, we assess the smoothing filter of continuous analysis of snow samples with respect to the discrete-19 signal, and use the discrete-15 dataset to address the storage-induced smoothing filter.

3.4.2 Diffusion induced by continuous analysis of snow-core samples

Due to the high-porosity of the upper-meters samples, a capillary action (Colbeck, 1974) forces the melted water at the Melt-Head to lift upwards, enabling percolation as illustrated in Figure 7.

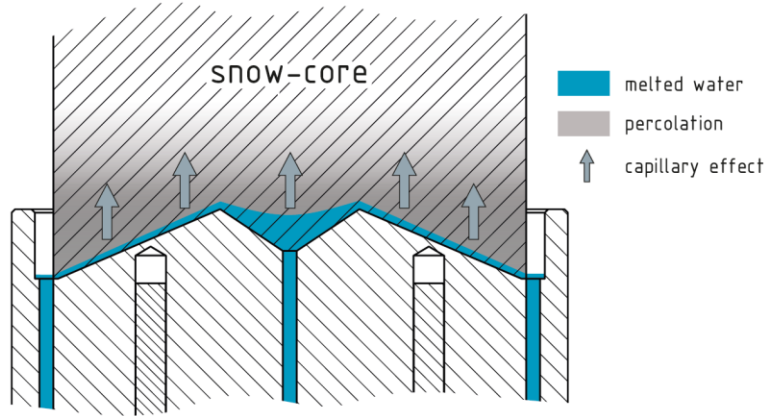


Figure 7. Illustration of the melting experiment showing the percolation induced by the low density of the sample combined to the melt-water reservoir within the inner concave volume of the Melt-Head.

In order to retrieve the diffusion length induced by the continuous analysis of snow-cores with respect to the discrete dataset, we convolved the discrete signal with a family of impulse responses of different diffusion lengths. A set of discrete-convolved signals of flattened extrema are obtained, and each signal is compared to the CFA signal (previously smoothed on 22 mm to ensure the same averaging than the discrete samples). Then, the minimum of root-mean-square (RMS = $\sqrt{\text{mean}((x_i - x_j)^2)}$) between convolved signals and the continuous record allows for the identification of the adequate diffusion length $\sigma_{CFA-discrete}$.

| | KF13 | KF14 | KF15 | KF16 | KF17 | KF18 |
|---|------|------|------|------|------|------|
| $\sigma_{CFA-discrete19}$ Normal-CDF | x | 29 | 32 | 31 | x | x |
| $\sigma_{CFA-discrete15}$ Normal-CDF | x | 49 | 52 | 57 | 56 | 57 |

Table 3. Diffusion lengths (in mm) of the continuous profiles of δD , as related to the discrete-19 dataset and to the discrete-15 dataset. No results are available for the core KF13 due to the too short continuous dataset.

Table 3 indicates a mean diffusion length for the continuous analysis $\sigma_{CFA-discrete19}$ of ~ 30 mm. Following equation (6), and assuming here independent smoothing filters induced by the percolation and the instrumental system, comes:

$$\sigma_{CFA-discrete(i)}^2 = \sigma_{CFA-system}^2 + \sigma_{percolation}^2 \quad (7)$$

$\sigma_{CFA-discrete(i)}$ refers to the diffusion length of the continuous record with respect to the discrete record(i) considered. If we assume a constant instrumental smoothing filter $\sigma_{CFA-system}$ of 14 mm (section 3.3) for all experiments, we can quantify by quadrature difference a diffusion length $\sigma_{percolation}$ of ~ 27 mm. This length being about twice the length induced by the experimental system, percolation is the contributor to address in priority to propose a suitable CFA-system for snow-cores.

3.4.3. Additional smoothing induced by storage

324 With a mean $\sigma_{CFA-discrete15}$ value of ~ 54 mm (Table 3), we can infer the storage-induced diffusion
 325 length. Assuming that the smoothing filter of the discrete-15 dataset corresponds to the smoothing
 326 filter of the discrete-19 dataset convolved with an independent smoothing filter induced by the
 327 storage, comes:

$$328 \quad \sigma_{CFA-discrete15}^2 = \sigma_{CFA-discrete19}^2 + \sigma_{storage\ 15-19}^2 \quad (8)$$

329 Using $\sigma_{CFA-discrete19} = 30$ mm, we estimate to ~ 45 mm the diffusion length induced by the 4 years
 330 storage in the cold facilities.

331
 332 We further computed for each 1-meter long snow core the mean and variability (standard
 333 deviation) of the both discrete datasets (Table 4). The decrease in variability indicates an averaged
 334 attenuation of 0.54 ‰ and 4.5 ‰ for $\delta^{18}O$ and δD , respectively. The changes in the means show
 335 an averaged enrichment of isotopic composition of +0.31 ‰ for $\delta^{18}O$ and +1.6 ‰ for δD . Rather
 336 than isotopic fractionation occurring within the bag, this enrichment is likely due to the repeated
 337 contact with laboratory-air when bags are opened, and the loss of sample (frost) in the bag.

| | $\delta^{18}O$ | $\delta^{18}O$ | δD | δD |
|------|----------------|----------------|-----------------|-----------------|
| | Discrete-15 | Discrete-19 | Discrete-15 | Discrete-19 |
| KF13 | -45.29 (1.3) | -45.076 (0.85) | -356.31 (11.93) | -355.77 (8.05) |
| KF14 | -45.14 (1.45) | -44.71 (0.85) | -354.85 (12.24) | -353.12 (7.69) |
| KF15 | -46.38 (2.39) | -45.91 (2.05) | -364.36 (19.53) | -361.51 (16.75) |
| KF16 | -44.95 (1.70) | -44.76 (1.16) | -353.87 (14.72) | -353.30 (10.23) |
| KF20 | -44.20 (2.35) | -43.92 (1.6) | -348.08 (20.4) | -345.72 (13.9) |

338 Table 4. $\delta^{18}O$, δD means (standard deviation) for each snow core discrete dataset, expressed in ‰.

3.5. Implementation to improve performances

As conclude in section 3.4.2, reducing strongly the percolation is essential and can be combined with the previous instrumental assessment, i.e. concave volume of the Melt-Head acting as a reservoir. We suggest the following Melt-Head, designed at the AWI (Fig. 8a). The inner-channel consists of a flat surface covered with boreholes and is located 10 mm higher than the outer-channel. Such inner-plate allows for an efficient and uniform evacuation of the melt-water, thus limiting the suction upward (Fig. 8b). The design also proposes a separation in 3 sub-channels to ensure the analysis of pure samples for paired chemical impurities (Fig. 8b).

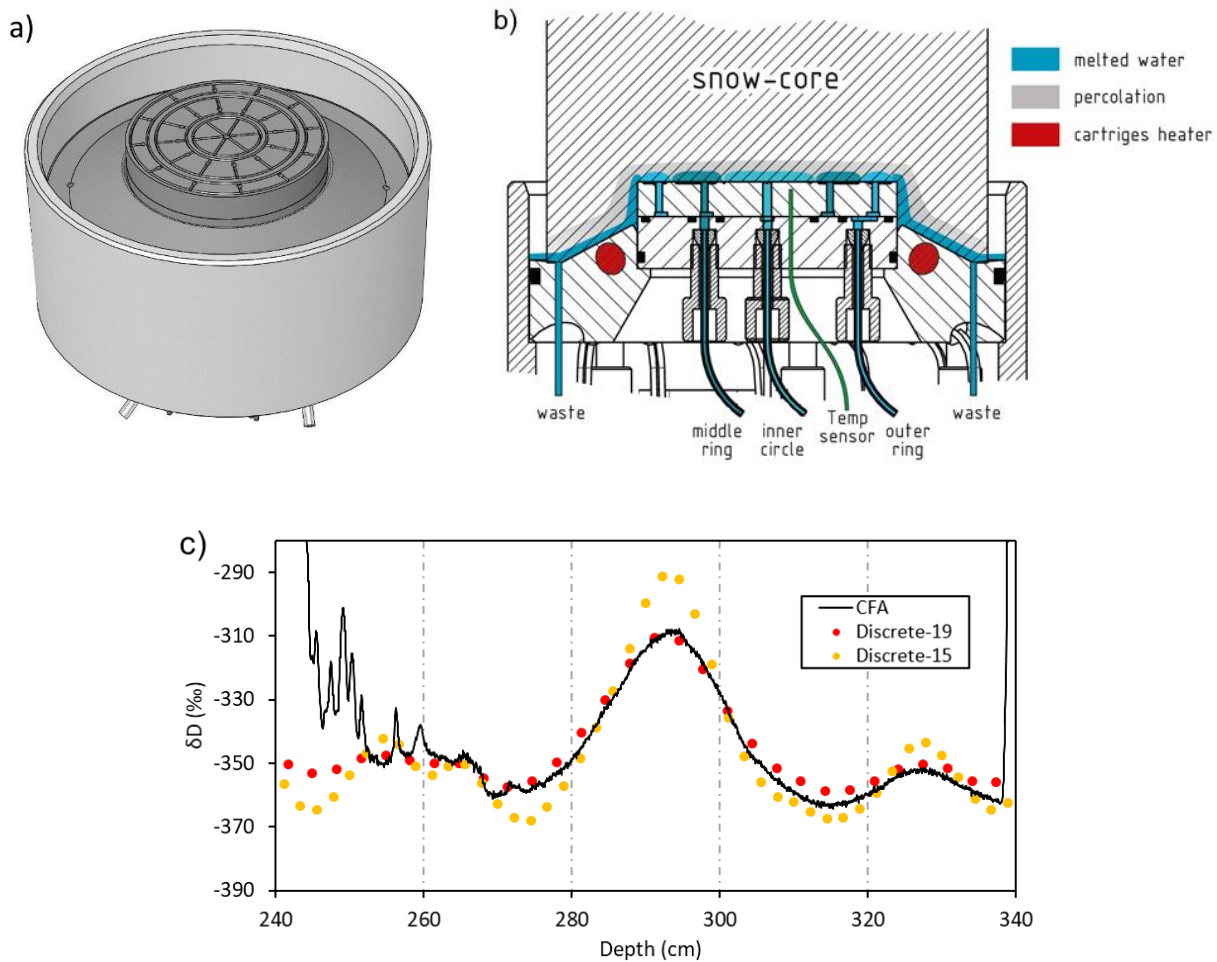


Figure 8. Implemented Melt-Head for snow-cores. a) Overview indicating the 2-levels physical separation between outer- and inner-channels, and the high number of bores covering the inner-plate. b) Sectional view showing the sub-channels and illustrating the increased evacuation of melted water and the reduced percolation. c) KF20 snow-core δD profiles (continuous in black line, discrete-19 in red marker, 33 mm depth-resolution, and discrete-15 in orange markers, 22 mm depth-resolution).

The results of the analysis of the snow-core KF20 are shown in Fig.8c. Despite troubles caused by an unstable vapor level in the top-30 cm, one can clearly see the improvement of the new design proposed. The quality of the calibration of the continuous signal can be discussed as indicates the slight shift towards lower composition than the corresponding discrete datasets. Nevertheless, we observe anomalously higher amplitude of the continuous dataset than the discrete-19 dataset, which we explain with the 33 mm averages of the discrete sampling.

4. Discussions

Despite the use of a Melt-Head acting as a water reservoir, the performances of our experimental system with regards to the isotopic signal diffusion are in line with prior improved CFA-CRDS systems (e.g. Jones et al., 2017). However, its application to low density cores ($<400 \text{ kg.m}^{-3}$, Laepple et al., 2016) requires overcoming the high level of diffusion induced by the percolation. Our improved design of Melt-Head allows for an efficient limitation of percolation and seems to offer the necessary quality to resolve the ~ 200 mm isotopic seasonal cyclicity in the snowpack in the Kohnen station area (Münch et al., 2017). More experiments must be conducted with the new device, its initial use suggesting technical improvements (e.g. temperature control). The

temperature is measured at the center of the inner-plate with heating-cartridges only surrounding the inner-plate (Fig. 8b). A poor regulation was observed due to the thermal inertia, and obtaining a sufficient melt-rate for a stable run required over-heating. Later on, controlling a stable melt-rate is not trivial as inhomogeneous density of the sample core over a few centimeters can cause rapid increase or decrease of speed.

Concerning very low accumulation rate sites, e.g. Vostock: ~60 mm annual snow layer thickness (Ekaykin et al., 2002); Dome F: ~74 mm (Kameda et al., 2008); Dome C: ~77 mm (Touzeau et al., 2016), further improvements are necessary. The significant contribution of the CRDS-line must here be addressed, and requires likely a collaboration with the manufacturer.

The observation of the significant smoothing induced by the storage of the core samples is of particular interest. We show in Fig. S2 (Appendix-2) the effect of storage on diffusion lengths for both isotopologues based on firn-diffusion model (Gkinis et al., 2014). Assuming a storage temperature of -20°C and a low density of 370 kg.m⁻³, 4 years lead to a very similar diffusion length for δD than our quantification (section 3.4.3). The diffusivity coefficients being positively correlated to temperature (Fig. S3, Appendix-2), the diffusion during storage is likely of stronger magnitude than on the East-Antarctic plateau.

Conclusions

Overcoming the increased stratigraphic noise in low accumulation areas and constraining the isotope signal formation within the upper-firn can be realized, but requires large number of high-quality stacked vertical profiles (Münch et al., 2017). In order to cope with the related challenge of high-pace -quality analysis and paired measurements of various proxies, we presented here a

CFA-system adapted for analysis of snow-cores. Based on the method of Gkinis et al. (2011), we developed algorithms to quantify the smoothing of the isotopic signal induced by the system and inferred its major contributors. We further investigated the strong additional smoothing induced by the low density of snow core samples and proposed a correction through an improved design of Melt-Head. Consequently, for an area of low accumulation rate such as Kohnen station, reliable high-resolution isotopic records paired with other climate proxies can be produced in a fast and clean way as compared to the classic discrete technique. For very low accumulation rate sites however, using a CFA technique requires likely modification of the CRDS analytical device itself. Finally, the isotopic diffusion during storage of snow-core samples requires further investigation, but underlines the need of (1) a strategy to preserve the original record (discrete samples cut in the field) or (2) prompt analysis with techniques such as the CFA. The coupling of our Melt-Head and isotopic setup to an on-site system (Kjaer et al. 2021) would present the double benefits of optimizing the quality of analysis and avoiding the cost of transportation of large number of snow-cores.

Data availability

- All snow-cores datasets (continuous, discrete-15, discrete-19) will be uploaded on PANGAEA.
- The technical drawings of all the components of the Melt-Head for snow-cores and their assembly will be published at the digital library Zenodo.
- The codes developed to characterize the isotopic diffusion are available at:
https://github.com/Ice-core-Paleo-Proxies/AWI_CFA_Isotope

413

414 **Acknowledgmment**

415 This project was supported by Helmholtz funding through the Polar Regions and Coasts in the
416 Changing Earth System (PACES) programme of the Alfred Wegener Institute. TL was supported
417 by the European Research Council (ERC) under the European Union's Horizon 2020 Research
418 and Innovation Programme (grant agreement no. 716092). We are grateful to Helle-Astrid Kjaer
419 and Paul Vallelonga for providing the design of the initial Melt-Head for snow-cores, and the
420 AWI-Workshop for manufacturing. We thank Thaddäus Bluszcz for his help at the first stage of
421 the instrumental development, and York Schlomann for providing all necessary isotopic standards.
422 We further thank Hanno Meyer for the discrete-15 isotopic measurement and Thomas Münch for
423 providing all information for the snow-cores investigation. Finally, the main author is very grateful
424 to Johannes Freitag and Sepp Kipfstuhl for their relevant inputs on the data analysis.

425

426 **Authors contribution**

427 Through her master-thesis HM participated to the experiments, developed all the algorithms to
428 characterize the isotopic diffusion using the R-software, and participated actively to the
429 preparation of this manuscript with the main author. In addition to the original algorithms, VG
430 provided his expertise on CFA and characterization of isotopic diffusion, and provided insights of
431 the storage-effect based on firn-diffusion. Through initiating the COMB-i project, MH and TL
432 motivated the use of CFA with snow-cores, and provided guidance to the main author. JL designed
433 the new Melt-Head with the main author, manufactured it at the AWI-workshop and provided
434 technical illustrations for the manuscript. MB conducted all discrete isotopic measurements at

AWI-Bremerhaven. FW. RD developed the CFA-system, designed and proceeded to the tests and experiments, co-supervised the diffusion characterization Master-thesis, designed the new Melt-Head, analyzed all data and prepared this manuscript.

References

- Allan, D. W.: Statistics of atomic frequency standards, P. IEEE, 54, 221–230, 1966.
- Bigler, M.; Svensson, A.; Kettner, E.; Vallelonga, P.; Nielsen, M.E.; Steffensen, J. P. Optimization of High-Resolution Continuous Flow Analysis for Transient Climate Signals in Ice Cores. Environ. Sci. Technol. 2011, 45, 4483–4489.
- Breton, D.J., Koffman, B.G., Kurbatov, A.V., Kreutz, K.J. and Hamilton, G.S. (2012): Quantifying Signal Dispersion in a Hybrid Ice Core Melting System. Environ. Sci. Technol., 46(21), 11922–11928, doi: 10.1021/es302041k.
- Colbeck, S. (1974). The capillary effects on water percolation in homogeneous snow. Journal of Glaciology, 13(67), 85–97. doi:10.3189/S002214300002339X
- Dallmayr, R., Goto-Azuma, K., Kjær, H. A., Azuma, N., Takata, M., Schüpbach, S. and Hirabayashi, M.: A High-Resolution Continuous Flow Analysis System for Polar Ice Cores, Bull. Glaciol. Res., 34, 11–20, <https://doi.org/10.5331/bgr.16R03>, 2016.
- Ekaykin, A. A., Lipenkov, V. Y., Barkov, N. I., Petit, J. R., and Masson-Delmotte, V.: Spatial and temporal variability in isotope composition of recent snow in the vicinity of Vostok station, Antarctica: implications for ice-core record interpretation, Ann. Glaciol., 35, 181–186, doi:10.3189/172756402781816726, 2002.
- Fisher, D. A., Reeh, N., and Clausen, H. B.: Stratigraphic noise in time series derived from ice cores, Ann. Glaciol., 7, 76–83, doi:10.3198/1985AoG7-1-76-83, 1985.
- Gkinis, V., Popp, T. J., Johnsen, S. J., and Blunier, T.: A continuous stream flash evaporator for the calibration of an IR cavity ring down spectrometer for isotopic analysis of water, Isot. Environ. Health S., 46, 1–13, 2010.

461 Gkinis, V., Popp, T. J., Blunier, T., Bigler, M., Schüpbach, S., Kettner, E., and Johnsen, S. J.:
 462 Water isotopic ratios from a continuously melted ice core sample, *Atmos. Meas. Tech.*, 4, 2531–
 463 2542, doi:10.5194/amt-4-2531-2011, 2011.

464 Gkinis V., Simonsen S. B., Buchardt S. L., White J. W. C. and Vinther B. M. (2014) Water isotope
 465 diffusion rates from the NorthGRIP ice core for the last 16,000 years – glaciological and
 466 paleoclimatic implications. *Earth Planet. Sci. Lett.*, 405.

467 Göktas, F., Fischer, H., Oerter, H., Weller, R., Sommer, S., & Miller, H. (2002). A glacio-chemical
 468 characterization of the new EPICA deep-drilling site on Amundsenisen, Dronning Maud Land,
 469 Antarctica. *Annals of Glaciology*, 35, 347-354. doi:10.3189/172756402781816474

470 Hoshina, Y., K. Fujita, F. Nakazawa, Y. Iizuka, T. Miyake, M. Hirabayashi, T. Kuramoto, S.
 471 Fujita, and H. Motoyama (2014), Effect of accumulation rate on water stable isotopes of near-
 472 surface snow in inland Antarctica, *J. Geophys. Res. Atmos.*, 119, 274–283,
 473 doi:10.1002/2013JD020771.

474 Jones, T.R.; White, James W C; Steig, Eric J.; Vaughn, Bruce H.; Morris, Valerie; Gkinis,
 475 Vasileios; Markle, Bradley R.; Schoenemann, Spruce W. (2017), "Improved methodologies for
 476 continuous-flow analysis of stable water isotopes in ice cores", *Atmos. Meas. Tech.*, 10, 617–632,
 477 doi.org/10.5194/amt-10-617-2017.

478 Jouzel J., Alley, R. B., Cuffey, K. M., Dansgaard, W., Grootes, P., Hoffmann, G., Johnsen, S. J.,
 479 Koster, R. D., Peel, D., Shuman, C. A., Stievenard, M., Stuiver, M., White, J. (1997). Validity of
 480 the temperature reconstruction from water isotopes in ice cores. *Journal of Geophysical Research*
 481 102(C12), 471–487 doi: 10.1029/97JC01283.

482 Kameda, T., Motoyama, H., Fujita, S., and Takahashi, S.: Temporal and spatial variability of
 483 surface mass balance at Dome Fuji, East Antarctica, by the stake method from 1995 to 2006, *J.*
 484 *Glaciol.*, 54, 107–116, doi:10.3189/002214308784409062, 2008.

485 Kawamura, K., A. Abe-Ouchi, H. Motoyama, Y. Ageta, S. Aoki, N. Azuma, Y. Fujii, K. Fujita, S.
 486 Fujita, and K. Fukui (2017), State 30 dependence of climatic instability over the past 720,000 years
 487 from Antarctic ice cores and climate modeling, *Science advances*, 3(2), e1600,446.

488 Kjaer et al., 2021, A portable Lightweight In Situ Analysis (LISA) box for ice and snow analysis,
 489 The Cryosphere, 15, 3719–3730, 2021 <https://doi.org/10.5194/tc-15-3719-2021>

490 Laepple, T., Hörhold, M., Münch, T., Freitag, J., Wegner, A., and Kipfstuhl, S.: Layering of
 491 surface snow and firn at Kohnen Station, Antarctica: Noise or seasonal signal? J. Geophys. Res.
 492 Earth Surf., 121, 1849–1860, doi:10.1002/2016JF003919, 2016.

493 Laepple, T., Münch, T., Casado, M., Hoerhold, M., Landais, A., and Kipfstuhl, S.: On the
 494 similarity and apparent cycles of isotopic variations in East Antarctic snow pits, The Cryosphere,
 495 12, 169–187, <https://doi.org/10.5194/tc-12-169-2018>, 2018

496 Maselli, O. J., Fritzsche, D., Layman, L., McConnell, J. R. & Meyer, H. Comparison of water
 497 isotope-ratio determinations using two cavity ring-down instruments and classical mass
 498 spectrometry in continuous ice-core analysis. Isotopes Environ. Health Stud. 387–398,
 499 <https://doi.org/10.1080/10256016.2013.781598> (2013).

500 Münch, T., Kipfstuhl, S., Freitag, J., Meyer, H., and Laepple, T.: Regional climate signal vs. local
 501 noise: a twodimensional view of water isotopes in Antarctic firn at Kohnen Station, Dronning
 502 Maud Land, Clim. Past, 12, 1565–1581, <https://doi.org/10.5194/cp-12-1565-2016>, 2016.

503 Münch, T., Kipfstuhl, S., Freitag, J., Meyer, H., and Laepple, T.: Constraints on post-depositional
 504 isotope modifications in East Antarctic firn from analysing temporal changes of isotope profiles,
 505 The Cryosphere Discuss., 2017, 1–21, doi:10.5194/tc-2017-35, 2017.

506 Münch, T. and Laepple, T. (2018). What climate signal is contained in decadal- to centennial-scale
 507 isotope variations from Antarctic ice cores? Climate of the Past, 14, 2053–2070, doi: 10.5194/cp-
 508 14-2053-2018

509 Osterberg, E.C., Handley, M.J., Sneed, S.B., Mayewski, P.A. and Kreutz, K.J. (2006): Continuous
 510 Ice Core Melter System with Discrete Sampling for Major Ion, Trace Element, and Stable Isotope
 511 Analyses. Environ. Sci. Technol., 40(10), 3355-3361, doi: 10.1021/es052536w.

512 Petit, R. J., D. Raynaud, I. Basile, J. Chappellaz, C. Ritz, M. Delmotte, M. Legrand, C. Lorius, L.
 513 Pe, J. R. Petit, J. Jouzel, D. Raynaud, N. I. Barkov, J. M. Barnola, I. Basile, M. Bender, J.
 514 Chappellaz, M. Davis, G. Delaygue, M. Delmotte, V. M. Kotlyakov, M. Legrand, V. Y. Lipenkov,
 515 C. Lorius, L. Pepin, C. Ritz, E. Saltzman, and M. Stievenard (1999), Climate and atmospheric

history of the past 420,000 years from the Vostok ice core, Antarctica, *Nature*, 399(6735), 429–436.

Ruth, U., D. Wagenbach, M. Bigler, J. P. Steffensen, and R. Röthlisberger, High resolution dust profiles at NGRIP: Case studies of the calcium-dust relationship, *Ann. Glaciol.*, 35, 2002.

Schaller, C. F., Freitag, J., Kipfstuhl, S., Laepple, T., Steen-Larsen, H. C., and Eisen, O.: A representative density profile of the North Greenland snowpack, *The Cryosphere*, 10, 1991–2002, <https://doi.org/10.5194/tc-10-1991-2016>, 2016.

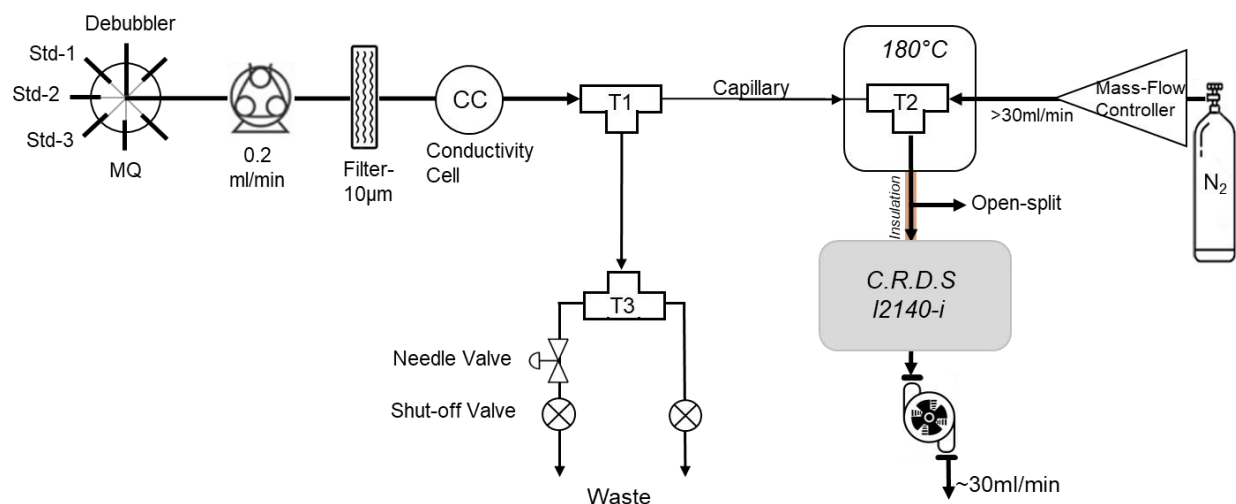
Steinhage, D., Kipfstuhl, S., Nixdorf, U., & Miller, H. (2013). Internal structure of the ice sheet between Kohnen station and Dome Fuji, Antarctica, revealed by airborne radio-echo sounding. *Annals of Glaciology*, 54(64), 163-167. doi:10.3189/2013AoG64A113

Touzeau, A., Landais, A., Stenni, B., Uemura, R., Fukui, K., Fujita, S., Guilbaud, S., Ekaykin, A., Casado, M., Barkan, E., Luz, B., Magand, O., Teste, G., Le Meur, E., Baroni, M., Savarino, J., Bourgeois, I., and Risi, C.: Acquisition of isotopic composition for surface snow in East Antarctica and the links to climatic parameters, *The Cryosphere*, 10, 837–852, doi:10.5194/tc-10-837-2016, 2016.

Van der Wel, L., Gkinis, V., Pohjola, V., & Meijer, H. (2011). Snow isotope diffusion rates measured in a laboratory experiment. *Journal of Glaciology*, 57(201), 30-38. doi:10.3189/002214311795306727

541

APPENDIX-1: Water-isotopes line



542

543 Figure S1. Detailed schematic of water isotopes line of the AWI CFA-system.

544

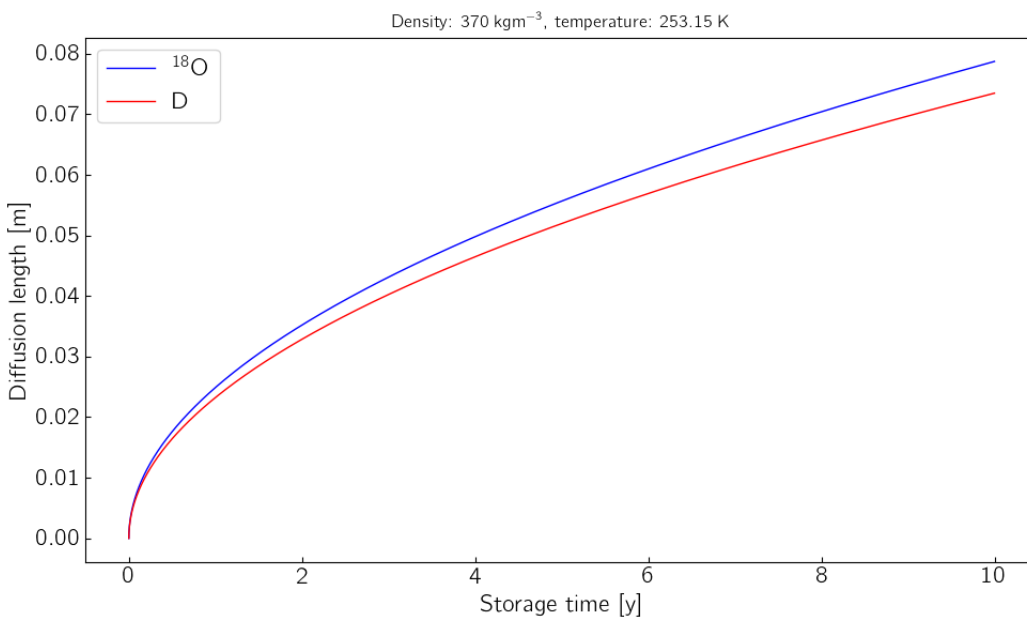
545 The selected sample steam is drained at a flow of $\sim 0.2 \text{ ml} \cdot \text{min}^{-1}$ through PFA tubes of 0.51 mm ID
 546 to a 10 μm frits-filter (A-107, Idex), then a synchronization conductivity cell before entering a
 547 stainless-steel micro-volume tee (U-428, Idex; T1 in Fig. S1). Here, a micro-flow is split from the
 548 incoming stream into a fused-silica capillary tube (50 μm ID), the rest going into the waste line.
 549 Due to the smaller ID of the waste line (0.25 mm ID), a back-pressure pushes the micro-flow
 550 through the capillary towards the oven. To control this back-pressure precisely and efficiently, the
 551 waste line is divided using a PEEK tee (T3) and added to one of the two sub-waste lines a 10-turn
 552 micro-metering needle valve (P-445, Idex).

553 The sample micro-flow is injected into the stainless-steel tee (T2, Valco ZT1M) mounted in the
 554 180°C oven, where it vaporizes instantly and mixes with a controlled flow of dry N_2 gas (Mass
 555 Flow Controller SEC-E40 N_2 100SCCM, Horiba company) to form a gas sample with the desired
 556 water vapor concentration.

557

558

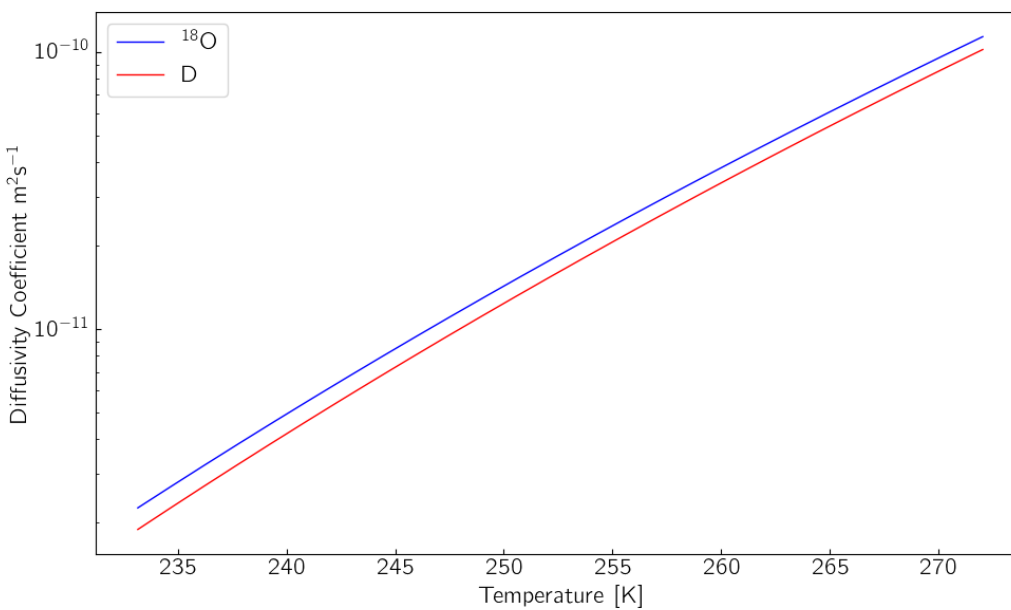
APPENDIX-2: Firn diffusion during storage



559

560 Figure S2: Firn-diffusion length for core samples (density of 370 kg.m⁻³) as function of the time
 561 of storage (-20°C).

562



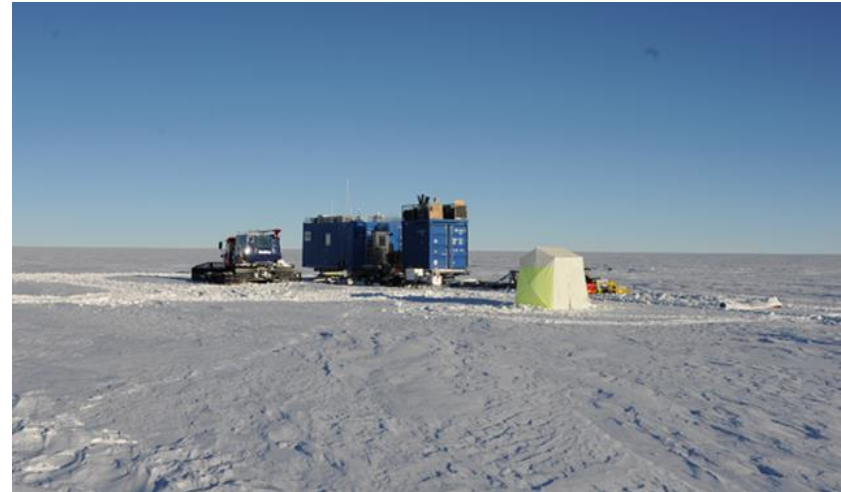
563

564 Figure S3: Diffusivity coefficients versus temperature.

PORT-FOLIO/ ANT LAND-18



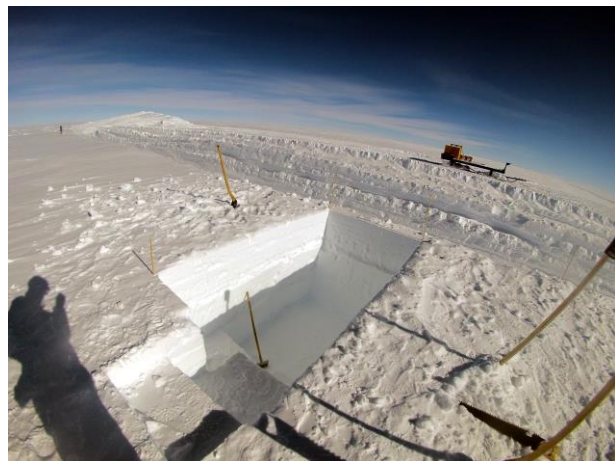
Kohnen station, Dronning Maud Land. Night of January 2nd (~20h) to January 3rd (~5h)

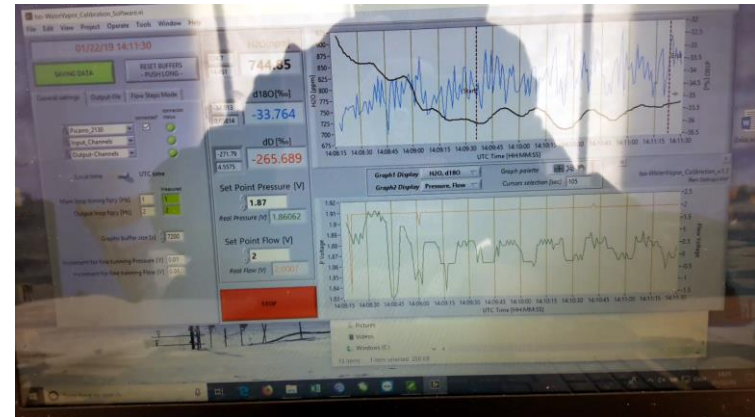
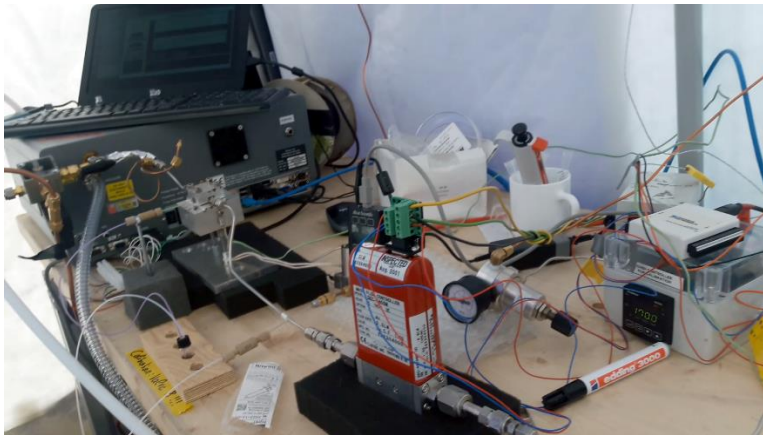
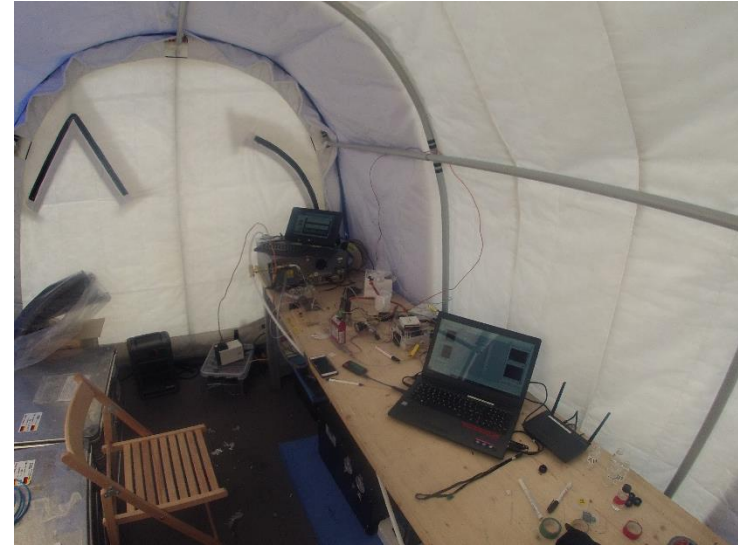
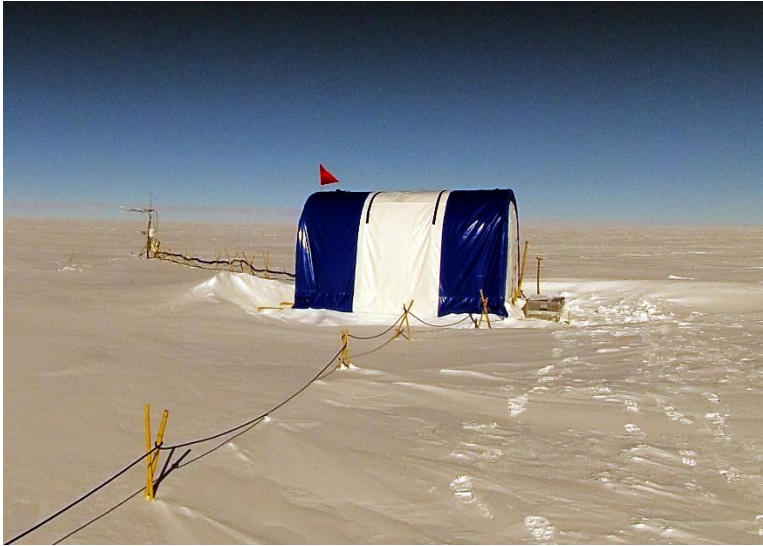


Kohnen-QK traverse: Sunny but cold; night camp; setup for transporting the dual-tubes sampler; surface snow after its passage



T4M trench, and cave (3 x 2 x 3m) juxtaposed. Light crossing the ~20 cm thick wall reveals the snow layers accumulated in the last ~15 years.





Seasonal laboratory in remote area for continuous measurements of the water-vapor isotopic composition: experimental setup; improvised software



Halos: ice crystals in the polar air acting as prisms & mirrors: they refract & reflect the light, creating "sun dogs" and lots of rainbows



well-deserved free time